Systematic investigation of organosiloxane derived surface modifications in tribochemical processes

Juretzka, Benjamin

(2020)

Systematic investigation of organosiloxane derived surface modifications in tribochemical processes

A dissertation approved by the Department of Materials and Earth Sciences, at TU-Darmstadt, in fulfilment of the requirements for the degree of Doctor−Ingenieur (Dr.-Ing.)

M. Sc. Benjamin Juretzka
Born on 03.29.1989 in Bensheim, Germany
24.11.2020 – Darmstadt

First referee: Prof. Dr. Dr. h.c. Ralf Riedel
Second referee: Prof. Dr. Robert Stark

TECHNISCHE UNIVERSITÄT DARMSTADT

Systematic investigation of organosiloxane derived surface modifications in tribochemical processes

Genehmigte Dissertation von M.sc. Benjamin Juretzka
Fachbereich Material- und Geowissenschaften, Technische Universität Darmstadt

Hauptberichter: Prof. Dr. Dr. h. c. Ralf Riedel
Mitberichter: Prof. Dr. Robert Stark

Tag der Einreichung: 27.05.2020
Tag der Prüfung: 01.09.2020

Darmstadt D-17

Jahr der Veröffentlichung der Dissertation auf TUprints: 2020

Declaration of Authorship

I hereby declare that the thesis submitted is my own unaided work. All direct or indirect sources used are acknowledged as references.

I am aware that the thesis in digital form can be examined for the use of unauthorized aid and in order to determine whether the thesis as a whole or parts incorporated in it may be deemed as plagiarism. For the comparison of my work with existing sources I agree that it shall be entered in a database where it shall also remain after examination, to enable comparison with future theses submitted. Further rights of reproduction and usage, however, are not granted here.

This thesis was not previously presented to another examination board and has not been published.

Ehrenwörtliche Erklärung

Ich erkläre hiermit ehrenwörtlich, dass ich die vorliegende Arbeit selbständig angefertigt habe. Die aus fremden Quellen direkt und indirekt übernommenen Gedanken sind als solche kenntlich gemacht.

Ich weiß, dass die Arbeit in digitalisierter Form daraufhin überprüft werden kann, ob unerlaubte Hilfsmittel verwendet wurden und ob es sich – insgesamt oder in Teilen – um ein Plagiat handelt. Zum Vergleich meiner Arbeit mit existierenden Quellen darf sie in eine Datenbank eingestellt werden und nach der Überprüfung zum Vergleich mit künftig eingehenden Arbeiten dort verbleiben. Weitere Vervielfältigungs- und Verwertungsrechte werden dadurch nicht eingeräumt.

Die Arbeit wurde weder einer anderen Prüfungsbehörde vorgelegt noch veröffentlicht.

Darmstadt, den 24. November 2020

_____

(Benjamin Juretzka)

Content

Abbreviations

α	Pressure viscosity coefficient
μ	Coefficient of friction
F_R	Friction force
F_N	Normal force
η	Viscosity
τ_x	Shear stress in x direction
$\dot{\gamma}$	Shear rate
v	Velocity
U	Entrainment speed
U_s	Sliding Speed
h	Lubricating film thickness
λ	Lambda ratio (lubricating film parameter)
ρ	Density
P	Pressure
a	Hertzian point contact radius
t	Time
F_{adh}	Adhesion force
E	Young's modulus
E'	Reduced elastic modulus
ν	Poisson's ratio
R	Reduced radius
R_q	Root mean square roughness (derived from line scan)
S_q	Root mean square roughness (derived over area)
ATR-FTIR	Attenuated toral reflection-fourier-transform infrared (spectroscopy)
AFM	Atomic force microscopy
AW	Anti-wear
cof	Coefficient of friction
EDX / EDS	Energy disperive X-ray spectroscopy
EHD	Elastohydrodynamic
EP	Extreme pressure
FTIR	Fourier-transform infrared (spectroscopy)
GPC	Gel permeation chromatography
MTM	Mini traction machine
NMR	Nuclear magnetic resonance (spectroscopy)
PDC	Polymer derived ceramic
PDMS	Polydimethylsiloxane
SiOC	Siliconoxycarbide

SLIM	Spacer layer imaging method
SRR	Sliding to roll ratio
TMS	Tetramethylsilane
VTMS	Vinyltrimethoxysilane
XPS	X-ray photoelectron spectroscopy
ZDDP	Zinc dithiophosphate

Abstract

By introducing low-viscosity engine and gear oils, the energy efficiency of oil lubricated drive trains and transmissions can be increased. However, by reducing the viscosity of lubricating oils, transmission components run for longer periods in component damaging conditions. In order to ensure protection by the lubricant in such severe conditions, surface-active additives are added.

The present work deals with surface modifications caused by organosilanes / -siloxanes in rubbing contacts. The investigations focus on the chemical changes and formed structures, as well as their influences on the lubricating behavior. For this purpose, vinyltrimethoxysilanes / -siloxanes were added to a mineral oil and investigated in ball-disc tribometers to investigate their influence on friction changes and lubricant film thicknesses. By varying test conditions, reactivity, chemical changes and influences on the lubrication behavior of the silane / siloxane oil additives were investigated. In addition, sol-gel coatings were applied and also subjected to tribological tests and chemical characterization.

It turns out that the used organosilanes and siloxanes deposit a multi-layered structure when exposed to tribological stress. While the top layer consists of weakly adhesive polysiloxanes with viscous properties, the bottom layer has an elastic character and is stronger bonded to the steel substrate. The different properties are based on the degree of crosslinking, which increases with increasing proximity to the substrate surface. The adhesive deposition is rich in SiO_2, which can be explained by a polymer into glass / ceramic conversion. The polymerization proceeds via condensation reactions and shows a strong dependence on the temperature. The adhesive layer results from the decomposition and further crosslinking of the polymers by the severe tribological stress. This transformation requires a certain contact pressure or shear stress. In addition, it has been shown that the formation of iron oxide is an important factor for the conversion and is as well part of the generated tribofilm.

With the knowledge of chemical analysis, a lubrication model for the multi-layer system is derived, which shows that both layers have opposing influences on the lubricating behavior of the lubricant. The *in-situ* generated polymers form thick polymer-rich boundary films which effectively increase the lubricating film thickness, especially at low entrainment speeds. This can reduce friction by up to 40 %. On the other hand, the adhesive tribofilm creates resistance to the oil drag in the lubrication gap and thereby increases the friction compared to the polished steel surfaces. Overall, a wear reduction and corrosion protection is also detected, however the present results only indicate tendencies from which layer the protective effects arise.

Furthermore, investigations show that big differences between the film formation and thereby tribological influences are found between the use of oligomeric and monomeric vinylmethoxysilanes / siloxanes. The monomeric precursor forms much lower polymeric film thicknesses but exhibits a more homogeneous and smoother tribofilm deposition. As a result, no reduction in friction and wear is achieved.

Zusammenfassung

Durch das Einführen niedrigviskoser Motor- und Getriebeöle kann die Energieeffizienz von ölgeschmierten Antrieben und Übersetzungen gesteigert werden. Durch das Verringern der Viskosität von Schmierölen laufen Antriebskomponenten allerdings längere Zeiten in komponentenschädigenden Bedingungen. Um trotzdem einen Schutz durch den Schmierstoff zu sichern, werden oberflächenaktive Zusätze beigemischt.

Die vorliegende Arbeit beschäftigt sich mit Oberflächenmodifizerungen, die durch Organosilane / -siloxane in Reibkontakten entstanden sind. Die Untersuchungen konzentrieren sich auf die chemischen Veränderungen und Strukturen, sowie Einflüsse auf das Schmierverhalten, welche die Änderungen mit sich bringen. Hierfür wurden Vinyltrimethoxysilane / -siloxane einem Mineralöl beigesetzt und in Kugel-Scheibe Tribometern hinsichtlich ihres Einflusses auf Reibungsveränderungen und Schmierfilmdicken untersucht. Durch variierende Testbedingungen konnten das Reaktionsvermögen, chemischen Veränderungen und Einflüsse auf das Schmierverhalten der Silan- / Siloxan-Öladditive untersucht werden. Darüber hinaus wurden Sol-Gel-Beschichtungen erzeugt und ebenfalls tribologischen Prüfungen und der chemischen Charakterisierung unterzogen.

Es zeigt sich, dass die verwendeten Organosilane und –siloxane eine mehrlagige Schichtstruktur auf den Antriebskomponenten abscheiden, wenn sie tribologischer Belastung ausgesetzt sind. Während die obere Lage aus schwach adhäsiven Polysiloxanen mit viskosen Eigenschaften besteht, bestitzt die untere Lage einen elastischen Charakter und weist eine stärkere Bindung an das Stahlsubstrat auf. Die unterschiedlichen Eigenschaften werden dem Vernetzungsgrad zugrunde gelegt, welcher mit zunehmender Nähe zum Substrat ansteigt. Die adhäsive Abscheidung ist reich an SiO_2, was durch eine Polymer in Glas- / Keramikumwandlung erklärt werden kann. Die Polymerisierung läuft über Kondensationsreaktionen und zeigt eine starke Abhängigkeit von der Temperatur. Die adhäsive Schicht resultiert aus der Zersetzung und weiterer Vernetzung der Polymere durch die heftige tribologische Beanspruchung. Diese Umwandlung zeigt sich erst ab einer gewissen Flächenpressung bzw. Schubspannung. Außerdem wurde nachgewiesen, dass die Bildung von Eisenoxid ein wichtiger Faktor für die Umwandlung sowie für den Bestandteil des erzeugten Tribofilms ist.

Mit den Kenntnissen der chemischen Analysen wird ein Schmierungsmodell für das Mehrlagensystem hergeleitet, welches zeigt, dass beide Lagen grundverschiedene Einflüsse auf das Schmierverhalten des Schmierstoffs aufweisen. Die *in-situ* erzeugten Polymere bilden dicke polymerreiche Grenzflächenfilme, die gerade bei niedrigen Einzugsgeschwindigkeiten

die Schmierfilmdicke effektiv erhöhen. Dadurch kann die Reibung um bis zu 40 % verringert werden. Der adhäsive Tribofilm erzeugt hingegen einen Widerstand gegen den Öleinzug im Schmierspalt und erhöht dadurch die Reibung im Vergleich zu den polierten Stahloberflächen. Insgesamt werden außerdem Verschleißverringerung und Korrosionsschutz nachgewiesen, wobei die vorliegenden Ergebnisse nur Tendenzen darstellen, von welcher Lage die jeweilige Schutzwirkung herrührt.

Des Weiteren zeigen Untersuchungen, dass es große Unterschiede zwischen der Filmbildung und den tribologischen Einflüssen zwischen oligomeren und monomeren Vinylmethoxysilanen / -siloxanen besteht. Der monomere Precursor bildet viel geringere polymere Filmdicken, zeigt dafür aber eine homogenere und weniger raue Tribofilmabscheidung. Dadurch können allerdings keine Verringerung der Reibung und des Verschleißes erreicht werden.

1. Motivation and aim of the study

Nowadays it is widely accepted that the climate change is highly affected by human-produced greenhouse gases. Especially the emission of carbon dioxide from the burning of fossil fuels is regarded as major driver of global warming. In order to suppress climate changes, the European Union has introduced regulations to reduce CO_2 emissions in the car industry. The regulations foresee that the whole car fleet of a car manufacturer needs to reach an average CO_2-target value of 95 g/km until 2020 [1]. The development and change to electric vehicles is one opportunity to reach these target values, however, since these vehicles are still not well developed and suffer from many disadvantages, they are not a sufficient instrument to reach the goals in such a short time. In addition it is still highly controversial whether electric vehicle will replace combustion engine driven cars in such extent. Therefore, the energy efficiency of passenger cars and commercial vehicles, driven by combustion engine, were and still need to be optimized by light weight design and reduction of friction.

The energy consumption by friction in passenger cars was presented in a study by Holmberg *et al.* The authors could show that in total one-third of the gain by fuel energy is lost by friction [2]. Being aware of this fact, the automotive industry developed many new low friction coating materials and surface designs. However, besides surface modifications especially low-viscosity and low-shear lubricants and additives are stated as the key to reduce the energy consumption.

The decrease in viscosity of lubricants is a comfortable parameter to increase energy efficiency. Besides lower shear forces in lubricated contacts, also churning losses, so the amount of energy being needed to move parts through oil can dramatically be decreased [3]. This has been done in the last decades and regulations and standards have been dictated by, for example, the International Lubricant Standardization and Approval Committee (ILSAC). The GF-6 licensing will start in mid-2020 and again introduce lower viscous lubricant classes. The decrease in viscosity is, however, a challenge for lubricant designer as lower viscous base oils support lower protection in starting and stopping motions, which are critical in terms of wear. This worsening performance is a big obstacle for the use of low viscous lubricants and must be adjusted by intelligent additive design.

Nowadays most anti-wear additives are phosphorous compounds, but their use became more and more restricted during the past lubricant standards. Therefore, new friction and wear reducing lubricant additives are being investigated and introduced in the last two decades. The smart additives range from ionic liquids over nanoparticles covering a vast range of materials [4, 5]. However, although these additives show promising performances in lab tests,

no commercial use has been achieved yet. Major obstacles like solubility, agglomeration and corrosive issues are still not fulfilled.

Phosphorous compounds are known to form glass like, protective reaction films in tribochemical processes. Silanes are the most investigated conventional glass building molecular compounds and have therefore recently been investigated for tribological purposes, with the aim to eliminate or substitute phosphorous compounds from engine oils [6]. The results show promising behavior in terms of wear protection, which is obtained by the formation of calcium silicate tribofilms. Unfortunately, no details about their lubricating influences have been presented yet and no detailed description whether a polymeric primary stage of the found silicate films is formed. Older works about the decomposition of silicone oils have shown, that polymeric, networked siloxane films can form upon rubbing on surfaces and influence the lubrication [7]. For future applications a detailed description of the tribochemical processes and reactions are necessary.

This work is building a bridge between these findings by giving a detailed description on the *in-situ* film formation and decomposition behavior of organosilane and organosiloxane in mineral oil lubricated tribological contacts. The focus of this work is held on dependences of the formation of silane based reaction films and on their influences on lubrication. This is done by providing a chemical, as well as structural description of the formed surface modifications under different testing conditions. In addition, the lubrication behavior is investigated and a lubrication model is presented. This thesis sets the basis for future development of organosilane based film forming oil additives.

2. State of the Art and Principles of Tribology

In this chapter, the science of tribology with its principles of friction and lubrication will be delivered. Further, focus will be on the physical and chemical properties of lubricant additives. Particularly friction modifier and anti-wear additives will be discussed, since they share similarities with the organosilane and organosiloxane investigated in this work. Finally, an introduction into organosilane and organosiloxane chemistry (sol-gel processing) and the state of the art of their tribochemical behavior will be provided.

2.1. Tribology and Lubrication

2.1.1. Friction

The term tribology is rather young and is defined as "The science and technology of interacting surfaces in relative motion and of related subjects and practices" in 1966 by Peter Jost [8]. However, the science and principles of friction, wear and lubrication is much older. Already the ancient Egyptians documented already the use of oils as lubricants [9], but the first fundamental "laws" of friction were discovered and stated by Leonardo da Vinci [10].

Friction is defined as the force which resists motion of solids, liquids or fluid layers in contact. The coefficient of friction μ (cof) is the ratio between the friction force F_R and the normal force F_N, see equation 1.

$$\mu = \frac{F_R}{F_N} \tag{1}$$

Where F_R is parallel to the direction of motion and F_N is normal to the contacting areas. For solid counterparts the friction force is proportional to the normal force and not dependent on the contact area. This can be described by the fact that each micro contact acts as a resistance to motion, while the number and size of contacts increase with pressure by elastic deformation [8]. The actual mechanism of friction can roughly be divided into adhesive interactions, plastic deformation, furrowing, as well as elastic hysteresis and damping.

2.1.2. Contact Mechanics

Accurate descriptions of tribological systems require models to predict real contact areas and pressure distributions. These models are important to compare loading conditions for the wide span of complex shapes and materials in tribological applications. For most purposes the Hertzian contact mechanics give an acceptable approximation to predict applied pressure and contact areas depending on elastic deformation [11]. Since only point contacts, such as

ball-ball / ball-disc contacts have been investigated in this work, only these equations will be given in the following.

Due to the high pressures and thus significant elastic deformation in most applications, it is of importance to derive the reduced elastic modulus E' for the contacting materials in the tribosystem:

$$\frac{2}{E'} = \left(\frac{1-\nu_1^2}{E_1} + \frac{1-\nu_2^2}{E_2}\right) \tag{2}$$

where $\nu_x$displays the Poisson's ratio and E_x the Young's modulus of material x, respectively. It should be noted that many textbooks use another version of the combined elastic modulus, which is half the value and often denoted as E*. Also a reduced radius is needed which can be obtained from equation 3:

$$\frac{1}{R} = \frac{1}{R_1} + \frac{1}{R_2} \tag{3}$$

For a concave surface R_1 or R_2 is negative, while for a flat surface R_1 or R_2 is infinite.

The Hertzian circular point contact radius a and maximum contact pressure p_0 is given in equation 4 and 5 respectively.

$$a = \left(\frac{3}{2}\frac{F_N R}{E'}\right)^{1/3} \tag{4}$$

$$p_0 = \left(\frac{1}{\pi}\right)\left(\frac{3F_N E'^2}{2R^2}\right)^{1/3} \tag{5}$$

2.1.3. Lubrication

Lubrication is essential to reduce friction as well as wear and fatigue in most transmission and bearing components. The main task of a lubricant is to provide a protective film between moving surfaces. Based on the continuity equation of Navier-Stokes, Reynolds derived in 1886 an equation, which describes the full fluid lubrication. The Reynolds equation depicts the pressure distribution in a fluid film which forms upon sliding and squeezing of two surfaces in contact with a fluid, see the simplified 2D form in equation 6 [12].

$$\frac{\partial}{\partial x}\left(\frac{h^3}{\eta}\frac{\partial p}{\partial x}\right) + \frac{\partial}{\partial y}\left(\frac{h^3}{\eta}\frac{\partial p}{\partial y}\right) = 12U\frac{dh}{dx} \tag{6}$$

Where h is the fluid film thickness, η the viscosity of the fluid, p the fluid pressure and U the entrainment speed. As noted, this equation is simplified since following assumptions have been made:

- No fluid slip at the solid boundaries
- Negligible variation in pressure through the thickness of the film (z-direction)
- Negligible variation in viscosity and fluid density
- The surfaces move in the x-direction
- Laminar flow
- Surfaces are rigid and do not deform
- Steadily loaded, elliptical contact

Especially the impact of elastic deformation of surfaces and the variation of fluid viscosity by pressure are essential for practical applications. The full fluid film lubrication regime, where elastic deformation of the surfaces and variation of the viscosity by pressure is significant, is called Elastohydrodynamic lubrication (EHD lubrication or EHL).

Figure 1 shows a schematic description of a ball / disc EHD contact with the theoretical Hertzian and the real pressure distributions. As the lubricant enters the contact region of body 1 (ball) and body 2 (disc) it experiences a strong increase in viscosity following the Hertzian pressure distribution, while maintaining a fluid film with thickness h_c. Approaching the outlet in direction of motion a pressure peak occurs which differs from the Hertzian pressure profile. The sharp decrease of pressure is accompanied by a decrease in viscosity as well as elastic deformation, which leads to a constriction and a minimum in lubricating film thickness h_0.

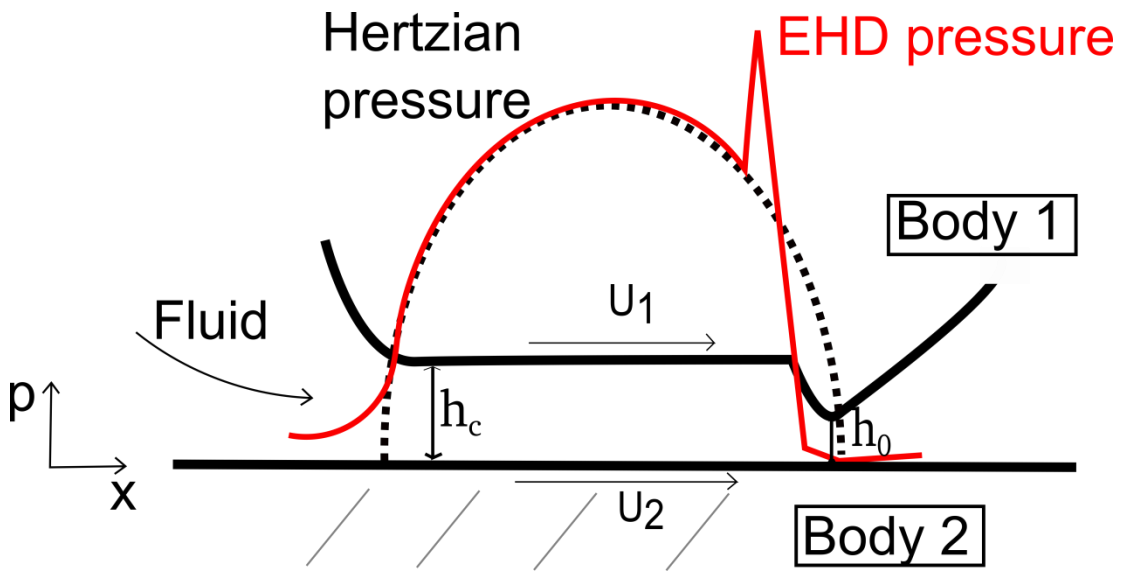

Figure 1: Schematic description of EHD contact shape and pressure distributions.

2.1.4. Fluid Properties and Solutions of Elastohydrodynamic lubrication (EHL)

In the following an overview of fluid properties and solutions to describe the EHL will be given.

The dynamic viscosity η of a fluid is given by:

$$\eta = \frac{\tau}{\dot{\gamma}} \tag{7}$$

where τ is the shear stress and $\dot{\gamma}$ represents the shear rate. In some applications the kinematic viscosity η_{kin} is also of interest and is in relation to the dynamic viscosity by:

$$\eta_{kin} = \frac{\eta}{\rho} \tag{8}$$

with the fluid density ρ. It is possible to give an easy approximate for the shear stress and shear rate in EHL contacts. Having a lubricant film with a thickness of h_c and a sliding speed U_s between the surfaces, it is possible to approximate the shear rate by:

$$\dot{\gamma} = \frac{U_s}{h_c} \tag{9}$$

If the friction force F_R is measured by a tribological test, then the mean shear stress $\bar{\tau}$ on the fluid can be approximated by:

$$\bar{\tau} = \frac{F_R}{\pi a^2} \tag{10}$$

Where πa^2 is the area of contact for a circular ball on flat.

As indicated in chapter 2.1.3 the change of viscosity by pressure is necessary to achieve a lubricating film which can maintain high pressures in EHL. A model to predict the viscosity change with pressure yields the Barus equation:

$$\eta(p) = \eta_0 e^{\alpha p} \tag{11}$$

With η_0 as the viscosity at standard atmosphere and the pressure viscosity coefficient α. Since the pressure viscosity coefficient shows dependencies on temperature and high pressures, in practice an "effective" α is estimated experimentally and then used for calculations to predict lubricating film thicknesses.

Coming to the prediction of lubricant film thicknesses in EHL contacts, two important and quite different speeds can be present. The first is the mean of the rolling speeds of two

surfaces. It is also called entrainment speed *U*, since this is the speed with which the lubricant is "entrained" into the contact:

$$U = \frac{U_1 + U_2}{2} \tag{12}$$

The entrainment speed determines the lubricating film thickness and is also present in the Reynold's equation 6. The second speed is the sliding speed U_s, which is the speed of the two surfaces relative to each other:

$$U_s = |U_1 - U_2| \tag{13}$$

The sliding speed has a large impact on the friction and heat generation, but only little on the film thickness. The slide-roll-ratio SRR is generally used to describe the speed distribution in an EHL contact, which is the ratio of the two presented speeds:

$$SRR = \frac{|U_1 - U_2|}{(U_1 + U_2)/2} \tag{14}$$

The SRR has a value of 0 in pure rolling conditions, so when $U_1 = U_2$ and value of 2 in pure sliding conditions, so when U_1, or U_2 is 0.

Due to the lack of applicable analytical solutions for the EHL problem, regression-fitted equations have been developed by Hamrock and Dowson, which predict the lubricating film thickness in adequate conditions [12]. The equations employ four non-dimensional parameters $\overline{U}$, G, W and k which are:

Speed parameter: $\overline{U} = \frac{U\eta_0}{E'R_x}$ (15)

Material parameter: $G = \alpha E'$ (16)

Load parameter: $W = \frac{F_N}{E'R_x^2}$ (17)

and Ellipticity parameter: $k = (\frac{R_y}{R_x})^{2/\pi}$, where k = 1 with ball on plate geometry, further with η_0 as the dynamic viscosity of the lubricant at atmospheric pressure plus R_x as the reduced radius in the entrainment direction.

Together with the presented parameter the minimal film thickness in an EHL contact can be calculated by [12]:

$$h_0 = R_x * 3.63\overline{U}^{0.68} G^{0.49} W^{-0.073} (1 - e^{-0.68k}) \quad (18)$$

and the central film thickness can be obtained by:

$$h_c = R_x * 2.69\overline{U}^{0.67} G^{0.53} W^{-0.067} (1 - 0.61e^{-0.73k}) \quad (19)$$

From equations 18 and 19 it is evident that the film thickness depends quite strongly on viscosity and speed.

All basics of contact mechanics and lubrication theory have been given to assess the most important parameter to determine the conditions in lubricated contacts. An intuitive way to describe liquid lubricated tribological conditions can be achieved with the help of Stribeck curves [13]. Stribeck curves provide an easy delineation of different lubrication regimes by the definition that the coefficient of friction is a function of the ratio:

$$\frac{\eta U}{F_N} \quad (20)$$

However, in general cases the viscosity and load is set constant and only the entrainment speed is changed in order to investigate the frictional behavior of the lubricant and tribo-couple on changes of speed.

An advanced way to describe Stribeck curves is by including lubricant film thickness parameter as well as roughness parameter with the frictional behavior. This is done by introducing a film parameter known as the lambda ratio λ, which is defined as:

$$\lambda = \frac{h_0}{\sqrt{R_{q1}^2 + R_{q2}^2}} \quad (21)$$

with R_{qX} as root mean square roughness for each contacting surface and the minimal lubricant film thickness. Figure 2 presents a schematic example of a Stribeck curve with indicated lubrication regimes and illustrative descriptions.

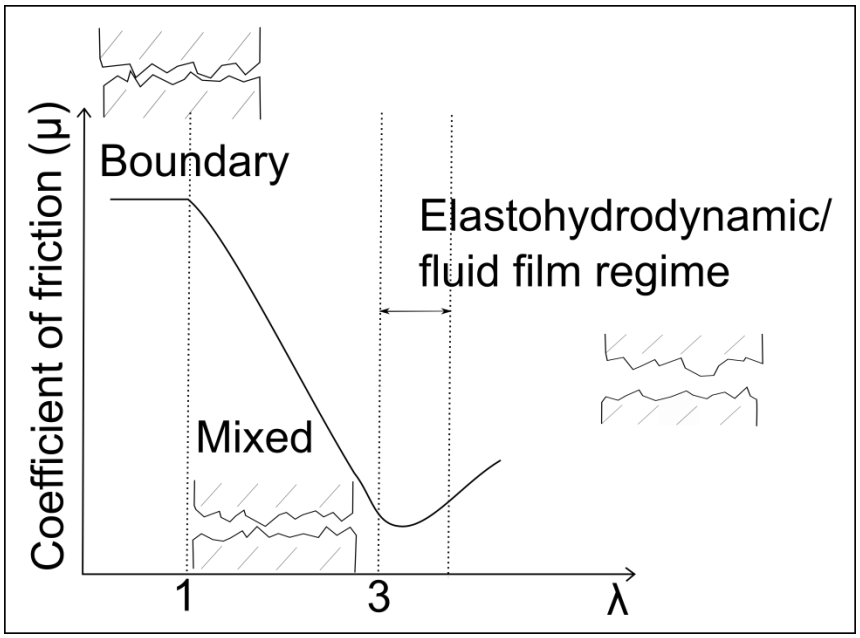

Figure 2: Schematic Stribeck curve with illustrative lubrication regimes.

The given image clearly separates the lubrication regimes by their frictional behavior, which are further described in the following.

For lambda values below unity, the lubricant film thickness is in the range below the surface roughness and therefore no pronounced hydrodynamic effects of the lubricant are visible on the frictional behavior. This regime is called boundary regime, as the surfaces are in contact. Most damage to the solid tribo-couples occurs in this regime, as the contacting asperities have to endure the applied load. The friction in this regime is mainly dependent on the solid surfaces or on special lubricating additives, like anti friction or anti wear additives, which will be further elaborated in the next chapters.

Lambda values between 1-3 mark the mixed lubrication regime, which describes the transition from the boundary to the fluid film regime. As visualized in Figure 2 most of the load is supported by a pressurized fluid lubricant film, while still some asperities are in contact.

Higher lambda values above >3 describe full fluid film lubrication where the load is fully supported by the lubricating film and all frictional contributions are governed by the physical properties of the lubricant. Generally, it is possible to even divide the fluid film regime into elastohydrodynamic lubrication, with $\lambda \approx$ 3-10 and hydrodynamic lubrication $\lambda > 10$, but no experiments have been performed in this work with $\lambda > 10$.

2.2. Friction modifier

As already mentioned in the section about boundary lubrication, special molecules or additives are added to lubricant mixtures to reduce friction in boundary lubricating conditions. Generally these additives have in common, that they produce boundary films with low shear strength on the surfaces. This way the contacting asperities are separated and for example, metal-metal contact is prevented.

The goal of investigations on friction modifier is generally to understand the tribochemical processes of the formation and the physicochemical properties of boundary films, which are formed by friction modifier additives [14]. Figure 3 presents a timeline describing the development of different oil additive classes and friction modifier. The first additive for engine oil applications was introduced in 1918 and has been a fatty acid. Back then it was found that fatty acids, when dissolved in mineral oils are able to reduce friction and wear, the ascribed effect was called “oiliness” [5].

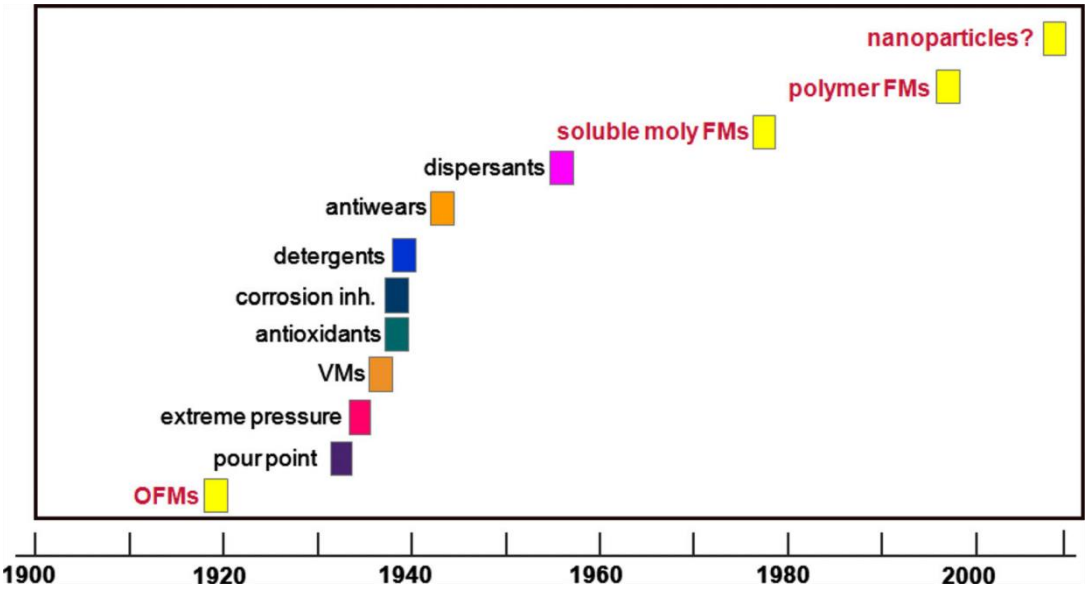

Figure 3:Timeline for development of lubricant additives including friction modifiers, also marked with yellow bars [5]. Y-axis is not defined in the reference but may classify the impact on lubricity.

Nowadays the most used organic friction modifiers (OFM) are oleylamide or glyceryl monoleate. These well-defined molecular structures exhibit polar head groups, which supply attraction to metallic surfaces, and long alkyl tail chains. By the adsorption on metallic surfaces, boundary films are formed and it has been shown that longer alkyl chains provide lower friction, besides this finding, it was shown that a minimum alkyl chain length is necessary to reduce friction [15]. However, the long alkyl tail can only support load when stable adsorption occurs and close packed layers are formed. Different organic polar groups have been investigated, such as amines, alcohols, acids, etc. and their adhesion and stability

depend not only on the substrate but also on temperature and even the possibility to chemically react. Carboxylic acids for example are able to form insoluble metal salts and thus increase their adhesion by chemical reactions with the metal atoms on the surface [14]. However, these salts can also lead to stronger corrosion for some metals, therefore extensive additive design is necessary for each individual tribological system [16].Unfortunately most organic friction modifier boundary layers break down at specific temperatures, as the rate of desorption increases with increasing temperatures.

Starting in the 1970s political and environmental crises and conflicts focused attention on fuel economy and thus also on friction reduction. During this time much effort was made to synthesize an oil-soluble lubricant additive able to keep colloidal MoS_2 stabilized. The result is still nowadays one of the most used friction modifier and known as molybdenum dialkyldithiocarbamate (MoDTC) [5]. The compound reacts under tribological stress and forms MoS_2 having a two dimensional crystal structure which exhibits very low shear strength and thus is able to reduce significantly the friction when present in a tribological contact [17, 18]. Again in the 2000s discussions on CO_2 emissions motivate investigations on new types of friction modifier additives. By the introduction and investigations on surface active functions on polymeric viscosity improver, the path for polymeric friction modifier was enabled [19]. In addition intensive investigations have been carried out on ionic liquids and on nanoparticles. However, in the case of ionic liquids no commercial breakthrough was achieved, mainly due to required optimization regarding corrosion and friction reduction aspects [4]. Nanoparticles show, besides molybdenum compounds, the best performance on friction reduction [5]. The vast range of materials, which have already been investigated in terms of their tribological performances is not only difficult to overview, but also the transfer from one material to another is hardly manageable, since sizes, structures and also used base oils depend strongly on their effectiveness [20, 21]. Despite their striking positive performances in terms of wear and friction, nanoparticles as oil additives are still not ready for industrial use, due to the weak stability of the dispersions. The prevention of agglomeration and precipitation of nanoparticles in severe tribological conditions is not yet achieved by simultaneously maintaining all functions of a lubricant mixture.

2.3. Extreme pressure (EP) and anti-wear (AW) additives

Besides friction modifier additives also anti-wear and extreme pressure additives are surface active additive classes, which act in boundary and mixed lubrication regime conditions. However, these additives are not developed and known for providing low friction, but for their formation of adhesive, protective reaction films, so called tribofilms, on the surfaces

[22]. Unlike adsorbed polar friction modifier species, which generally exhibit poor high temperature or high pressure properties, these reaction films are generally chemically bonded to the metal surface and exhibit strong adhesion [23]. The formed reaction layers are sacrificial buffer layers to prevent metal-metal contact and thus prevent abrasive wear or even micro welding processes. Extreme pressure (EP) and anti-wear (AW) additives behave quite differently, as EP additives generally even increase wear, while AW additives are designed to repress volume loss.

Sulfur carriers are the oldest and still most common EP additives and have been added in early days especially for metal working fluids. Most EP additives are organic sulfur compounds with the general formula of R-S_x-R [23]. Where R denotes organic groups, such as alkyl, phenyl, etc., which impact the reactivity and solubility of such compounds [24]. The other main factor for the reactivity and performance is the number of sulfur atoms X, which highly impacts the reactivity and concentration of active sulfur. The general mechanism of EP additives is degradation of these compounds at elevated temperatures and severe stress, which thereupon leads to chemical reactions between the sulfur atoms and the metal surfaces. After chemisorption of the sulfur atoms on the metal generally also the S-C bonds break, which then results in the formation of surface layers of for example FeS, in case of iron alloys [25]. The inorganic sulfur layers are designed for a directed wearing procedure, which suppress micro welding processes and thus prevents total failure of components. It is thus of importance to choose suitable EP compounds for each individual conditions, to not promote abrasive wear, but only prevent micro welding.

Contrary to EP additives anti-wear additives are designed to restrain wear of the tribo-couples, by generally forming sacrificial tribofilms. Most common AW additives are phosphorus compounds or compounds containing sulfur and phosphorus. These compounds are generally based on neutral or acidic phosphoric acid ester derivatives, which exhibit organic groups to control their reactivity and solubility. Again, the thermal stability increases with increasing chain length of alkyl groups [23]. From all anti-wear additives zinc dithiophosphate (ZDDP) is not only the most used but also the most investigated oil additive [26]. The compound serves besides anti-wear also extreme pressure and anti-corrosive performances. The good performances are achieved by the around 100 nm thick, strongly adhesive and densely packed pad like reaction film, see Figure 4 for schematic illustration.

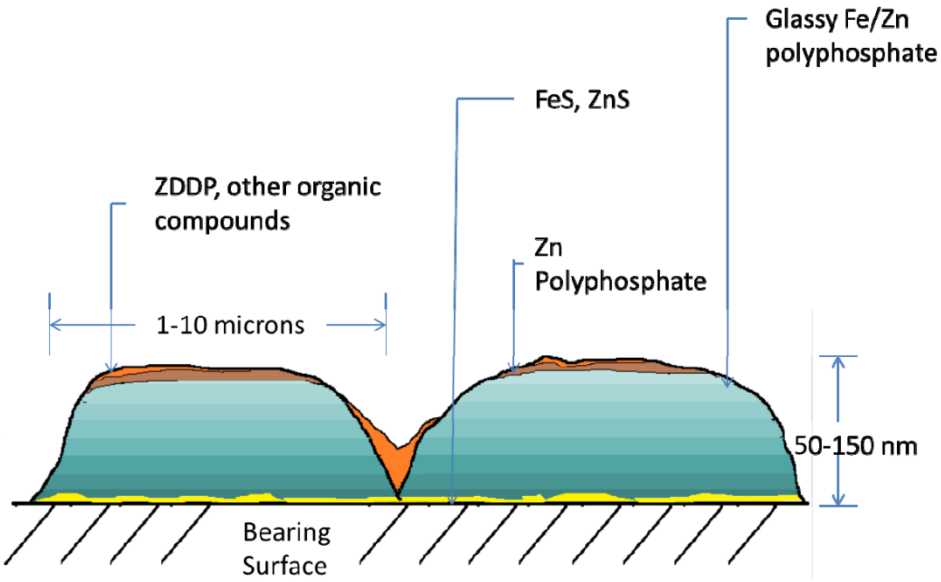

Figure 4: Schematic structure of surface films formed from ZDDP [27].

Depending on the cross-linking state from polyphosphate to glassy film, the hardness and stiffness increases, however, the mixture of this structure, together with the ability to form different phosphates under pressure is stated as the key for the good anti-wear behavior [28-30]. The mechanical stability fits the operating conditions, meaning it is hard and stiff enough to withstand the high forces, but not too hard to damage the metallic surface during a wearing procedure [28]. ZDDP degrades over the formation of polyphosphates into layers of zinc phosphate glass either thermally above 120 °C or by rubbing already at much lower temperatures starting at 40 °C [26, 31, 32]. Although, the additive is in use since the 1950's due to its complex mechanisms the major contributions and differences between the thermal film formation and the deposition under tribological stress have been investigated rather recently. It was shown, that the film formation does not necessarily require solid-solid rubbing contact, but is also driven by applied shear forces [33]. Nevertheless, rubbing does promote the chemical reactions leading to film formation due to catalytic activity of "fresh" iron as well as frictional heat [34]. As mentioned earlier, the films provide negative effects in terms of friction performance. Increased roughness due to the formation of tribofilms leads to a retarded transition of the lubrication regimes and thus to larger speed ranges for the boundary and mixed regime, see equation 21 and Figure 2. However, investigations show that even comparable smooth reaction films exhibit high friction and retarded transitions of mixed and boundary regimes. Therefore, also starvation and inlet blocking of the tribological contact by reaction film material, as well as slip at the lubricant/ZDDP reaction film boundary was proposed [22, 35]. It will later be discussed, that a precise explanation for variations on friction by tribofilms is difficult, due to many different effects which act simultaneously.

2.4. Sol-Gel processing and ceramization

2.4.1. Sol-Gel processing

Sol-gel processing is a wet chemical procedure to create oxide or hybrid organic inorganic materials by progressive polycondensation reactions [36]. Advantage of this processing route is the use of nanoscale tailored building blocks to create either nanoparticles or macroscopic networks in form of coatings, fibers or monolithic objects. First steps in sol-gel science have become available by the first synthesis of silicon alkoxides from $SiCl_4$ and alcohol by Ebelman in 1846 [37]. However, it nearly took a century until the Schott glass company developed and investigated the sol-gel process to use it for an industrial process for coatings [38, 39]. Nowadays the sol-gel processing is used for a broad variety of applications which include all types of functional coatings, such as scratch-resistant, barrier properties, etc., catalysts or catalyst supports, ceramic fibers, optical and insulating materials or biomaterials [40-44]. The broad range of applications is achieved from the multiplicity of properties, which can be introduced into the materials by the tailoring of the building blocks.

The used chemical compounds in this work can be assigned to the group of organosilanes and organosiloxanes, which means that the silicon compounds contain carbon-silicon bonds. Furthermore, all used silicon compounds belong to the category of metal alkoxides or more precise in this case: silicon alkoxides. The name refers to at least one alcohol group bonded to the silicon atom. Silicon alkoxides are popular precursors (starting compounds) for the sol-gel process, as they form colloidal suspensions and react readily with water. A colloid is defined as a suspension in which the dispersed phase is so small, around 1 – 1000 nm, that gravitational forces are negligible and interactions are dominated by short-range forces, such as van der Waals attraction and surface charges [45]. The term sol defines a colloidal suspension of solid particles, whereas an emulsion is a suspension of two liquid droplets in another liquid, both types of colloids are used to generate polymers or particles based on the starting precursors and cross-linking conditions. If the starting precursor can make more than two bonds, then there is the possibility to form macroscopic molecules, whose network extends throughout the solution, this substance is referred as gel [45]. A gel is thus a continuous porous solid network with elastic or viscoelastic properties. Figure 5 illustrates different possible processing routes and products which can be obtained from sol-gel systems.

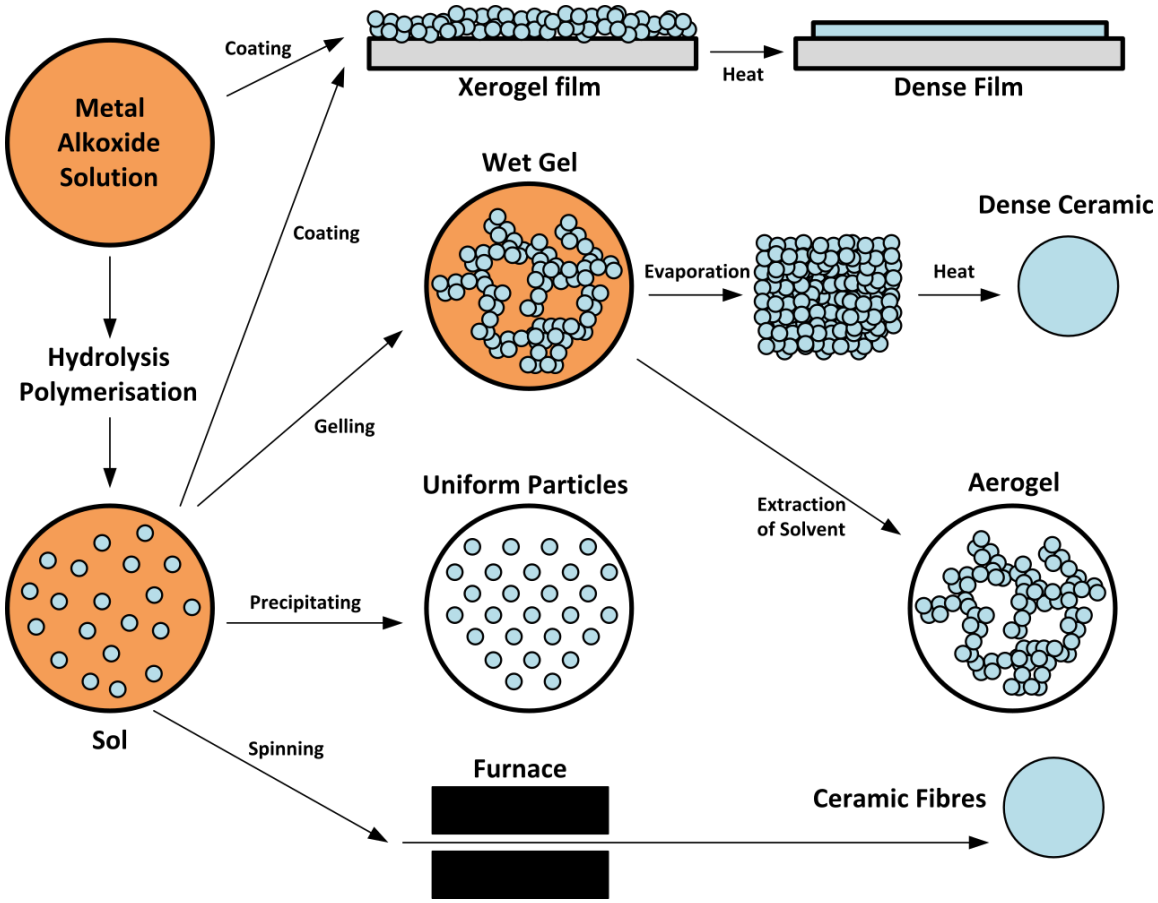

Figure 5: Schematic representation of possible processing routes of the sol-gel approach [46].

The whole sol-gel process is based on mainly two chemical reactions, first a hydrolysis reaction between the alcohol group with water following a subsequent condensation reaction between either an alcohol with a hydroxy group or between two hydroxy groups. Figure 6 shows possible hydrolysis and condensation reactions. The overall goal of the sol-gel process is the cross-linking by the formation of Si-O-Si bonds, also called siloxane bonds.

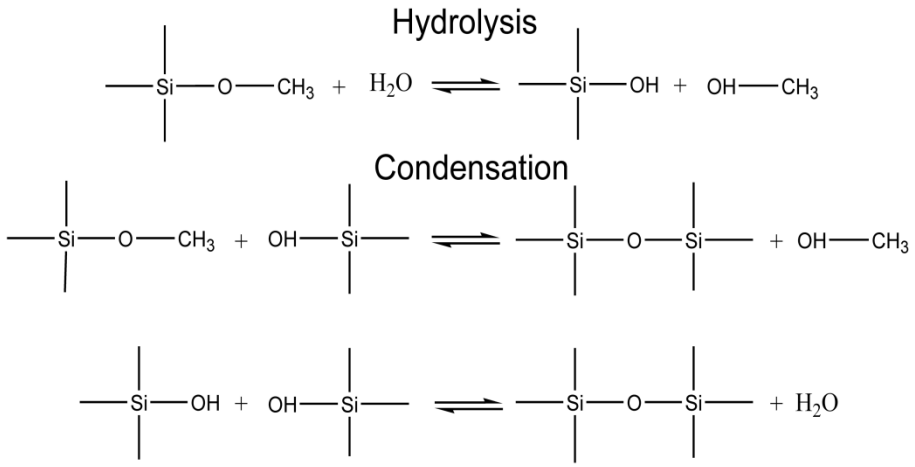

Figure 6: Schematic hydrolysis and condensation reactions of silicon alkoxides.

Despite the simple description, the overall process is very complex, since the hydrolysis and condensation reactions depend on many parameters, where the most important are discussed in the following.

Since most alkoxysilanes are not miscible with water, alcohols are used as solvents to achieve homogenous mixtures. As indicated in Figure 6 the hydrolysis, as well as condensation reactions are reversible, which means that the alcohols in the mixtures influence the cross-linking behavior. The reesterification is the reversible reaction of a condensation reaction with an alcohol group. If the alkoxy groups attached to the used precursors differ from the alcohols in the solution, different colloids will be achieved, which then affects the properties of the resulting gel or even glass/ceramic. Another aspect is the steric hindrance of bulky phenols or long chain alcohols, which significantly decrease the reactivity and thus the whole cross-linking procedure [47]. It should be mentioned, that already the change from methoxy to ethoxy groups is quite significant in terms of the hydrolysis reaction rates. Depending on the organic group of the silicon alkoxide more polar or nonpolar solvents can be used, however, the dipole moment of a solvent affects and determines the length over which the charge on one species can be "felt" by surrounding species [45].

Another important parameter is the water content, which is often given as H_2O to alkoxide ratio *r* and promotes the hydrolysis rate. To fully hydrolyse a tetravalent alkoxide r values of at least 4 are necessary, while a ratio of 2 is enough for the full conversion into an oxide. Higher values will increase the hydrolysis reaction rates and also affect the relative rate of alcohol- or water-producing condensation reactions in favor to the water-producing reactions.

Without catalysts the reaction rates and thus time to gelation would be very slow and no industrial production could be thinkable. Hydrolysis and condensation reaction rates are most influenced by strength and concentration of an acid or base and thus the pH value of the sol. This is due to different reaction mechanisms for acidic or basic conditions. In acidic conditions positive charge carrier H^+ will try to find electrons and therefore attack the oxygen atom of the Si-OR group. Thereby the electronic cloud from the silicon to oxygen will be shifted and silicon becomes more electrophilic and thus more reactive to the attack of water in hydrolysis or of silanols in condensation reactions. Another influence in this context is the change of reactivity from unreacted alkoxides ($Si\text{-}(OR)_4$) over partially hydrolyzed ($Si(OR)_{4-x}(OH)_x$) to condensed species (Si-O-Si). As more hydrolysis and condensation occurs, the pH of the sol will change and silanol groups become more acidic when more Si-O-Si bonds are present.

In basic conditions hydroxyl ions (OH^-) attack directly the silicon atom in hydrolysis reactions, which leads to a 5-coordinated intermediate of silicon with a following dissociation of the

alcohol group. The most accepted mechanism for the condensation reaction is a nucleophilic attack of a deprotonated silanol on a neutral silicate species [45]. Depending on the pH value, different reaction rates for hydrolysis and condensation occur and are depicted Figure 7.

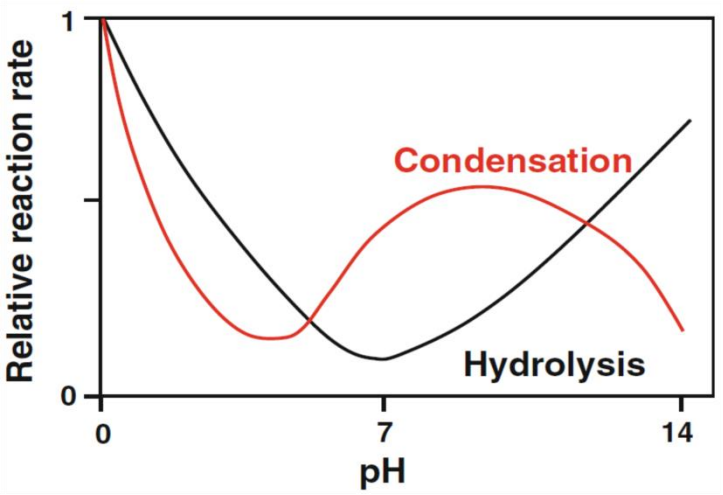

Figure 7: Relative hydrolysis and condensation rates as a function of pH for silicon alkoxides [48].

Below and above a pH value of 7 the concentration of the catalysts increase, which also increases the hydrolysis reaction rates. As stated before, the electron density of silicon decreases from alkoxide over hydrolyzed to condensed species. Therefore, in acid catalyzed systems the hydrolysis is faster than condensation. In case of the condensation reaction rates a minimum at low pH values is seen around the point of zero charge of the silica surface, which is pH 1.8-4.2 depending on extent of condensation of the silica species [48]. Due to net neutrality between solution and species no attraction is present and reaction rate is minimized. Highest condensation rates are observed for pH values of around 10. Above the reaction rates for hydrolysis are higher and are in competition with condensation reactions due to cleavage of siloxane bonds.

Also the organic fraction on the silicon affects the rates of hydrolysis and condensation reactions. Generally the introduction of Si-C bonds leads to a higher electron density at the silicon atom compared to a Si-O bond. Therefore, the reaction rates are higher in acidic conditions for organically modified silicon alkoxides, however steric hindrance again decreases reaction rates when bulky groups are attached on silicon, especially in basic conditions [49].

Finally the whole colloid, polymer or even gel structure depends on the conditions and reaction rates of hydrolysis versus condensation. In acidic conditions rather linear or weakly branched silica species are preferentially formed. In basic conditions denser agglomerated clusters condense, see Figure 8 for a schematic representation. When particles reach a critical

size Ostwald ripening sets in and no gel formation but precipitation occurs. In total the physical properties such as stiffness, but also porosity of the final gel is strongly dependent on the chosen conditions of a sol-gel process.

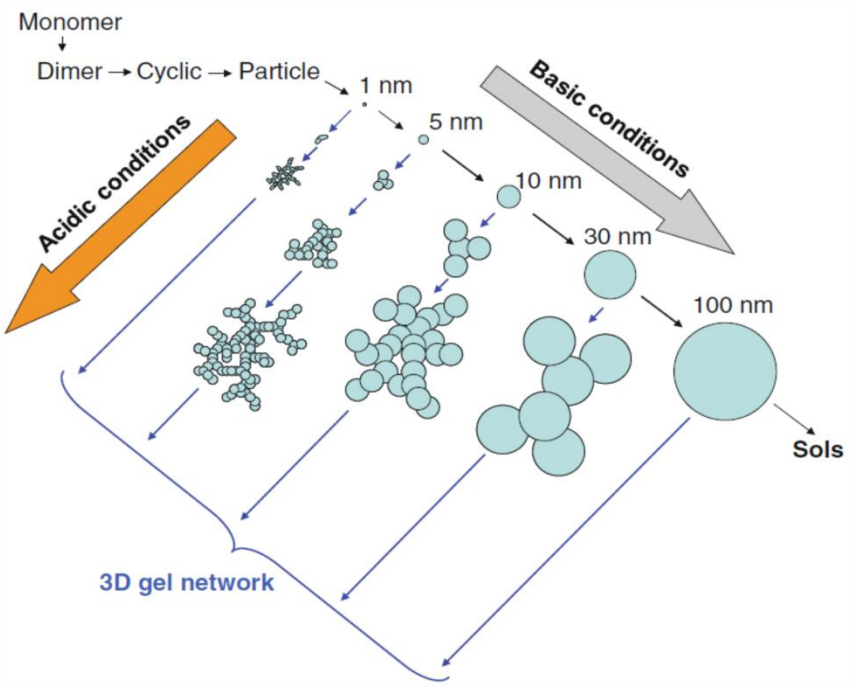

Figure 8: Schematic evolution of colloidal and gel structures for different sol conditions [50].

2.4.2. Ceramization

Sintering is the classical process to densify and produce ceramic work pieces from powder compacted green bodies and sol-gel derived materials. The sintering process is driven by minimization of the surface energy and thus reduction of porosity. However, the sintering process for organically modified silicon polymer, such as xerogels or gel coatings differs quite strongly compared to the powder route. The ceramization mechanisms to obtain ceramics from polymeric materials (polymer derived ceramics, PDC) were deeply investigated by Chantrell and Popper in the 1960s and gained again a lot attraction when Yajima presented a spinning process to produce silicon carbide (SiC) fibers from organosilicon polymers [51, 52].

The polymer-to-ceramic transformation consists generally of two steps, the cross-linking procedure at temperatures of 100 to 400 °C and the ceramization step from 600 to 1400 °C [53]. Cross-linking involves the solidification of the mostly liquid precursors into near end-shape thermosets, which can be processed by the sol-gel route or by reactive organic groups [54]. A well networked green body is crucial to minimize loss of low molecular weight components and defragmentation processes, which would decrease the ceramic yield and could lead to cracking or porosity. The ceramization process of polysiloxane gels leads to

silicon oxycarbide (SiOC) glasses via the evolution of hydrocarbons, like CH_4 and hydrogen [55]. The defragmentation of low molecular weight organic fractions and silane species leads to shrinkage and porosity of the material. However, together with defragmentation, also redistribution reactions occur, which involve homolytic cleavages between Si-O, Si-C or Si-H bonds and guarantee further densification. In case of hybrid silica thin film gels, defragmentation and ceramization start at up to 150 to 200 °C lower temperatures than for bulk materials, so already at 250 °C and 500 °C, respectively [56].

Besides the incorporation of carbon into the amorphous SiOC network, also residual carbon in form of graphene like free carbon can form, depending on the starting organic fractions and annealing temperature [55].

2.5. Silicon compounds and thin films in tribology and lubrication

In the following the state of the art about chemical reactions, physical properties and influences on lubrication of silane and organosiloxane compounds in tribologically stressed contacts will be presented. Polysiloxane, such as silicones, are often denoted as inorganic polymer due to their siloxane backbone, which gives them special properties. Compared to C-C bonds Si-O bonds are more than 30 % stronger additionally the Si-O-Si angles from 140° to 180° provide a high chain flexibility [54, 57]. This results in a higher oxidative and thermal stability, but also small viscosity-temperature coefficients, which make them high performance candidates as bulk lubricants [54, 58]. Their overall lubricating abilities and properties like pressure viscosity coefficient and temporary shear thinning are highly dependent on their molecular structure, especially on the hydrocarbon branches [59, 60]. Nevertheless, the comparable high prices restricts their use to high performance lubricants [23].

For this work their chemical degradation, in combination with the formation of surface films is of central importance. This aspect was discovered and has been investigated in the 1960s. Mixtures of polysiloxane in hydrocarbon oils were tested and it was found that anti-friction or anti-wear behavior is mainly found due to the degradation of liquid polysiloxanes into surface films. The effect of anti-friction and anti-wear increases with decreasing oxidative stability of the tested polysiloxane, depending on their organic branches, but also on the hydrocarbon oil [61]. Also the oxygen feed affects the stability of the polyorganosiloxane and the higher the oxygen amount in the atmosphere, the lower is the stability. The film formation was further investigated by Tabor and Willis who used a polydimethylsiloxane (PDMS) with stearic acid on copper tribo-couples. They observed that the low friction performance of stearic acid is provided at much higher temperatures in the polysiloxane mixture than in hexadecane. The higher stability is ascribed to a boundary film of copper stearate in a gel-like polysiloxane

matrix, which forms under rubbing, already at 90 °C and thus at lower temperatures than thermal oxidation would occur [62, 63]. In addition, it was shown by electrical contact resistance measurements, that these gel-like films increased in thickness with increasing temperatures from 90 °C to 150 °C, but break down at contact pressures of around 1 GPa. FTIR analysis demonstrated cross-linking of the polymers by bond cleavage of Si-C bonds and predicted the formation of formaldehyde and formic acid. Furthermore the residual Si-OH groups condense to a cross-linked polymeric surface film, see Figure 9 for illustration [62]. As stated earlier, the breaking of Si-C bonds appears at lower temperatures in thin films and on metal oxide surfaces, which was also observed in this work, without any tribological stress. Earlier Willis could show by thermal annealing that the formation of such polysiloxane films depends also on the metal oxide, as no films could be observed on gold or platinum.

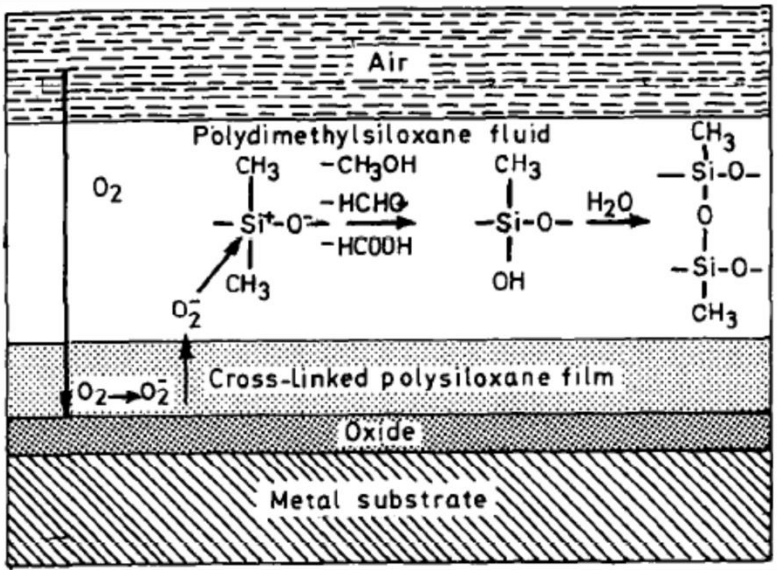

Figure 9: Illustrating mechanism of thermal decomposition of polydimethylsiloxane [63].

Jemmett summarized the findings about the structure of the siloxane films tribofilms in a review. However, due to limited characterization methods in this time, no formation of silicate tribofilms could be proven and clear picture of the microstructure stayed unclear [64].

A first attempt to elaborate the microstructure of these films was done around 30 years later by Kuribayashi and Yamamoto, who used a lubricant dispersion of magnetite particles in silicone oil (PDMS) and investigated these particles after rubbing tests by GC-AES and XPS [65]. The results did not show a silicate formation on the iron oxide particles, but could confirm the elimination of methyl-groups and cross-linking of the silicone fluid on the oxide surfaces.

The specific use of organosilanes as film forming oil additives was tested and film structures were investigated by Yu and Bancroft et.al. [6], who tested a silane compound in combination with Ca detergents and B- and N- containing dispersants. Unfortunately, no information about the molecular structure of the tested precursor is given, however, the patent of the co-author highlights the results from tetraethoxysilane and octyltriethoxysilane [66]. Comparative experiments with state of the art anti-wear additives could show that the silane additives can show superior behavior in terms of anti-wear. Simultaneously they do not show significant effects on friction in reciprocating sliding tests. The anti-wear performance is attributed to silicon and oxygen containing tribofilms, which have further been investigated by X-ray photoelectron spectroscopy (XPS) and X-ray absorption near edge structure spectroscopy (XANES). The XANES results show, that the silane species reacts already in the oil blend via hydrolysis and condensation reactions into dispersed SiO_2 particles. The obtained tribofilms consist of a $CaSiO_3$ phase, which is described as thin and hard ("concrete") coating. Although these results state the formation of a silicate film for the first time, the presence of detergents and dispersants is claimed as necessary for film deposition. In addition no information of a gel-like film is given, which is supposed to be the primary stage towards the formation of a silicate film, when organosilanes are used. Nevertheless, the presence of detergents and dispersants in the oil fits with the background about sol-gel processing, since basic detergents catalyze the formation of silicate particles.

Also just recently silicon containing ionic liquids are in development. They show outstanding anti-wear and low friction behavior, when used as lubricant additive [67, 68]. The ionic liquid additive is a mixture of trimethylsilylakylsulfonate and a tetraalkylphosphonium. Again the good tribological performance is attributed to the formation of a silicon and oxygen rich reaction film. Unfortunately, no detailed information about film structure is given. However, the generated tribofilms are tribochemically formed without any influence of further additives and they show pad like adhesive films, similar to other anti-wear additives.

As mentioned, research on silane or silicate lubricant additives is limited, but tribological studies on silica and sol-gel siloxane films may give additional information about their wearing and tribological performance. Dense 1 µm thick silica films, produced by a sol-gel route with tetraethylorthosilicate and annealed at 500 °C, show in dry pin on disc tests no gain in anti-wear behavior compared to the AISI304-L stainless steel substrate. The silica film was worn away quite easily and no significant contribution on friction was present [69]. Hanetho *et al.* prepared sol-gel derived films with 3-(Aminopropyl)triethoxysilane under different water and pH conditions and tested them in rubbing experiments [70]. They observed, that coatings, which were deposited from acidic conditions had better abrasion

resistance and also delamination occurred later. Coatings derived with low water content and neutral conditions are disrupted very fast, but showed a smearing and thus lubricating ability, which could protect the steel surface for a certain time. In total, the organosilane derived sol-gel films could show friction reducing abilities, as long as the coatings were not delaminated.

Silicon nitride (Si_3N_4) and silicon carbide (SiC) are popular ceramic materials in tribological applications, due to the low weight, high hardness and thermal stability, compared to steel alloys. The important feature of this ceramics for this work is their tribochemical degradation. Generally these ceramics show after a run in procedure low friction performance, which is not only due to polishing effects, but also due to self-lubricating aspects. It has been shown that these ceramics form silica layers on the surface upon rubbing in moist atmosphere [71, 72]. The lubricating feature is referred to hydroxylated silicon species, which act as boundary lubricant and their formation can be amplified by the use of alcohols, which promote reesterification reactions with the silica surface [73].

3. Experimental

The following chapter describes the properties and structures of the used chemicals as well as the experimental methods used to investigate the tribological behavior and the obtained surface modifications.

3.1. Lubricants and additives

3.1.1. Base oil

Base oils are classified by the American Petroleum Institute and the Association Technique de l'Industrie Européenne des Lubrifiants by their chemical composition and properties [23]. Base oils are divided in 5 groups, where mineral base oils comprise the groups I to III. Mineral base oils are derived from crude oil by fractional distillation and contain a variety of hydrocarbons, as well as organosulfur and organonitrogen species. The classification into these groups depends on the content of saturates, sulfur and the viscosity index. The viscosity index describes the dependence of kinematic viscosity on temperature with the relation that the lower the index is, the stronger is the dependence on temperature. With extensively processing of the oils, the group number increase as the content of saturates, as well as cyclic paraffins, aromatics and sulfur decreases. The consequences of extensively processing are oil products, which contains high contents of saturates, leading to a high viscosity index. Group IV and V are classified as synthetic base oils, meaning that these oils are produced mainly from ethylene as source. Group IV denotes to polyalphaolefins, which are fully saturated aliphatic or branched paraffinic hydrocarbons, while Group V comprises all other synthetic base oils like polybutenes, polyalkylene glycols or silicones.

In this work a group III base oil "Nexbase® 3050" by Neste is used. The base oil meets the standards having sulfur content of below 0.03 %, more than 90 % of the hydrocarbons are saturated and the viscosity index is above 120. The kinematic viscosity at 40 and 100 °C is 25 mm^2/s and 5 mm^2/s, respectively and the density is 0.83 g/cm^3 at 15 °C [74]. The water content was characterized by Karl-Fischer-titration and lies below 0.01 wt.%.

3.1.2. Organosilane/-siloxane blends and sol-gel coatings

A Vinyltrimethoxysilane [VTMS] and a condensed oligomeric ester of VTMS have been investigated in this work. Figure 10 shows schematic chemical structures of the precursors. The oligomeric vinylmethoxysiloxane is commercially available as "Dynasylan® 6490" and consists of mainly 3 to 7 monomeric units. All base oil mixtures were prepared by 2 wt.% addition of the organosilicon precursor. The mixtures are colorless liquids and are fully

soluble with each other. The amount of organosilane/-siloxane was prepared to have near application conditions.

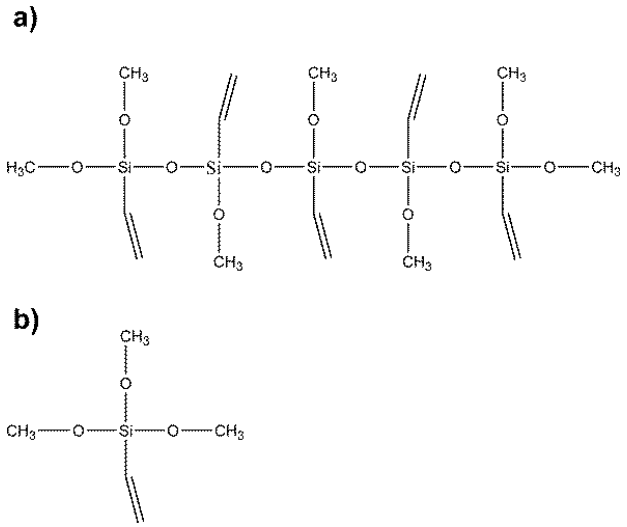

Figure 10: Schematic molecular structure of a) oligomeric vinylmethoxysiloxane „Dynasylan® 6490" and b) vinyltrimethoxysilane.

Besides testing of the organosilicon mixtures as lubricants, also sol-gel coatings were fabricated. Therefore sols with molar ratios of 1 : 19 : 31 of Dynasylan® 6490 : ethanol : water were prepared. Whereas, the ratio of H_2O to alkoxide is 4.4 and the ratio of ethanol to alkoxide is 2.7. After mixing of the sols, the pH value of these sols was adjusted with HCl to a value of around 2 and then kept for around 30 min to promote hydrolysis reactions of the organosilicon species. Afterwards the pH value was adjusted with an ammonia solution to 3.5-4 and stored in a sealed glass container at 40 °C. The sols have been aged for different duration prior deposition. Coatings have been deposited on standard 100Cr6 steel test specimen of a Mini Traction Machine, see next subchapter for more information about the Mini Traction Machine. The deposition followed a static spin coating procedure, where the polished ring of the steel disc was first fully covered with the sol and then the substrate was spun at 2500 rotations per minute (RPM) with an acceleration of 250 RPM/s for 45 seconds. Afterwards a drying step was performed for 10 seconds with a speed of 500 RPM. The deposited sols were once tested as deposited, so without a curing step after deposition and also in cured conditions. Curing was proceeded at 100 °C for 4 days before testing and stored in normal atmosphere.

3.2. Tribological and rheological tests

3.2.1. Ball on disc friction measurements

In order to investigate the influences of the lubricants on friction, ball on disc tests have been performed with a Mini Traction Machine (MTM) by PCS Instruments. The MTM is additionally equipped with a 3D spacer layer imaging (3D-SLIM) set-up, which uses optical interferometry to record and measure formed tribofilms on the ball wear track, during the test.

As presented in Figure 11 the disc specimen is immersed in a lubricant pot surrounded by heating elements. The ball is mounted and connected to load sensors, which measure the loading force onto the disc, as well as the friction force. The rotating speeds of the ball and the disc is controlled separately, thus different slide to roll ratio (SRR) can be set.

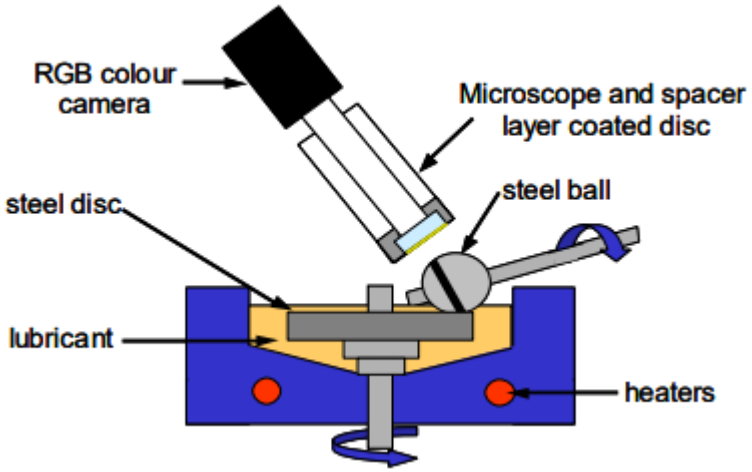

Figure 11: Scheme of the Mini Traction Machine [75].

The 3D-SLIM set-up consists of a glass disc with a layered glass / Cr / SiO_2 build-up in direction to the ball, see Figure 12 for clarification. The ball can be mounted towards the glass disc and the contact is then illuminated by a white light source. Part of the light is reflected from the chrome layer and part travels through the silica layer and tribofilm which is then reflected back from the steel ball. When the light paths recombine, they form an interference image, which is taken by a RGB camera. By a calibration step before each test the silica layer thickness is first analyzed and therefore the tribofilm thickness can be calculated [76].

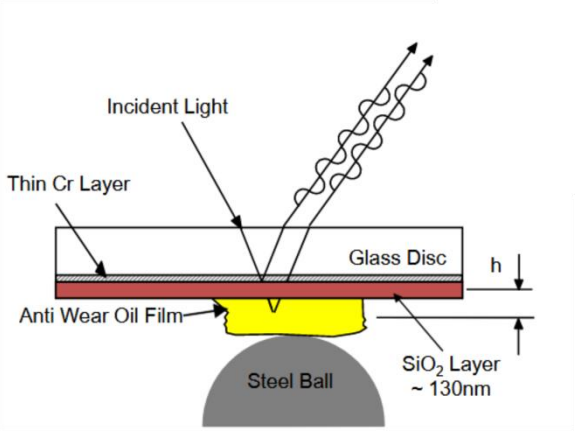

Figure 12: Principle of optical interferometry [75].

The test specimen are made of AISI 52100 steel, where the ball has a diameter of 19.05 mm, a surface roughness of Ra < 0.02 µm and a hardness of 800-920 HV. The steel disc has a diameter of 46 mm a surface roughness of Ra < 0.01 µm and hardness of 720-780 HV [77].

For this work a standardized MTM test procedure was configured, which consists of three different sequences, a rubbing sequence, where the mean speed is set constant to a value of 100 mm/s, a Stribeck measurement, where the mean speed runs from 2500 to 5 mm/s and a SLIM sequence, where an image of the ball wear track is taken. The main sequences during a test are the rubbing sequences, which sum up to around 121 min in total. In between the rubbing sequences Stribeck measurements are done, which are followed by SLIM imaging sequences. This way a continuous energy input by the rubbing sequences is applied on the wear tracks and the influences of the generated surface modifications, tribofilms, on friction in different lubricating regimes can be analyzed by Stribeck curves. The SLIM images additionally show optically a tribofilm formation. If not further noted, the tests following the standard procedure are run at a load of 30 N and a SRR of 50 %, at a lubricant temperature of 100 °C.

Some measurements are done at different load, Table 1 shows the corresponding Hertzian contact pressures for the applied loads with the steel specimen.

Table 1: Applied load on steel ball and corresponding Hertzian contact pressure

Load [N]	Hertzian contact pressure [GPa]
10	0.66
20	0.83
30	0.95
40	1.04
50	1.12
60	1.19

3.2.2. Ultra-thin film interferometry

The influence of the organosilicon precursors on the lubricating film thickness is investigated by optical interferometry with an EHD2 Ultra Thin Film Measurement System by PCS Instruments (in the following abbreviated with EHD).

In this set up a glass disc is loaded against a 19.05 mm diameter AISI 52100 steel ball. The steel ball is mounted on a bearing, so that pure rolling motion is achieved when the glass disc gets into contact while rotating. The ball is half immersed in the lubricating liquid. By motion of the glass disc, the lubricant is dragged into the glass disc / steel ball contact. The glass disc / steel ball contact is investigated by white light interferometry similar to the 3D-SLIM method, described in 3.2.1. The equation to evaluate film thickness for constructive interference is:

$$h_{oil} = \frac{(N - \varphi)\lambda - 2n_{SiO2}h_{SiO2}}{2n_{oil}} \text{ with N} = 1,2,3 \ldots \quad (22)$$

Where h_{oil} is the lubricating film thickness, N is the fringe number, φ is the phase, λ is the wavelength of the light, and n_x is the refractive index of the SiO_2 layer or the oil and h_{SiO2} is the thickness of the SiO_2 layer. The EHD2 system is equipped with spectrometer in order to disperse the reflected light. This way the wavelength at which maximum constructive interference occurs is used for calculation.

The refractive index for the used oil was set to 1.396 for all measurements. The SiO_2 layer thickness was measured prior to each measurement and the refractive index was given by the manufacturer. Organosiloxane polymer exhibit refractive indices, generally range from 1.39 to 1.5, where the indices increase with increasing alkyl or phenyl substituents on the silicon [78, 79]. Since the precise refractive index is not known, the refractive index of oil is used, for clearance, an estimated refractive index of 1.44 for vinylsiloxane polymer would account to an error in lubricating film thickness of around 1 %.

3.2.3. 4-Ball wear test

Wear tests have been carried out with a 4-Ball wear tester Shell VKA following the DIN 51350-3. An illustrative example is given by Figure 13. The balls have a diameter of 12.7 mm and are made of 100Cr6 steel with an average hardness of 63 +/- 3 HRC. The standard test is carried out according to DIN 51350-3 for one hour with a revolution speed of 1425 min^{-1} and a load of 300 N, corresponding to a Hertzian pressure of 2.12 GPa. The sample volume was 10 ml.

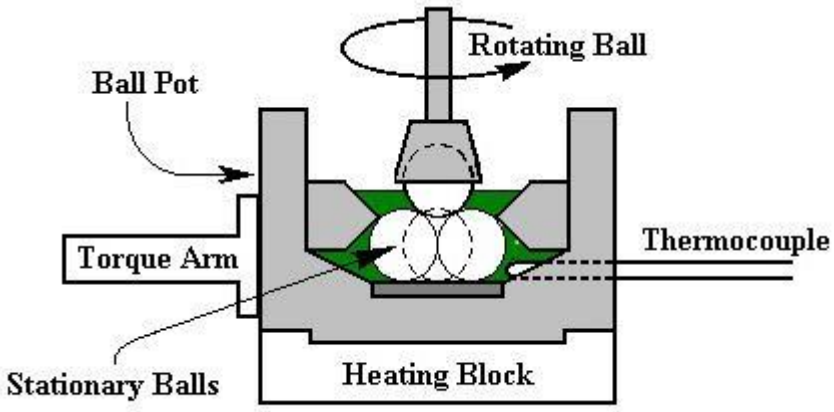

Figure 13: Illustrative working principle of the 4-ball wear test [80].

3.3. Surface / chemical characterization

In order to investigate the formed tribofilms on the wear tracks, the surfaces have been cleaned by two different procedures. First directly after all tribological tests, the surfaces have been rinsed with benzene in order to remove all oil residues. Second a small part of the wear track was polished with acetone and a fine tissue. Investigated areas which were polished with a tissue are labeled in the following as “cleaned”.

3.3.1. Attenuated total reflection fourier transform infrared spectroscopy (AT-FTIR)

The lubricants, sols and wear tracks were investigated by AT-FTIR using a FT-IR spectrometer Varian 670 FT-IR in attenuated total reflection geometry. For the characterization of surface modifications on the wear tracks, backgrounds had to be recorded with an unused MTM steel disc.

3.3.2. Raman spectroscopy

Visible Raman spectra were recorded with a Horiba HR800 micro-Raman spectrometer by Horiba Jobin Yvon GmbH with 633 or 488 nm emissions. The excitation line has its own interference filter to filter the plasma emission and a Raman notch filter for laser light

rejection. All measurements were obtained with a grating of 600 g/mm. The used confocal microscopes with magnifications of 50x and 100x have NA values of 0.55 and 0.9, leading to a beam spot diameters of less than 1 µm, respectively. The power of the laser was attenuated by neutral density filters, thus the power on the sample was in the range from 0.6 to 6 mW.

3.3.3. Nuclear magnetic resonance spectroscopy (NMR)

Liquid samples were diluted in benzol-D_6 (C_6D_6), tetrahydrofuran-D_8 or methanol-D_4. ^{1}H, ^{13}C and ^{29}Si nuclei were measured with a 500 MHz spectrometer DRX 500 (Bruker). In case of ^{13}C and ^{29}Si nuclei also distorsionless enhancement by polarization transfer (DEPT)-spectra were recorded, for easier assignment also 1H correlation spectra (COSY) were recorded.

3.3.4. X-ray photoelectron spectroscopy (XPS)

The measurements were conducted at the daSIy-mat (Technical University Darmstadt) with a Phi5700 spectrometer by Physical Electronics. The spectra were recorded with a monochromatic Al-Kαradiation with hν = 1486.6 eV and a beam diameter of 120 µm.

Only cleaned wear track surfaces were investigated by XPS spectroscopy in order to make sure, that only adhesive tribofilms were investigated. The measurement of the sol-gel coating was performed at the rim of the coating to prevent sample charging. Additionally the charging of the coating was checked by applying an electric field on the specimen. Since no influence of the coating could be observed, the measurements have been performed without applied electrical field.

3.3.5. Scanning electron microscopy (SEM) and energy dispersive X-ray spectroscopy (EDX / EDS)

Scanning electron microscope images and energy dispersive X-ray measurements were performed with a JEOL JSM-IT100 set-up. The images are obtained by detection of low-energy secondary electrons. The acceleration voltage for imaging and EDX measurements was set to 5 kV in order to obtain near surface signals and adequate intensities for light elements. Only the EDX measurements for the sol-gel derived coatings are obtained from Philips XL30-FEG with integrated "Genesis" EDS from EDAX.

3.3.6. Profilometry and optical microscopy

A BRUKER DektakXT profilometer was used to measure the tribofilm height. The profilometer was equipped with a diamond tip having a radius of 12.5 µm and the testing force was set to 6 mg. Profiles were leveled by a linear or a quadratic curvature removal. The tribofilm height

was then obtained by the average height difference of the unworn, polished steel surface and the wear track surface.

Optical microscopy was performed with an Olympus Lext-OLS4000. Several tribofilm heights were calculated from 3D laser measurements with the same microscope. Also in this case the tribofilm height was calculated from the average height difference between the unworn polished steel surface and the wear track surface.

3.3.7. Atomic force microscopy (AFM)

Atomic force microscopy (AFM) has been used for determination the topography of the MTM discs. A Dimension Icon by Bruker with a cantilever from Nanosensors and the Nanoscope software has been used for the measurements. All measurements have been performed in tapping mode. The measurements have been evaluated with the Gwyddion software.

4. Results and discussion

The structure of this thesis is chosen in such a way that at first in chapter 4.1. the tribochemical and tribological behavior of a model precursor is introduced and discussed. The chapter starts with investigations on the influence of the precursor on friction by tribological tests. Afterwards the formed tribofilms are chemically and structurally characterized. In the following, deeper insights into the film formation, will be given by variation of tribological testing conditions, coupled with chemical tribofilm characterization.

With the knowledge about the formation of the reaction films and their chemical structures, their properties in terms of lubrication and wear prevention are described and discussed in chapter 4.2. Finally a lubrication model is presented.

In chapter 4.3 influences of different molecular sizes of the model precursor will be discussed. The findings are compared with the film formation and lubrication model of the model precursor.

4.1. Systematic tribological and chemical investigation of vinylmethoxysiloxane as model precursor

As indicated, in the state of the art, not much work has been published about the behavior of organosilane oil additives in tribologically stressed contacts. Therefore, a vinylmethoxysiloxane oligomer "VTMS-oligomer" is chosen as a model precursor to investigate the polymerization and film formation of organosiloxanes in oil lubricated tribologically stressed contacts. The model precursor is chosen, since it induces pronounced effects and influences on lubrication. It will be shown in chapter 4.3. that for different molecular structures these observed influences are not as distinct and yet crucial to understand and derive the lubricating behavior of cross-linkable organosiloxanes.

The chapter starts with the results of rheological and tribological tests, where the influences of the model precursor on viscosity and friction are compared to base oil test results. The reaction films, which have been obtained by this test, are chemically and structurally investigated. Then a detailed view on the dependences and influences of the reaction film formation is given at the end of the chapter.

A low viscous group III base oil "Nexbase 3050" was chosen in order to have application near test results. All mixtures have been prepared with 2 wt.% siloxane precursor without further additives, such as viscosity index improver or detergents in order to track the influences and reactions on film formation by the precursor alone. Since the precursor is expected to act as a

friction modifier or anti-wear additive the treat rate is set to 2 wt.%, again to have application near test results [23].

4.1.1. Influence of vinylmethoxysiloxane on lubrication and friction

By discussing influences on lubrication, the viscosity of the sample or the viscosity change by an additive is often the most pronounced property. Therefore viscosity measurements of the used samples have been performed with a rotational rheometer as well as glass capillary viscometers by Cannon Fenkse following ASTM D445-18.

Figure 14 illustrates the measured kinematic viscosity of the base oil and base oil / siloxane mixture. The kinematic viscosity changes from 26.44 to 25.03 cst at 40 °C and from 5.08 to 4.94 cst at 100 °C after precursor addition. The small shift can be explained by the strong difference in viscosity of the base oil and the precursor. The VTMS-oligomer has significantly lower kinematic viscosity of around 3 cst at 20 °C [81]. However the change at higher temperatures is of particular interest because it defines stability of the precursor in oil mixture. The observed insignificant change of viscosity at 100 °C shows the stability of the precursor at given conditions, since a viscosity increase would be expected in case of polymerization. This means, that any influences on lubrication and friction by the precursor must arise from interactions with surfaces.

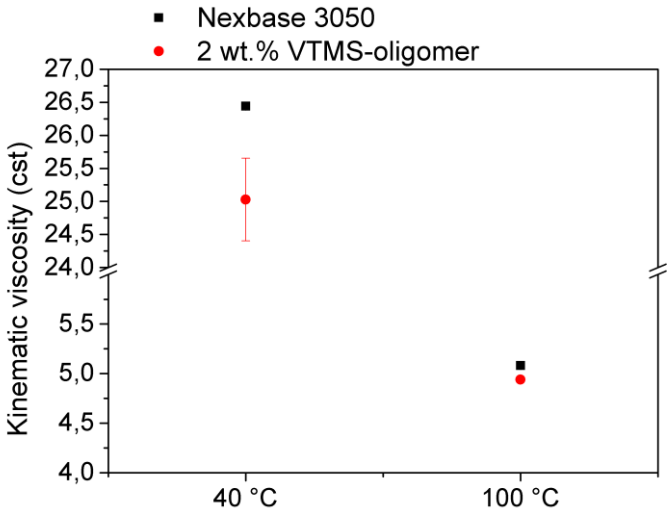

Figure 14: Kinematic viscosity over temperature of the base oil and the precursor + base oil mixture, obtained following ASTM D445-18. Other error bars are too small to visualize.

The film formation and influence on friction is investigated with a ball on disc set-up following the “standard film former” procedure, described in chapter 3.2.1. The testing

conditions are designed to study film forming oil additives, like ZDDP due to the high energy input on the surface by long rubbing sequences [82].

Figure 15 a) shows the comparison of the coefficient of friction during the rubbing sequences between the pure base oil and the precursor mixture. In case of the base oil rubbing sequences a linear increase in the coefficient of friction (cof) from 0.055 to 0.093 during the first 240 min is observable. Afterwards the cof stays constant. This tendency suggests the occurrence of wear and / or degradation of the mineral oil. Also the presented Stribeck curves in Figure 15 b) show an increase in the cof between the first measured Stribeck curve and the last, measured after 330 min testing time. The Stribeck curve after 330 min is shifted in the direction of higher entrainment speeds. Such a shift can be correlated to a retarded lubricating film build up, caused by either changes of the lubricant viscosity, for example shear thinning, or by increased surface roughness, since the lubricating film has to overcome larger asperities. It will be shown later in chapter 4.1.2 that the curves from Figure 15 a) and b) are in consistence with the occurrence of wear.

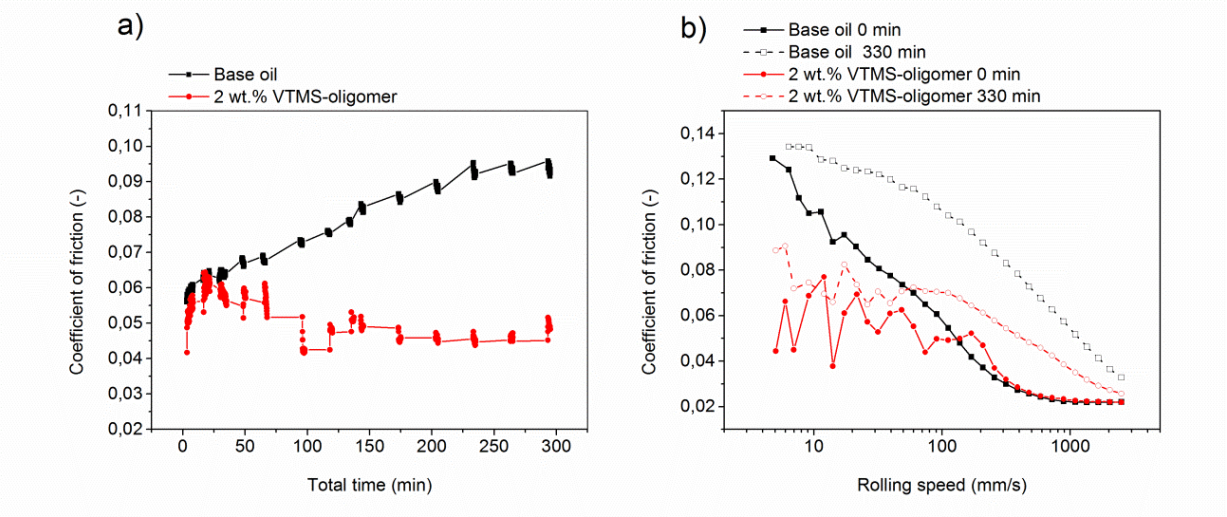

Figure 15: a) Friction coefficient in rubbing steps (100 mm/s) over testing time and b) Stribeck curves measured at the beginning of the test and at the end of the test (30 N, 100 °C, 50 % SRR).

The addition of the oligomeric vinylmethoxysiloxane strongly affects the tribological behavior of the lubricant, which can be deduced from Figure 15. The change of the cof over testing time follows not a continuous increase as shown for the pure base oil, but only a slight increase from 0.05 to 0.063 during the first 30 minutes. Afterwards the cof decreases until around 120 minutes testing time to a value of 0.055 and stays then constant until the end of the test. Also the Stribeck curves show a completely different behavior by the addition of the precursor. The initial Stribeck curve, measured before the first rubbing sequence exhibits a low cof of around 0.05 in the boundary to mixed lubrication regime until around 300 mm/s

and then follows the base oil curve, matching the same cof. Also the last Stribeck curve, measured after 330 min testing time, shows a decreased cof in the boundary to mixed regime of around 0.075 compared to both base oil Stribeck curves. However, approaching medium speeds of around 100 to 200 mm/s shows a friction increase in contrast with the initial Stribeck curve at 0 min. The slope of the curve at medium to high speeds suggests that the whole Stribeck curve is shifted to higher mean speeds, as observed for the base oil Stribeck curve at 330 min.

From the ball on disc test results, it can be concluded that the model precursor directly interacts with the steel surfaces at the beginning of the test. The friction reduction at slow to medium speeds shows a similar behavior like friction modifier additives, which also act on surfaces by physi- and chemisorption. However, the friction increase and shift of the Stribeck curve to higher speeds, after longer rubbing times shares rather similarities with rough tribofilms from antiwear additives or worn surfaces [35]. The constant speed test also indicates that the oligomeric precursor protects the surfaces and maintains a low cof.

In order to have a better understanding of the interactions from the precursor with the surfaces SLIM images have been recorded and are shown in Table 2.

Table 2: MTM SLIM (ball wear track) images recorded at different testing times, always after 100 mm/s rubbing steps, at 30 N loading.

Time [min]	8	21	45	67	136	175	330
Base oil	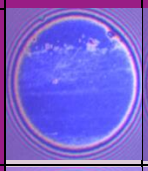	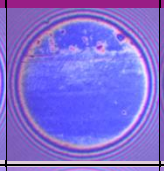	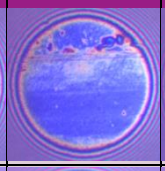	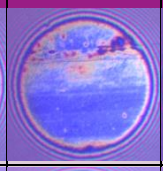	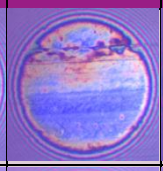	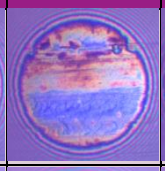	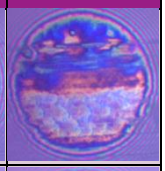
2 wt.% VTMS-oligomer				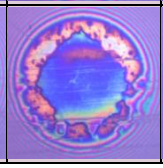	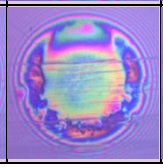	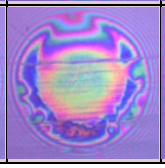	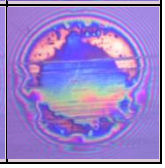

The SLIM images from the base oil test are in consistence with the friction curves and show the formation of wear or oil degradation products on the ball wear track with increasing testing time. In the case of the VTMS-oligomer test all images display a colorful deposit on the ball wear track. However, the images do not give a clear trend of film formation or even tribofilm structure, but prove interactions of the precursor with the surfaces.

4.1.2. Investigation of the formed films and description of the multi-layer nature

The investigation of the formed products by the tribologically stressed precursor is necessary to follow the interactions in the tribo-contact and to align them with the friction curves. Therefore images of the wear tracks of the used MTM discs were recorded and are presented in Table 3. The table illustrates the wear tracks in two conditions. The not cleaned description indicates that the MTM discs have only been rinsed with benzene to get rid of the oil mixture. The cleaned condition specifies that the MTM disc has additionally been polished with an acetone soaked tissue.

Table 3: Wear track images of tested MTM discs obtained with optical microscope. The yellow scale bar represents in the case of X20 magnified 100 µm and in the case for X50 magnified 50 µm. "Not cleaned" indicates that the MTM discs were just rinsed with benzene after testing, while "Cleaned" indicates that the wear tracks were polished with an acetone soaked tissue.

Disc wear track Optical Microscope	Not cleaned X20 magnified	Cleaned X20 magnified	Cleaned X50 magnified
Base oil			
2 wt.% VTMS-oligomer			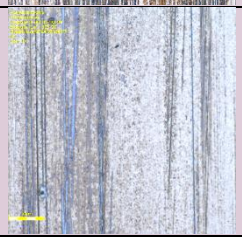

The appearance of the wear track from the base oil test is in accordance with the SLIM images, showing a clear color change. The dark color of the wear track can be attributed to oxidation of steel and/or oil decomposition, since no other chemical compounds are present in the system. Light microscope images of the MTM disc wear track from the VTMS-oligomer test also have colorful deposits. As mentioned, the discs have been rinsed extensively with benzene prior to recording, indicating that the deposits are not only mineral oil remains, but are supposed to be siloxane-based products. However, these siloxane deposits do not withstand the cleaning procedure, which can be seen by the images marked as "cleaned". The cleaned wear track appears also darker than the pristine steel surface, but much brighter than the wear track from the pure base oil test.

With the help of the wear track profiles in Figure 16, it becomes clear, that a coating like adhesive tribofilm is deposited on the wear track. The average height of the wear track is around 40 nm higher than besides the wear track, for the cleaned region. The not cleaned profile exhibits polymeric deposits up to a thickness of several hundred nm.

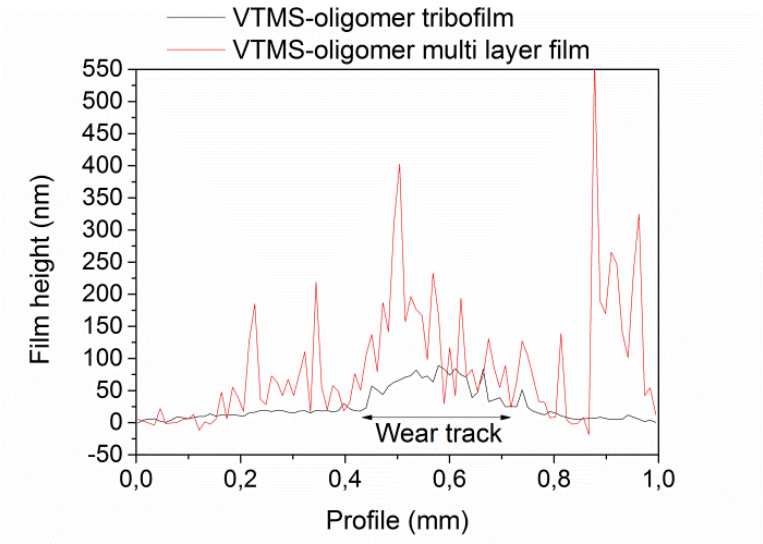

Figure 16: Wear track profiles of cleaned and uncleaned region of a tested VTMS-oligomer MTM disc, obtained by profilometry.

The findings listed above allow deriving following hypothesis which is visualized in Figure 17. The siloxane precursor cross-links during the rubbing experiments and forms a multi-layered film structure. The film consists of at least two layers, where one layer is an adhesive coating like tribofilm on the wear track. The other layer is a rather weakly bonded or adhering polysiloxane on top of the tribofilm. This polymer is further denoted as “tribopolymer”.

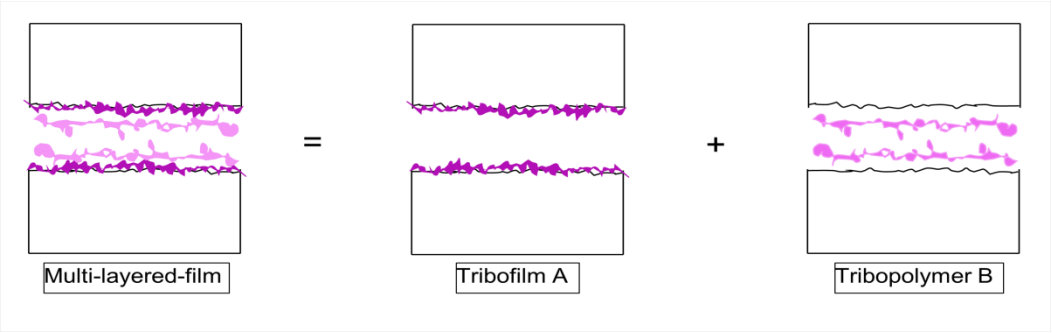

Figure 17: Schematic organosilane based reaction film with multi-layer architecture, consisting of an adhesive tribofilm and a viscous tribopolymer.

4.1.3. Tribopolymer characterization

In the following, the proposed hypothesis that the colorful residues on the wear track are siloxanic polymer will be validated by means of ATR-FTIR and Raman spectroscopy. Figure 18 presents the ATR-FTIR spectra of the base oil, the pure precursor and of the multi-layered film. The spectra of the multi layered film are measured in the "not cleaned" condition. As the deposits are much thicker than the tribofilm beneath, the findings from the multi layered film are denoted to the chemical structure of the tribopolymer, which is in consistence with the results from 4.1.4. The main IR-absorption sites of the oligomeric VTMS precursor are associated to C-H (2950-2850 cm^{-1}), Si-O-CH_3 (2840, 1190, 1100-1080 cm^{-1}), Si-CH=CH_2 (1600, 1410, 1275, 1010, 967 cm^{-1}) and Si-O-Si (1000 to 1200 cm^{-1}) as assigned according to the literature [83-85]. Unfortunately, some absorption bands, especially Si-O-C and Si-O-Si overlap in the region of 1000 to 1200 cm^{-1} and are not easy to differentiate. This makes an interpretation of unreacted alkoxy groups difficult [86].

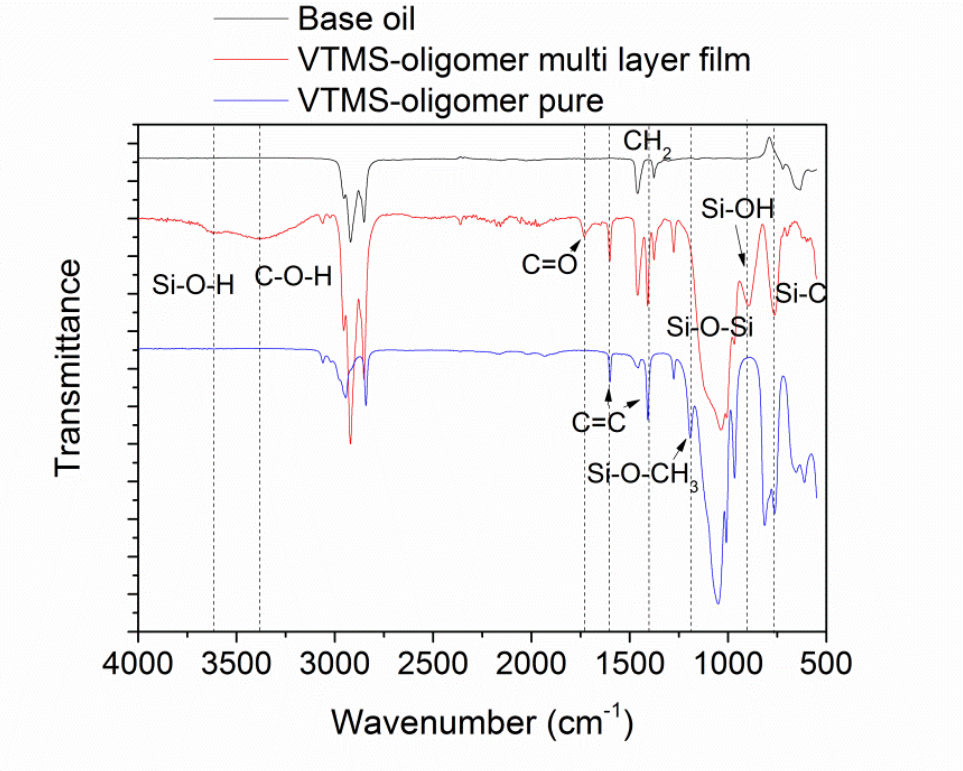

Figure 18: ATR-FTIR spectra of MTM disc wear tracks tested with 2 wt.% VTMS-oligomer blends and of the pure precursor. "multi layer film" refers to the tribopolymer.

The shown spectra prove the formation of polymeric siloxane layers on the wear track. The appearance of Si-O-H and C-O-H bands and the broadening of the Si-O-Si band is a clear indication for the polymerization of the VTMS-oligomer by hydrolysis and condensation type of reactions. Also the clear presence of the Si-O-H bands reflects that the polymers are not

fully cross-linked. Interactions from vinyl groups cannot be proven due to no clear vanishing of C=C bands. The appearance of a C=O band is a clear evidence of further reactions. In order to have a better understanding of the chemical reactions and products which may be formed by the precursor, TGA and FTIR with sol-gel annealing experiments have been performed. The spectra can be found in the appendix and the results demonstrate the formation of C=O bonds at 250 °C, which goes in hand with the vanishing of vinyl groups.

Another important aspect is degradation of oil in lubricated contacts above 100 °C, which is schematically described in Figure 19. The oxidation products of hydrocarbons are well investigated and play an important role for the formation of tribofilms. The degradation generally starts with the formation of hydroperoxide groups. These groups further decompose and form different compounds like alcohols, carbonyls up to carboxylic acids [87]. By means of this information a multitude of reactions originating from oxygen introduction may be present in the system. A precise reaction pattern and interactions between base oil and the precursor is thus not predictable under these conditions.

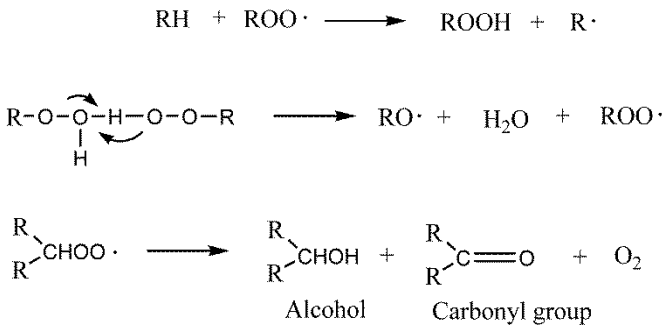

Figure 19: Schematic presentation of the reactions involved in oil degradation and possible products, excerpt from [23].

To get more information, the used oil mixtures are investigated by NMR analysis. As already mentioned the tribopolymer is not strongly bonded to the surfaces and may be sheared off the surfaces during the test and therefore stays in solution. The NMR spectra are shown in the appendix 6.2. Unfortunately, the NMR analysis cannot prove the presence of condensed precursors, which are solved in the oil mixture. However, indications for alcohol groups suggest the occurrence of hydrolysis reactions, which supports the FTIR analysis.

As already described in section 2.4.1, hydrolysis and condensation reactions are the main cross-linking mechanism for silanes. However, this holds especially for acid or base catalyzed conditions in moist environments. The water content of the base oil was measured by Karl-Fischer titration and is less than 0.01 wt.%. A water content of 0.01 wt.% yields a molar ratio of hydrolysable Si-O-CH_3 groups to H_2O of around 51 to 1 for the used mixture. Therefore,

from the presence of unreacted Si-O-H groups and the low water content it is concluded in this context, that the siloxanic tribopolymer are only weakly cross-linked. Furthermore, no clear details about reactions between base oil and the precursor can be stated. NMR investigations did not show indications for this in the used oil, which however, does not hold for the precursors attracted or bonded to the surface. In total no clear influence of oil decomposition products could be observed and are therefore not considered to take part in the polymerization reactions.

4.1.4. Tribofilm characterization

A first indication that a coating like tribofilm was deposited on the wear track is illustrated in Figure 16, where an average step height of around 40 nm between the wear track and steel surface can be analyzed. This tribofilm is further investigated by SEM and AFM and images are given in Figure 20. All records have been obtained after the cleaning procedure. The top view images show a clear contrast between the polished steel surface and the tribofilm, also the tribofilm appears darker in the center of the wear track. Higher magnified images show that the tribofilm is not homogenously deposited, but has a rather pad-like morphology. As the density of these pad-like deposits increase the tribofilm appears darker and therefore thicker. The clear rim of the tribofilm indicates that the deposition process is triggered by frictional influences, like stress or heat, since no deposits are seen besides the wear track. The cross-sectional images cannot resolve whether an iron oxide or different bond coat formed underneath the tribofilm. The shattered steel below the tribofilm may result from tribologic stress and/or from the heavy ion bombardment by the focused ion beam procedure. Also the images obtained by AFM show the pad-like morphology of the tribofilm. Such kind of morphology has also been reported for other anti-wear film forming additives, especially ZDDP [82]. The pad-like topography is consistent with the results, obtained by profilometer analysis from Figure 16, proving that the tribofilm is rougher than the polished steel surface.

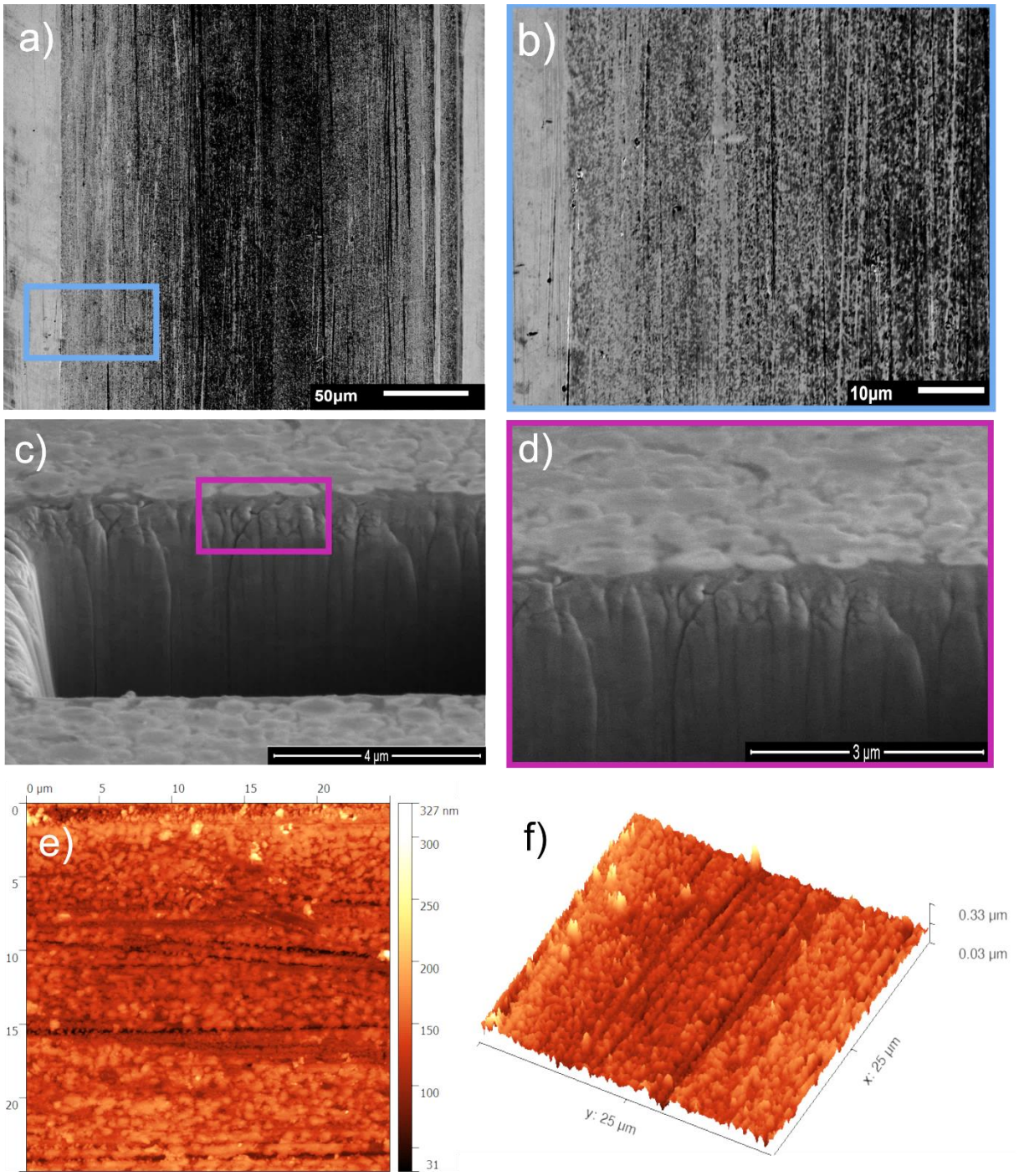

Figure 20: Images of VTMS-oligomer derived tribofilm obtained by SEM a) – d) and by AFM e) + f). a) and b) are top view images of the tribofilm, while c) and d) show cross-sectional images obtained by FIB preparation. Image e) is again a top view contour image and f) is the corresponding 3D image.

To prove, that this film is siloxane derived, EDX analysis is performed and the results are shown in Table 4. The table contains EDX results of the pristine steel disc, the wear track compositions from the test with base oil and from the test with the VTMS-oligomer base oil mixture. When comparing the reference steel composition and the disc from the base oil test, a strong increase in oxygen concentration can be observed, which is attributed to iron oxide formation and suits the results from the friction curves. The increase in carbon concentration

can be referred to products from oil degradation or oil rest overs. On the other hand the VTMS-oligomer derived wear track shows increased silicon and oxygen concentrations. A prediction of the tribofilm composition is difficult as it cannot be said how strong the substrate influences the measurement results. A rough estimation would be to assume that all detected oxygen is bonded to silicon, due to its strong affinity with each other. Further the elemental concentrations from the reference disc are subtracted from the tribofilm concentrations, which in total give a tribofilm composition of $SiO_{1.66}C_{0.47}$. The initial Si:O:C ratios of the used organosiloxane precursor corresponds to approximately $SiO_{2.2}C_{3.4}$. If all methoxy groups ideally cross-link, then a ratio of $SiO_{1.5}C_2$ would be obtained. The estimated elemental composition of the tribofilm comes close to a strongly cross-linked Si:O:C ratio, however the carbon concentration appears much lower. First it must be said, that quantitative analysis of light elements is not very accurate with EDX measurements. Second, as mentioned, the influence of the carbon concentration of the steel is difficult to predict. Nevertheless, loss of organic content by cleavage of Si-C bonds under tribological stress or increased temperatures have been reported already and is expected under the tested conditions [7, 53].

Table 4: EDX results of MTM disc wear tracks. The values are the average of five point measurements on the wear track and two measurements besides the wear track. All measurements are performed with 5 kV acceleration voltage.

Sample	Wear track composition [atom %]			
	Si	O	C	Fe
Reference Disc	0.4	0.2	4.7	94.7
Base oil	0.6	19.1	6.6	73.7
2 wt. % VTMS-oligomer	4.8	7.5	6.8	80.9

In the following, differences of the tribopolymer and tribofilm in terms of their chemical structure are discussed with the help of FTIR characterization results in Figure 21. The most striking features of the tribofilm spectrum compared to the tribopolymer spectrum are shift of broad Si-O-Si band to much higher wavenumbers and the loss of bands corresponding to organic groups. The shift to higher wavenumbers is related to stretching vibrations of Si-O-Si in $RSiO_{1.5}$ and SiO_2 coordination, which is investigated by thermal treatment of vinylsiloxane coatings [88]. Another relation is the activation of longitudinal optical modes which are generally not active in normal incidence transmission spectroscopy. However, with occurrence of porosity and free-volume these modes become also active due to light scattering [89, 90]. Whether the tribofilm is of porous nature can only be suspected, but also rough morphology would activate these modes, what is consistent with the topographic investigations discussed above. Due to the low thickness, also the intensity and signal to noise ratio is not very high. Nevertheless, hardly any bands belonging to organic groups can be observed for the tribofilm. Only very weak C-H stretching signals at 2930 cm^{-1} as well as a tiny tip at 1275 cm^{-1} give signs of residual organic groups in the tribofilm. These findings match the estimated composition from the EDX results, which also recommend a loss of organic fraction and an increase in $SiO_{1.5\text{-}2}$ coordination, indicating stronger cross-linking.

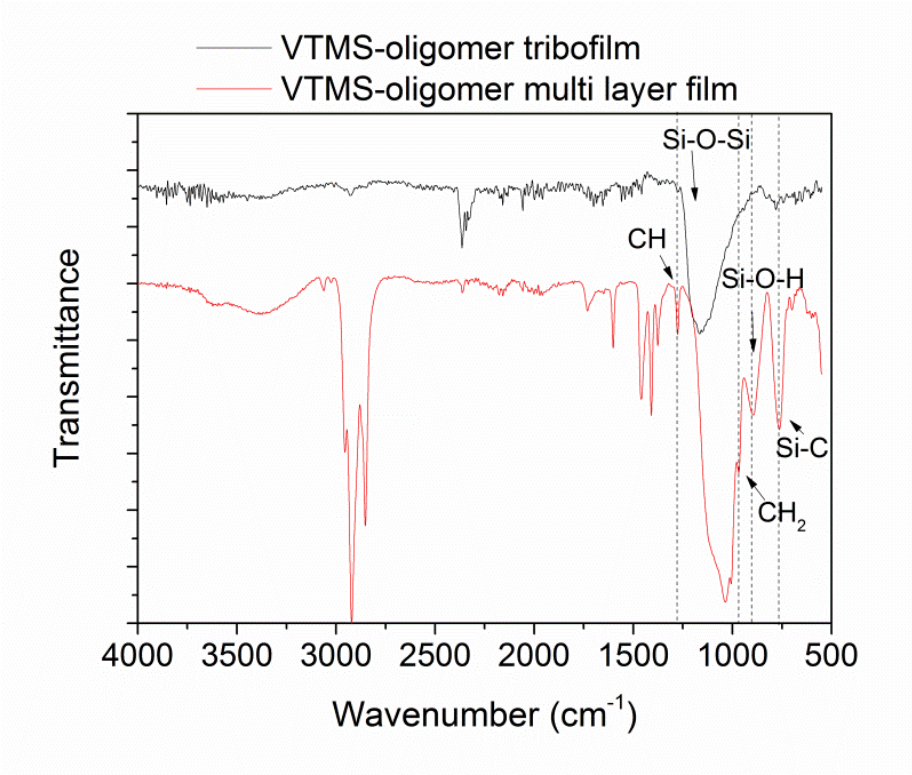

Figure 21: ATR-FTIR spectra of MTM disc wear tracks tested with 2 wt.% VTMS-oligomer blend. "multi layer film" refers to the tribopolymer. "tribofilm" refers to the adhesive coating like reaction film.

It can be concluded that the intensive tribological stresses cause the tribofilm to become much stronger cross-linked than the tribopolymer. As mentioned above, the transformation process from siloxane gels to SiOC glasses starts at 500 °C. This transformation process is reported to be shifted to lower temperatures in presence of fresh steel surfaces which act catalytically as well as low coating thicknesses [56, 65]. Additionally, the high pressures and strong shear forces can lead to degradation of polymer and promote cross-linking [64]. Therefore, a strongly cross-linked SiOC coating with glass-like and residual organic fractions is expected as tribofilm.

As the FTIR investigation show limited sensitivity for organic groups, micro-Raman measurements have been performed and the spectra are shown in Figure 22. First the spectrum corresponding to the base oil derived wear track is discussed, since it gives information about the substrate and oil interactions. Many distinct signals can be observed for hematite-Fe_2O_3 with sharp peaks at 218, 288, 406 and 1319 cm^{-1} and magnetite with its highest intensity peak at 660 cm^{-1}. From the shape of the broad peak centered at 660 cm^{-1} as well as the strong and broad band from 1100 to 1650 cm^{-1} also FeOOH might be present to small extent [91, 92]. Iron carbonate can form as corrosive product from base oil degradation, as implied in the FTIR discussion, however, the highest intensity peak at around 1070 cm^{-1} can only be estimated as shoulder and therefore will not be further discussed [93].

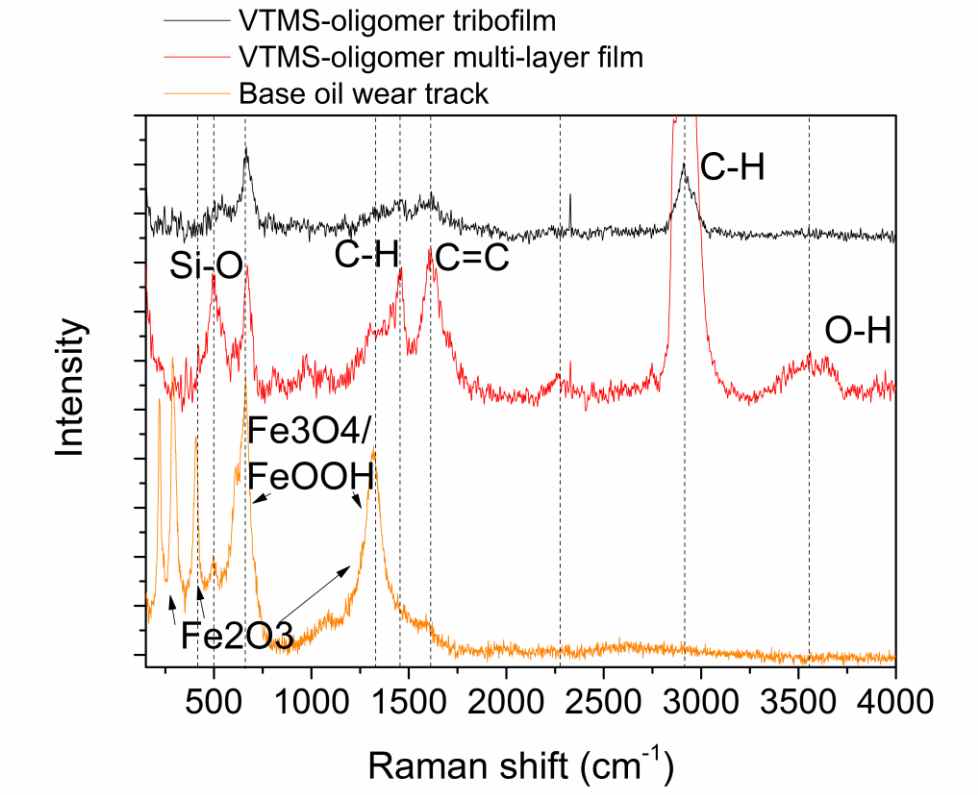

Figure 22: Micro-Raman spectra of MTM disc wear tracks tested with base oil as well as 2 wt.% VTMS-oligomer blend. "multi-layer film" refers to the tribopolymer. "tribofilm" refers to the adhesive coating like reaction film.

Table 5: Investigated Raman signals and the corresponding chemical and vibrational assignments.

Assignment	Raman signal (cm^{-1})	References
Fe2O3 hematite	218, 288, 406, 498, 613,	91, 92
Fe3O4 magnetite	550, 660	91, 92
FeOOH div.	245, 373, 493, 522, 1116,	91, 92
Si-O-Si sym. stretch	490, 804	84, 94
C-H asym. bend	1460	84, 85, 94
C=C stretch	1614	84, 85, 94
C-H sym. stretch	2800-3000	84, 85, 94
O-H stretch	3400-3600	84

In the spectrum corresponding to the tribopolymer, many broad bands are found. The polymeric siloxane shows broad bands at around 490 cm^{-1} for Si-O-Si vibrations, at 1460 and 1614 cm^{-1} corresponding to C-H and C=C vibrations, the very intense band from 2800 to 3000 cm^{-1} correspond to C-H vibrations, a band at 3400 to 3600 cm^{-1} can be attributed to O-H vibrations [84, 85, 94]. Only the band at around 670 cm^{-1} cannot be assigned to the polymer, as it stands for Fe_3O_4 from the substrate. The Raman spectrum confirms the findings from the FTIR characterization and again shows no clear evidence for the degradation of C=C bonds.

In case of the tribofilm spectrum only weak signals matching Si-O-Si, Fe_3O_4 vibrations and C-H vibrations can be observed. As the band from 2800 to 3000 cm^{-1} from C-H is strongly Raman active it can be deduced that the organic fraction of tribofilm is rather small. The weak bands from 1400 to 1600 cm^{-1} may be attributed to amorphous carbon residues, which could form by oil degradation or decomposition of organics from the polymer. Interestingly, no hematite signals can be detected, in contrast to the base oil derived wear track. The magnetite signals prove that the tribofilm is not grown on top of the steel surface. Together with the SEM images from Figure 20, it is concluded that the SiOC tribofilm is deposited on top of a magnetite layer. More details on the formation of the tribofilm will be given in the next chapter. With the help of Ellingham diagrams the thermodynamic stable phases of iron oxides for different atmospheres can be predicted. The observed suppression of hematite formation is referred to interactions between the steel surfaces with the VTMS-oligomer. In the following, three main reasons for this suppression are discussed. First the precursor acts as oxygen and water scavenger reducing the oxygen concentration which might come into contact with the steel surface, second the polymeric layer acts as barrier as it lies on top of the steel and third the precursor/tribofilm might even act as reducing agent stabilizing the magnetite phase.

To prove these expectations XPS measurements have been carried out and the results are discussed in the following. For clear assignment of the binding energies of the atoms, a sol-gel derived coating from the VTMS-oligomer was deposited and dried at 100 °C and is shown in

Figure 23 (right). Thus the results from the sol-gel coating can be used as a reference for binding energies in a polymeric cross-linked state. This way any shifts in binding energies between the tribofilm and the polymer coating can be addressed to changes in the molecular structure by extensive tribological stress.

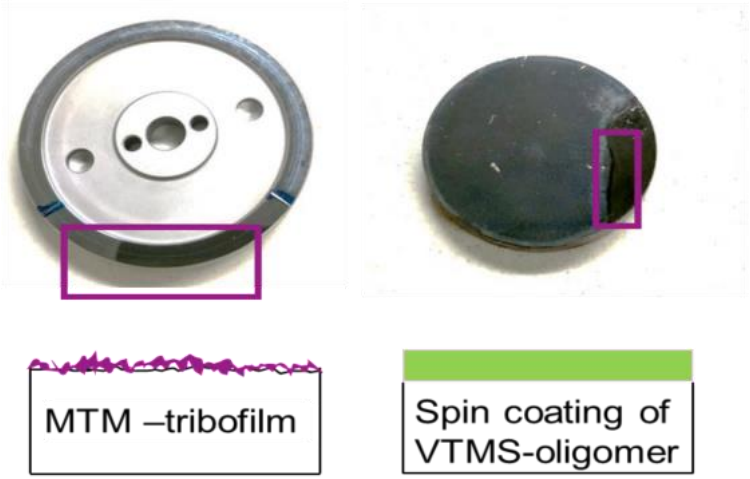

Figure 23: Exemplary specimen for XPS analysis. A sol-gel derived coating from the VTMS-oligomer is used as polymeric reference sample for easier binding energy assignment.

The XPS technique is a surface sensitive technique with a depth of information of about 10 nm, which is suitable in case of the deposited tribofilms to avoid substrate signals. Figure 24 and Figure 25 show the Si2p, O1s, C1s and Fe2p curve fitted spectra of the tribofilm (upper) and sol-gel coating (bottom). All assigned chemical environments are based on results from FTIR and Raman spectroscopy characterization. Although much information about the bonding situation of the elements is known, a precise quantification of the different species is still difficult. This comes primarily from uncertainties in chemical shifts due to variations in bond length and angle, which is pronounced in amorphous materials.

A comparison of the Si2p spectra between the tribofilm and the sol-gel coating gives information about the chemical environment of the silicon, after the tribological stress. The comparison shows a strong shift of the Si2p peak to higher binding energies in case of the tribofilm. From FTIR analysis it is known, that the sol-gel coating is a polymeric network with different bonding situations of silicon. A fully condensed coordination would be SiO_3C, where the silicon is bonded to three bridging oxygen and a carbon atom from a vinyl group. The FTIR investigation does also show unreacted Si-O-H groups present in the sol-gel coating. As the binding energies would be similar for both groups a cumulative peak fit was chosen. This peak is centered at 102.2 eV, which corresponds to unreacted SiO_3C silicon coordination. Another peak appears at 102.8 eV for the fully condensed coordination as the binding energy increases with bridging oxygen [95]. The tribofilm Si2p peak shows also two peaks. One peak

fits with 103 eV the fully condensed SiO_3C state. However, peak broadening also indicates presence of unreacted groups. The more prominent peak at 104.3 eV represents a SiO_4 coordination and fits with higher binding energies compared to the SiO_3C coordination, also it is in accordance with references from literature [96, 97]. These findings are a clear indication that the tribofilm exhibits indeed an amorphous silica rich fraction. Also it proves a polymer to glass transformation during the rubbing process.

Furthermore, the O1s spectra of the tribofilm and sol-gel coating also confirm polymer to glass conversion. For the sol-gel coating three different peaks can be seen. One at 530.06 eV corresponding to Fe_xO_y, 531.8 eV corresponding to C-O/C=O bonds and 532.7 eV corresponding to the SiOC network. The iron oxide is naturally present on the surface of the substrate and was measured on the rim of the sol-gel coating. The intermediate peak is designated to C-O bonding environments from unreacted groups, trapped methanol or acetone, as well as C=O bonds from further oxidation upon thermal curing, the binding energy matches with literature references and signals from the C1s spectrum in Figure 25 [87, 98]. The peak standing for the SiOC network appears rather small. However, the binding energies of C-O / C=O bonds coincide with the siloxanic bonds. In case of the tribofilm spectrum a new peak appears at around 533.6 eV, which is related to SiO_4 tetrahedra. Interestingly the fitted peak attributed to C-O/C=O bonds from the tribofilm is stronger in intensity as expected from the results of FTIR and Raman investigations. It will be shown, in the C1s and Fe2p spectra that residual organics and different iron oxide compounds are also present. Therefore a precise estimation of the polymeric content in the amorphous tribofilm is difficult.

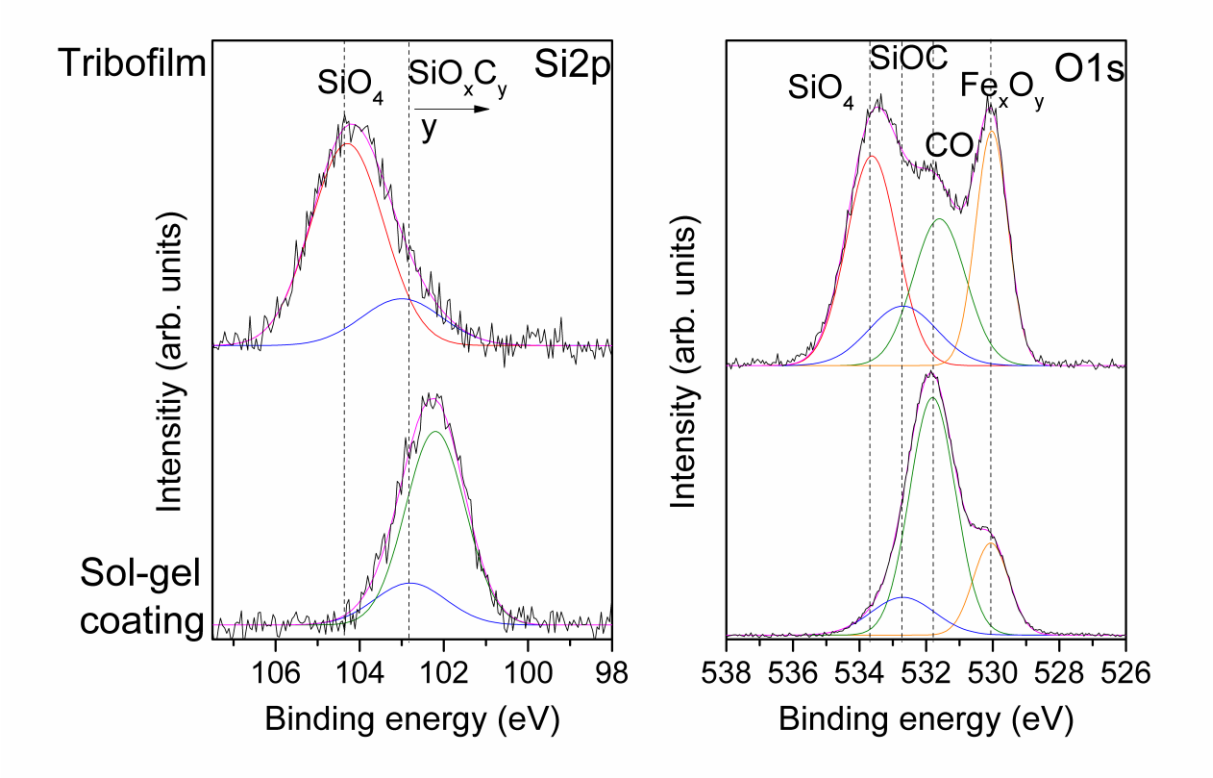

Figure 24: Curve fitted Si2p and O1s spectra of a tribofilm (upper) and Sol-gel coating (bottom) obtained by XPS.

The characterization of the C1s and Fe2p spectra give further information on the decomposition of the polymer and base oil. The C1s XPS spectrum of the sol-gel derived coating shows four peaks where the peaks at 285.2 and 285.7 eV stand for C=C and C-H bonds, respectively. Also a shoulder corresponding to C-O bonds at 286.5 eV is present. A strong peak at 288.6 eV can be attributed to C=O bonds. All binding energies from the C1s spectrum match with the binding energies from organic bonds found in the O1s spectrum of the sol-gel derived coating. In case for the C1s spectrum of the tribofilm, three peaks are fitted in the broad peak. The peak center is shifted to higher binding energies at 285.2 eV. The shift is due to the loss of C=C bonds and a stronger contribution of C-O bonds, compared with the peak from the sol-gel film. A small shoulder corresponding to C=O bonds can also be observed, which might be due to solvent rest overs and oxidized carbon species.

No fitting was performed for the Fe2p spectra, due to multiplet peaks and spectral overlaps, which makes fitting for mixed oxides very difficult and is not of primarily interest in this work [99]. However, as guidance binding energies for different iron species have been added from the work of Lin *et al.* for rough estimations [100]. The main differences in the Fe2p spectra of the tribofilm and sol-gel derived coating are the presence of elemental iron in the tribofilm sample and satellites, which can be attributed to Fe^{3+} species, which is however present in Fe_2O_3 and Fe_3O_4.

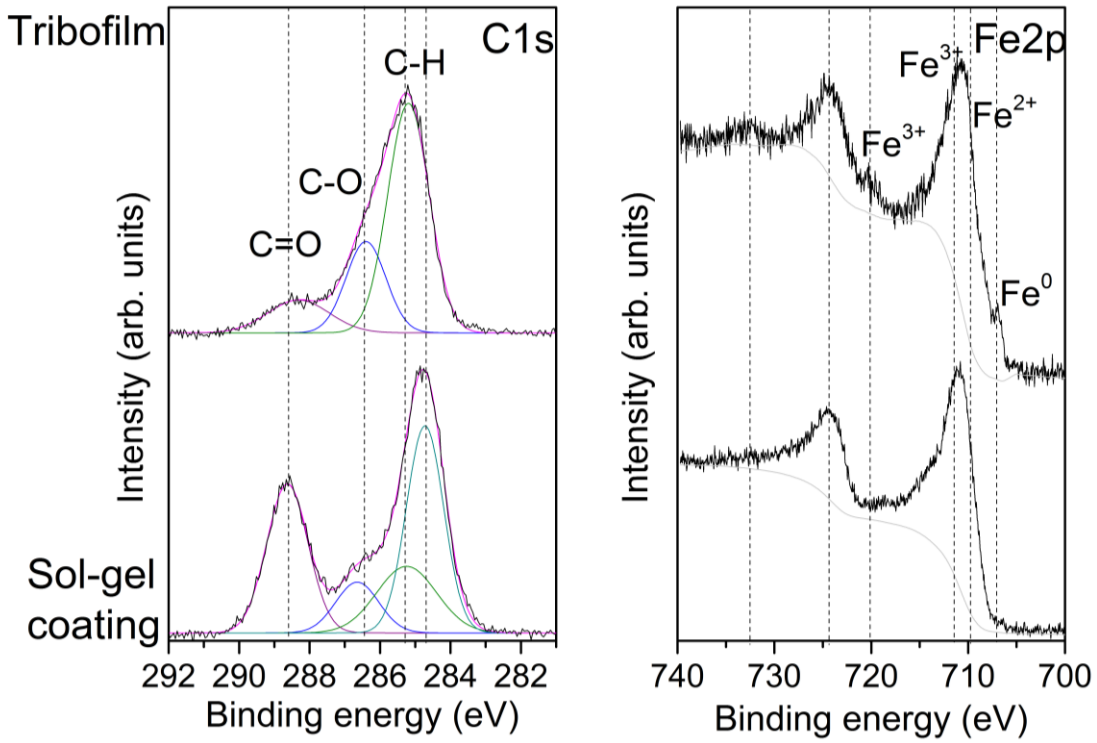

Figure 25: Curve fitted C1s spectra and raw Fe2p spectra with baseline of a tribofilm (upper) and Sol-gel coating (bottom) obtained by XPS.

In summary, the hypothesis from chapter 4.1.2 is proven as the multi-layer film consists of a polysiloxane top layer and a stronger cross-linked, silica containing bottom layer. The top layer is formed mainly by hydrolysis and condensation reactions, which result in a polymeric gel-like material. It cannot be proven, if the tribopolymer shows additional interactions with the base oil or decomposition products from the base oil. However, the adhesive bottom layer is a result of further cross-linking, with a high yield of silica. Since silica cannot be formed via hydrolysis and condensation reactions by the starting precursor, also redistribution and / or defragmentation reactions must have occurred. As the notation “tribofilm” highlights, these reactions are triggered by the intensive tribological stress on the contacting surfaces, as no proof of silica species can be found besides the wear track.

Also some properties of the reaction films can be highlighted, which have an impact on their lubricating ability. Similar to common used friction modifier the formed tribopolymer exhibits polar groups which show attraction to polar surfaces and tribofilms. In addition, the tribopolymer is of the same nature as the tribofilm, which means that they can share bonds, which further increases the adhesion. By comparison of the base oil and the precursor derived wear tracks, a strong decrease in iron oxide signals is obtained. As mentioned, the tribofilm and tribopolymer act as corrosion resistance for the substrate, which will be discussed further in the next chapter.

4.1.5. Tribological influences and dependences on film formation of vinylmethoxysiloxane as model precursor

The previous chapter described how the formed tribological reaction films are built up in terms of their chemical, as well as morphological manner. However, it has not been cleared, which and how testing parameters influence the formation of the tribopolymer and tribofilm. Therefore, in the following chapter first the influences of the rubbing time, then contact pressure and also temperature are discussed. It still needs to be revealed whether the iron oxidation and the sequence of the formed films affect the tribological performance and film formation in general.

First the influence of testing / rubbing time is presented and discussed in the following. For this purpose MTM-tests with different rubbing times have been performed and the formed reaction films have been analyzed afterwards. Figure 26 shows the Stribeck curves measured after different rubbing times and rubbing curves. Figure 27 gives the corresponding tribofilm thicknesses for the base oil reference tests and the tests with the VTMS-oligomer mixtures. The testing conditions are kept similar to the previously presented tests only the time was varied. A mean speed of 100 mm/s correlates to a minimum lubricating film thickness of h_0 = 7.6 nm and lambda ratio of $\lambda(h_0)$ = 0.67, calculated with equation 21 and 19. This means, that the system is under boundary conditions with a lubricating film thickness in the range of surface roughness, so any influences of surface roughening are detected easily.

The first Stribeck curve is measured before any rubbing sequence and has therefore the same profile like in Figure 15. With the information from the previous chapter it can now be concluded, that the organosiloxane precursor crosslinks and forms siloxane layers on the steel surfaces. The cross-linking reactions take place without any frictional stress or energy and are activated by the increase of temperature to 100 °C. The friction reduction is the result of a low shear strength polymeric layer, which still provides lubrication at low speeds, where the used base oils film thickness is too thin. Exact proof and description about the lubrication behavior of the polymeric layer will be given in the next chapter.

The rubbing curves show an increase in friction during the first 10 min and stay nearly constant afterwards with a cof at around 0.0625. The corresponding tribofilm heights prove the formation of the adhesive tribofilm layer during the first minutes of rubbing. Similar to the coefficient of friction the film thickness increases until 10 min and then stays rather constant at a height of around 20 nm until at least 30 min. This proves that the tribofilm

formation is dependent on the frictional stress at the ball-disc contact. As already explained in the previous chapter, the severe conditions during rubbing sequences lead to further cross-linking and redistribution reactions of the organosiloxane polymer, which results in a microstructure with fractions of silica. From the Stribeck curves it becomes clear that the polymeric layer forms first and then gradually decomposes and further networks to a more cross-linked adhesive film, due to the high energy input at the surface. The tribofilm formation can also be read from the Stribeck curves.

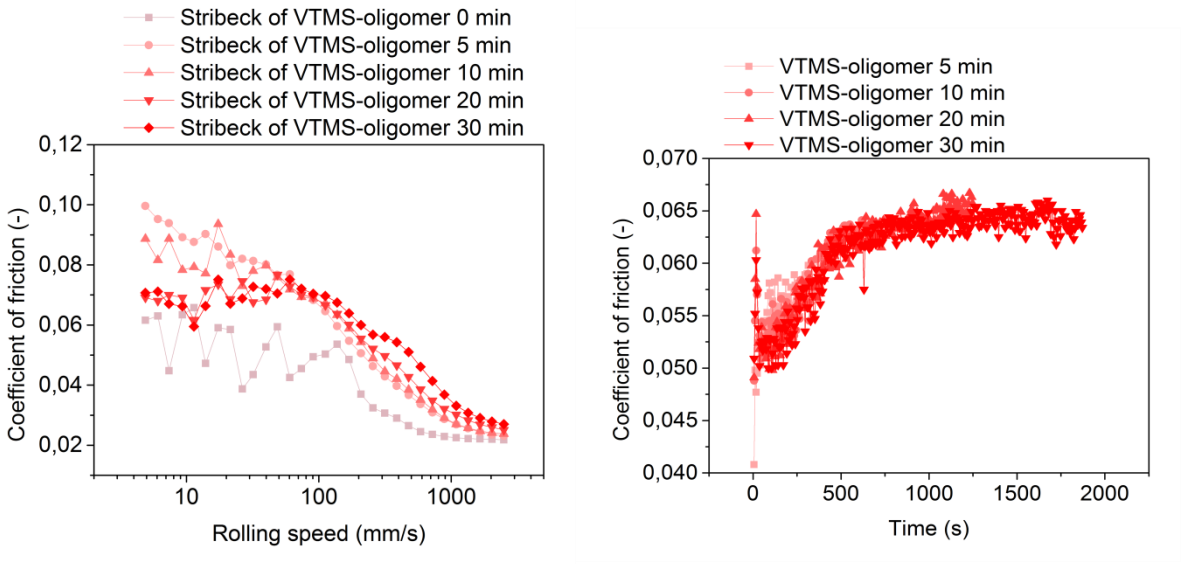

Figure 26: Left) Stribeck curves measured after different rubbing times (30 N, 100 °C, 50 % SRR) and right) Friction coefficient over rubbing time (100 mm/s).

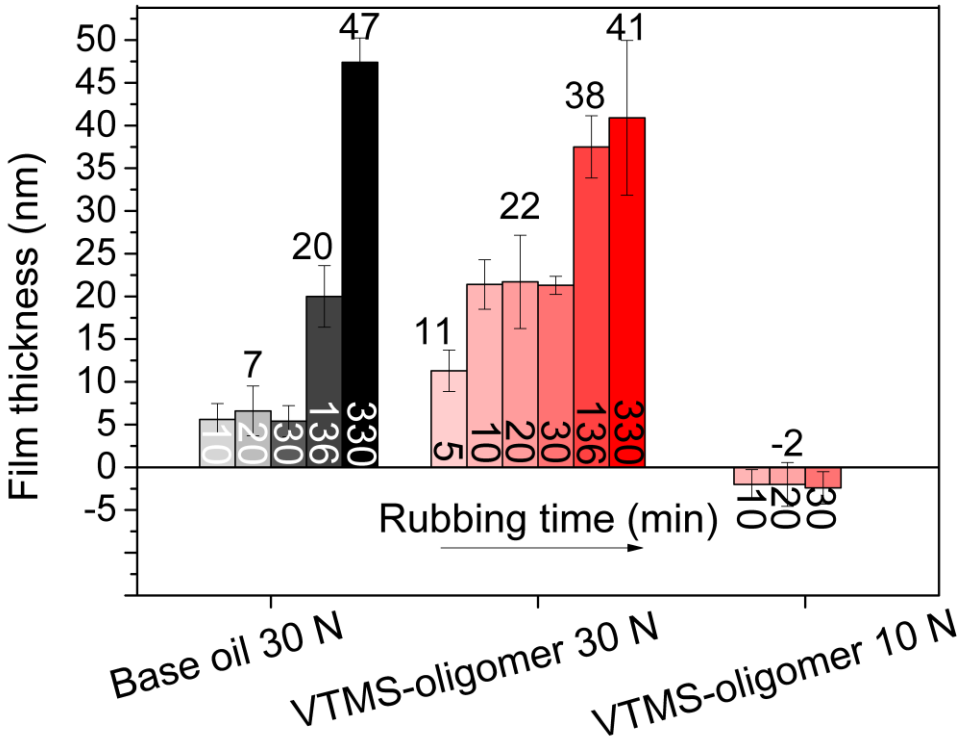

Figure 27: Measured average tribofilm step heights of tribofilms corresponding to the different rubbing tests.

After five minutes rubbing the corresponding Stribeck curve shows an increased cof in all regimes compared to the Stribeck curve before rubbing sequence. With the formation of the adhesive film an increased roughness is present. Therefore, the lambda ratio changes to lower values, which is synonymous for retarded full film lubrication. This behavior is clearly observable for all Stribeck curves above 5 min rubbing, from mean speeds between100 to 1000 mm/s. Interestingly, with the growth of the tribofilm until 10 min, also the reduction of the friction at low speeds from 0 to 70 mm/s vanishes. This is consistent with the sequence of layer formation, as the adhesive tribofilm is the decomposition product of the tribopolymer. Due to the adhesion and stronger networking, the film shows an increased resistance to shear, which is represented by increased friction. With increasing rubbing time, up to 30 min, no increase in tribofilm height is present. However, the reduction of friction takes place again after 10 min rubbing. This is attributed to the equilibrium between the formation of the polymeric layer and the decomposition of the polymeric to a stiffer and rough tribofilm. This equilibrium maintains also for at least 330 min testing time when comparing with the results in Figure 15. The Stribeck curves do not change after 30 min of rubbing the tribofilm, however, growths until around 2 h with only minor changes afterwards. Since the reduced friction in the boundary regime is connected to a minimum of tribopolymer concentration, it

can be deduced that the equilibrium between polymer degradation and tribofilm formation becomes stable after 20 to 30 min of rubbing under the given conditions.

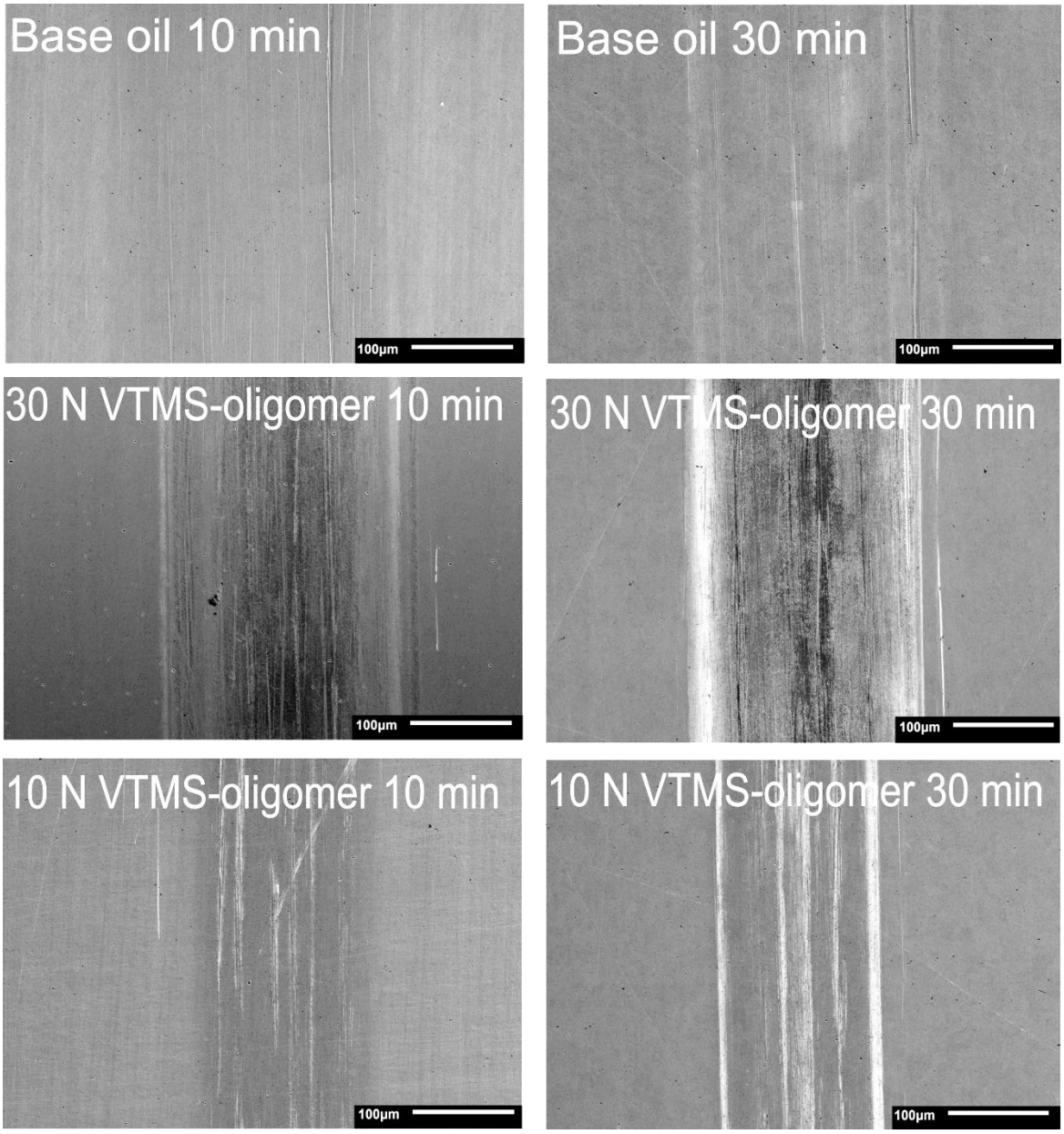

Figure 28: SEM images of wear tracks derived from different lubricants at different loading and rubbing times.

Figure 28 presents the obtained wear tracks and tribofilms from the rubbing experiments. Together with the results from EDX in Table 6 the continuous film growth can be followed by the increasing silicon and oxygen concentrations. Although no clear increase in tribofilm height is observed in the first 30 min, the silicon and oxygen concentrations raise with increasing rubbing time. Also the SEM images show slight changes between 10 min and 30 min rubbing. The wear tracks appear more uniform in damage or film formation with increasing testing time. Therefore it is concluded that the tribofilm height does not increase after a certain threshold, but deposits more uniform across the wear track. In addition, a

continuous but slower growth of film thickness beyond 30 min testing time can also be observed.

Table 6: EDX results of MTM disc wear tracks after different rubbing times. All area measurements are performed under similar conditions across the wear track, with 5 kV acceleration voltage.

Sample and rubbing time	Wear track composition [atom %]			
	Si	O	C	Fe
Reference Disc	0.4	0.2	4.7	94.7
Base oil 10 min	0.4	1.6	4.9	93.1
Base oil 30 min	0.4	2.4	5.1	92.1
30 N VTMS-oligomer 10 min	2.0	2.9	6.0	89.2
30 N VTMS-oligomer 30 min	3.7	5.5	7.0	83.8
10 N VTMS-oligomer 10 min	0.42	-	5.0	98.7
10 N VTMS-oligomer 30 min	0.54	-	5.31	98.5

Experiments with lower contact pressure have been performed in order to investigate the influence of load on film formation. Further it must be pointed out that lower loads are connected to lower tribological stress. Especially the influence of temperature increase by rubbing and influences by wear or oxidation on the steel surfaces is discussed more in detail. Therefore, tests with a load of 10 N have been performed, which corresponds to a Hertzian pressure of 0.66 GPa. The standard conditions run with a load of 30 N which corresponds to a Hertzian pressure of 0.95 GPa. The change of pressure on the lubricating conditions is negligible at mean speeds of 100 mm/s, as the lambda ratio results to $\lambda(h_0) = 0.72$ with a minimal lubricating film thickness of $h_0 = 8.2$ nm. This means the system runs still in boundary lubrication, but the surfaces experience lower stress.

The results concerning the tribofilm height and wear track images are shown in Figure 27 and Figure 28, respectively. Whereas, the term tribofilm is misleading since no tribofilm is formed. Neither the silicon or oxygen concentrations from EDX measurements in Table 6 nor the profilometer characterization give any confirming results in respect to the formation of a SiOC containing tribofilm. The corresponding friction curves are shown in Figure 29. The Stribeck curves after different rubbing times show no increase in friction by a tribofilm in the region of 100 to 1000 mm/s, which is consistent with the previous discussed findings. However, at speeds below 100 mm/s a slightly lower friction compared to pure base oil can be observed. This is again due to the formation of polymeric layers, which is a thermally activated process

and already known from the former tests. Similar to the Stribeck curves, the rubbing curves do not show an increase in friction, which can be attributed to no formation of an adhesive tribofilm. Instead the rubbing curves show a decrease in friction with a cof of around 0.04 to 0.032 after 30 min of rubbing. This behavior is again attributed to the formation of a lubricating siloxanic polymer layer. In total, these findings highlight the necessity of tribological stress, for the formation of precursor derived tribofilms. Furthermore a threshold and dependence of pressure on the adhesive film formation is observed.

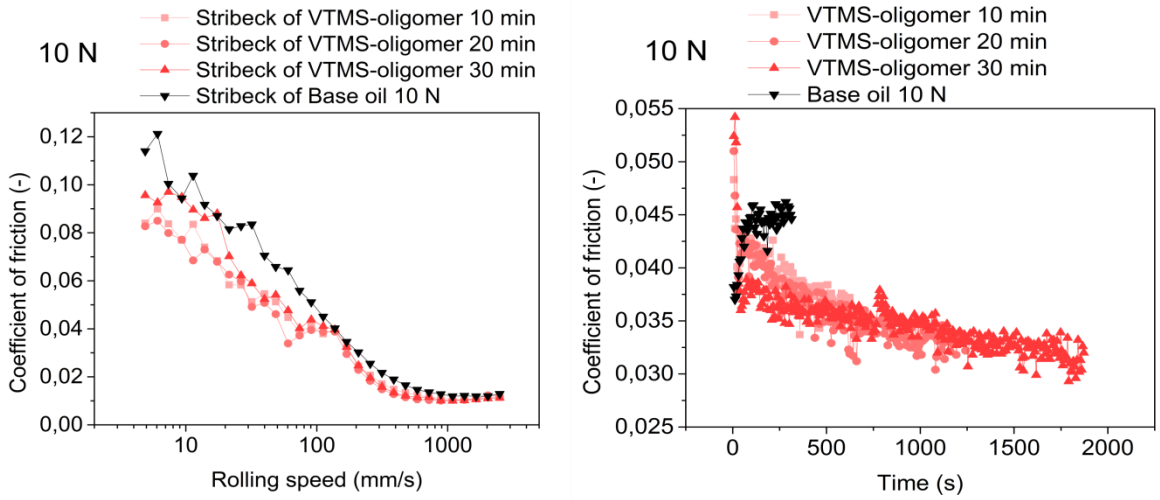

Figure 29: Left) Stribeck curves measured after different rubbing times (10 N, 100 °C, 50 % SRR) and right) Friction coefficient over rubbing time of the corresponding tests (100 mm/s).

Tribological stress is a big term, which includes factors like flash temperature rise, contact pressure, triboemission and surface catalysis. The influence of static pressure on the formation of zinc dithiophosphate glass-like tribofilms was investigated by Tse *et al.* and the authors could not observe significant influences of pressures of up to 18 GPa on the transformation and cross-linking of phosphate groups [101]. Fujita and Spikes have investigated the raise of oil temperature by frictional heat and its influence on the zinc ditiophosphate tribofilm formation [26]. They observed that the temperature raise is not the key driver for the formation of such films. However, the increase in heat can become quite significant with high sliding speeds. In order to estimate the raise of oil temperature equation 23 is used [102].

$$T_{oil} \approx T_s + 1.1\frac{\mu p_0 U_s a}{2K_s} \tag{23}$$

Where T_{oil} is the oil temperature between the contacting surfaces, T_s the temperature of steel specimens and K_s is the thermal conductivity of the steel specimens. T_s can be taken as 100 °C, since the total frictional heat $\Delta T_{Fr} = \mu \cdot p \cdot U_s$ would account to 1.9 W, which would not significantly increase the steel specimen's temperature. K_s is taken as 30 W/mK, the cof as

0.065 and *a* corresponds to 123 µm at a load of 30 N. So at a sliding speed of 50 mm/s T_{oil} would account to 107 °C. The change of around 7 °C is not significant but nevertheless it is still an influence which should not be neglected. The change to 10 N results in an oil temperature raise of only ≈ 3 °C to 103 °C, so the temperature raise of the lubricating oil film, by the different load conditions is concluded as not the primary influence.

As mentioned, with reduction of contact stress, also less wear and oxidation is possible, which is shown to influence the deposition behavior of the tribofilms in the following. How the state of the surface impacts the polymer to ceramic transformation was already addressed in the theory section and in literature [56, 65]. A clear indication for contributions by the surface can be seen by the development of tribofilm thickness over time. A fast increase in film thickness can be tracked during the first 10 minutes, which declines afterwards for the tests with a load of 30 N. The formation and influence of iron oxides on tribofilm formation is known to have an impact and information can be gathered from the wear tracks corresponding to short rubbing tests. Figure 30 presents micro-Raman spectra from different disc wear tracks and regions of 30 N and 10 N loading tests.

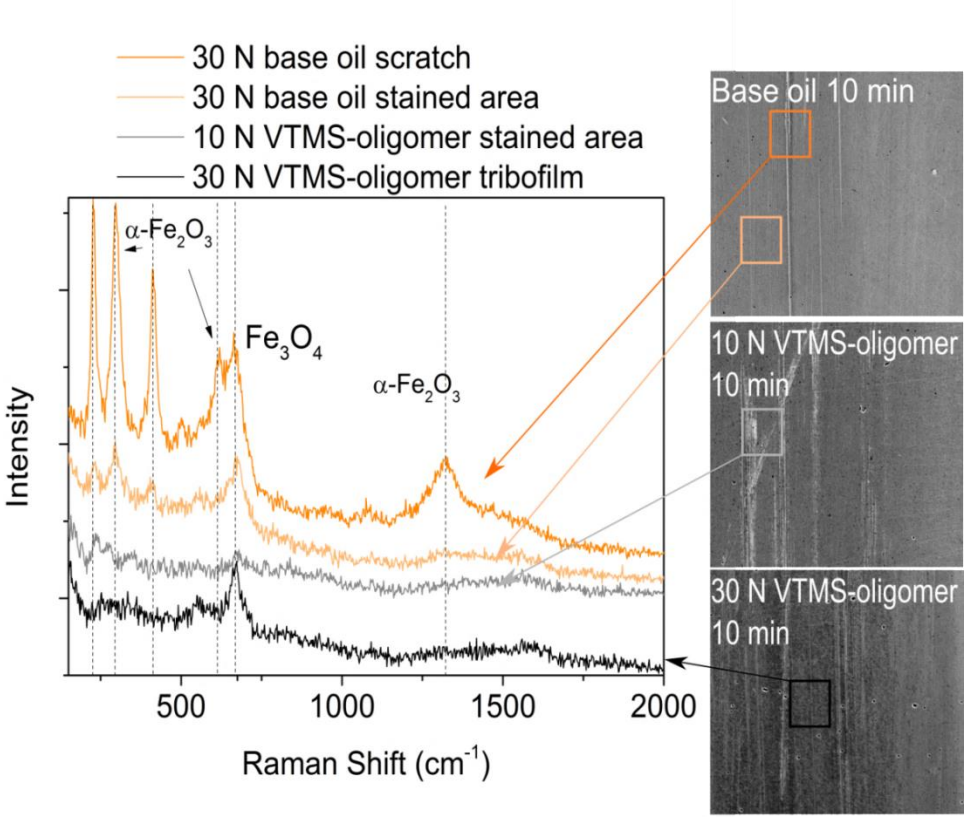

Figure 30: Micro-Raman spectra of MTM disc wear tracks tested with base oil as well as 2 wt.% VTMS-oligomer blend. The spectra are obtained on different spots on the wear track, see images for clarification.

The two top spectra are obtained on a scratch and besides a scratch, on a wear track after 10 min rubbing with the base oil. Signals from the scratch suggest that hematite is the major iron oxide. However, besides the scratch the intensity ratios between hematite and magnetite signals swap and magnetite is the major component. Therefore, it can be deduced that wear in form of scratches is influencing quite significantly the formation of hematite. The Raman spectra are in consistence with the EDX results from Table 6, as the oxygen values increase with the presence of iron oxides. The light grey spectrum corresponds to a stained region on the wear track, obtained after 10 min rubbing at a load of 10 N with the addition of the VTMS-oligomer. Although small scratches can be seen, no clear signals for iron oxides can be observed, only a very small hump might be attributed to oxidation. In contrast the spectrum obtained at 30 N with precursor addition shows clear signals from magnetite. Again signals of magnetite match with the presence of a SiOC containing tribofilm, which is not the case for the wear tracks obtained under a load of 10 N. The results exhibit, that magnetite is formed in the early stage of film formation. Further, the transformation from magnetite to hematite is hindered by the formation of the SiOC tribofilm. At this point, it is possible to conclude that the low intensities of the magnetite signals indicate the tribofilm growth on top of the magnetite layer. Also it can be deduced that this layered structure is stable for longer testing times, which can be seen from the six h test results in Figure 22. The complex role of oxidation and its necessity for tribofilm growth is cleared together with the dependences of temperature, after the next section.

The dependence of the testing temperature on polymer and film formation has been investigated by MTM tests running at 40, 60, 80 and 100 °C. Figure 31 presents the measured Stribeck curves after around 2 h testing time for the base oil and the VTMS-oligomer/base oil mixtures. Additionally SLIM images have been recorded after Stribeck curve measurements at different testing times and are given in Table 7. The Stribeck curves from the tests with base oil in Figure 31 show how the viscosity at different temperatures influences the lubricating conditions.

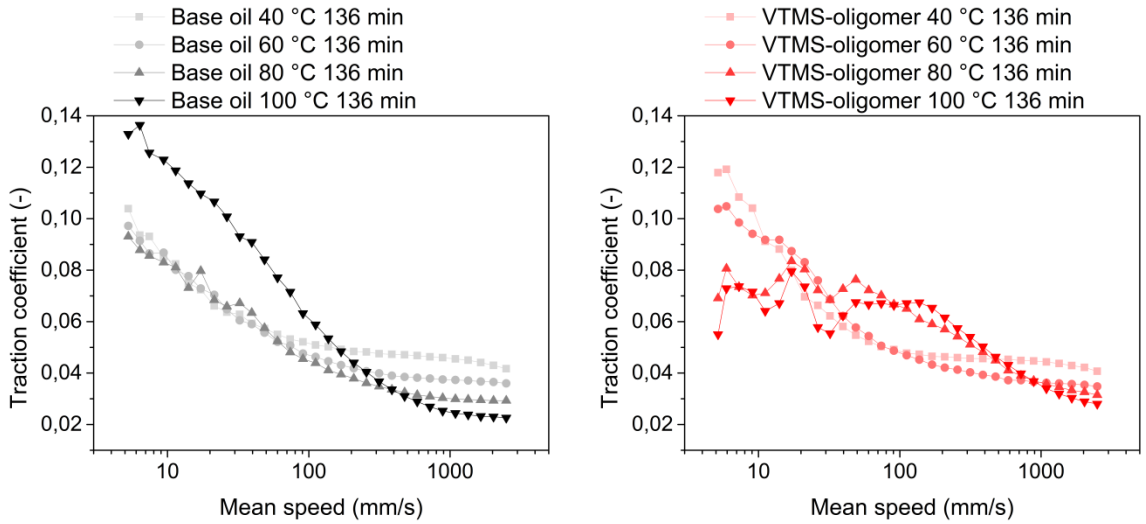

Figure 31: Stribeck curves measured after around 2 hours testing at different temperatures (30 N, 50 % SRR) with base oil and 2 wt.% VTMS-oligomer samples.

The viscosity decreases with increasing temperature, therefore thicker lubricating film thicknesses are achieved with the same speed at lower temperatures. The entrance to the EHD regime can easily be observed by the change of the slope to a nearly constant cof at high speeds. Thus, at lower temperatures the EHD regime is reached at lower mean speeds. However, also the strong influence of viscosity on EHD friction can be seen, as the friction in EHD is mainly influenced by the viscosity of the fluid. The boundary friction is similar for all temperatures, except for the test at 100 °C. This shift to higher cof is attributed to a higher roughness from corrosive products, compared to the tests at lower temperatures. The SLIM images illustrate similar deposits for temperatures below 100 °C. Although stains on the wear tracks from 40 to 80 °C tests are obtained, no significant increase in average tribofilm height is detected. Nevertheless, the wear tracks are roughened due to few scars and dark deposits, which reach in case of the 60 and 80 °C sample up to 20 nm. But the wear tracks do not show a uniform step height over the wear track, except at 100 °C. An overview of average film heights is given in Figure 32.

Polymerization and film formation are displayed with the images in Table 7. First polymeric deposits can be seen in case of the 60 °C test, it appears that the amount or size of deposits increase with testing time and testing temperature. Although, first signs of polymeric deposits can be seen at 60 °C no influence on lubrication can be derived from the friction curves in Figure 31. It was stated already, that the friction reduction in the boundary regime is caused by the polymeric film. However this does only apply if the polymeric film is thick or stable enough to separate the contacting surfaces. So it needs to be at least thicker than the

roughness of the surfaces. In case of the test at 60 °C the volume of polymeric species on the surface is insufficient, which will be proven in detail in the next chapter.

Table 7: MTM SLIM (ball wear track) images recorded at different testing times, from tests at different temperature with base oil and 2 wt.% VTMS-oligomer addition.

Time [min]	3	27	136	Time [min]	3	27	136
VTMS-oligomer 40 °C	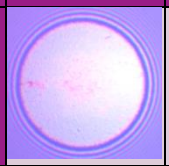	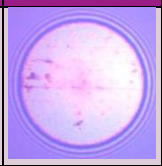	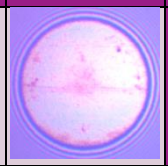	Base oil 40 °C	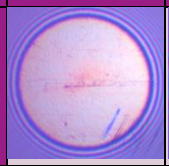	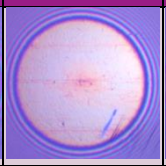	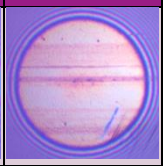
VTMS-oligomer 60 °C	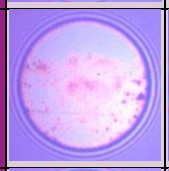	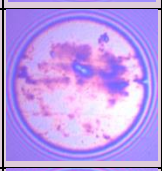		Base oil 60 °C	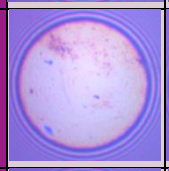	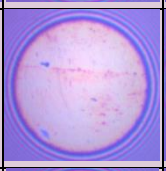	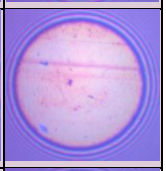
VTMS-oligomer 80 °C		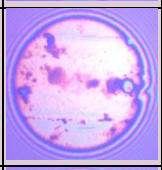		Base oil 80 °C	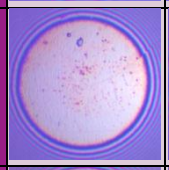	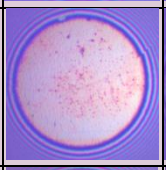	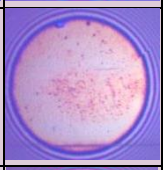
VTMS-oligomer 100 °C		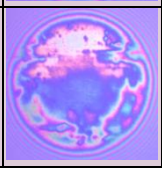	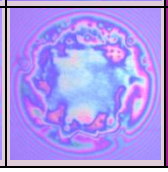	Base oil 100 °C	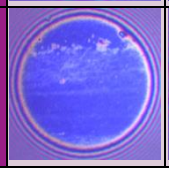	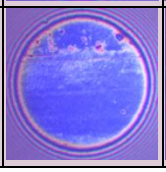	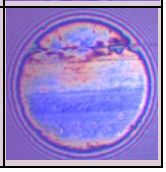

The Stribeck curves at 80 and 100 °C exhibit the familiar profile with the delayed EHD regime and lower friction in the boundary regime. Interestingly, the Stribeck curves for both temperatures do not differ from each other. Only slightly higher cof values above 2000 mm/s reflect the higher viscosity at 80 °C in the EHD regime. Also no influences of temperature on the cof in boundary conditions can be seen for the tests at 80 and 100 °C. It appears that the viscosity or shear strength of the polymer film does not depend significantly on the temperature above certain threshold, which will be discussed in the next chapter.

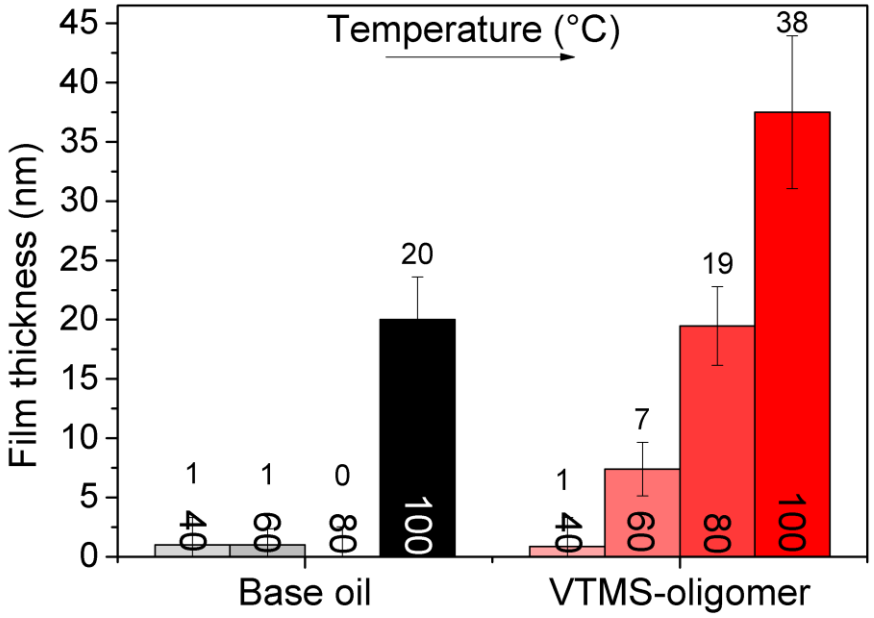

Figure 32: Measured average tribofilm step heights with profilometer for the different testing temperatures and oil samples.

The average tribofilm heights from the temperature tests are given in Figure 32 and SEM images from the precursor derived wear tracks are displayed in Figure 33. First signs of film formation are obtained at 60 °C, also with appearance of polymeric deposits in Table 7. Similar to the polymer deposits displayed in the SLIM images, also the tribofilm thicknesses increase with testing temperature. Together with the results from the timed tests, it becomes obvious, that the tribofilm formation depends on the existence of polymeric layers. It may be deduced that higher polymer concentration favors the deposition of tribofilms, as the source for tribofilm formation increases. On the other hand higher temperatures favor the bond breaking of Si-C bonds and redistribution reactions to a more silica like structure, which is the main mechanism for the silica rich adhesive tribofilm. Whether higher polymer concentrations or only a threshold is necessary for tribofilm formation is not clear from the results. The increase in volume of polymer in the rubbing contact can be seen either from SLIM images and/or from a critical polymer film thickness in the tribocontact, at which lower friction is obtained. This critical polymer film thickness will be further investigated in the next chapter.

Finally the discussion about the role of iron oxide on the tribofilm deposition is now continued with a detailed view on the SEM images and Raman results in Figure 33 and Figure 34, respectively. The SEM images are in consistence with the average film thicknesses from Figure 32, since a growing film height can be seen with increasing testing temperature. While no signs of deposits can be seen on the wear track from the 40 °C tests. First deposits are

obtained on the wear track from the test at 60 °C. The average film thickness of around 7 nm results from an inhomogeneous film deposition, which is exemplary displayed in the image with higher magnification. The images show, that tribofilm formation appears concentrated on more stressed areas, which suffer from wear. This similarity with iron oxide formation was given in the previous section and is now further discussed.

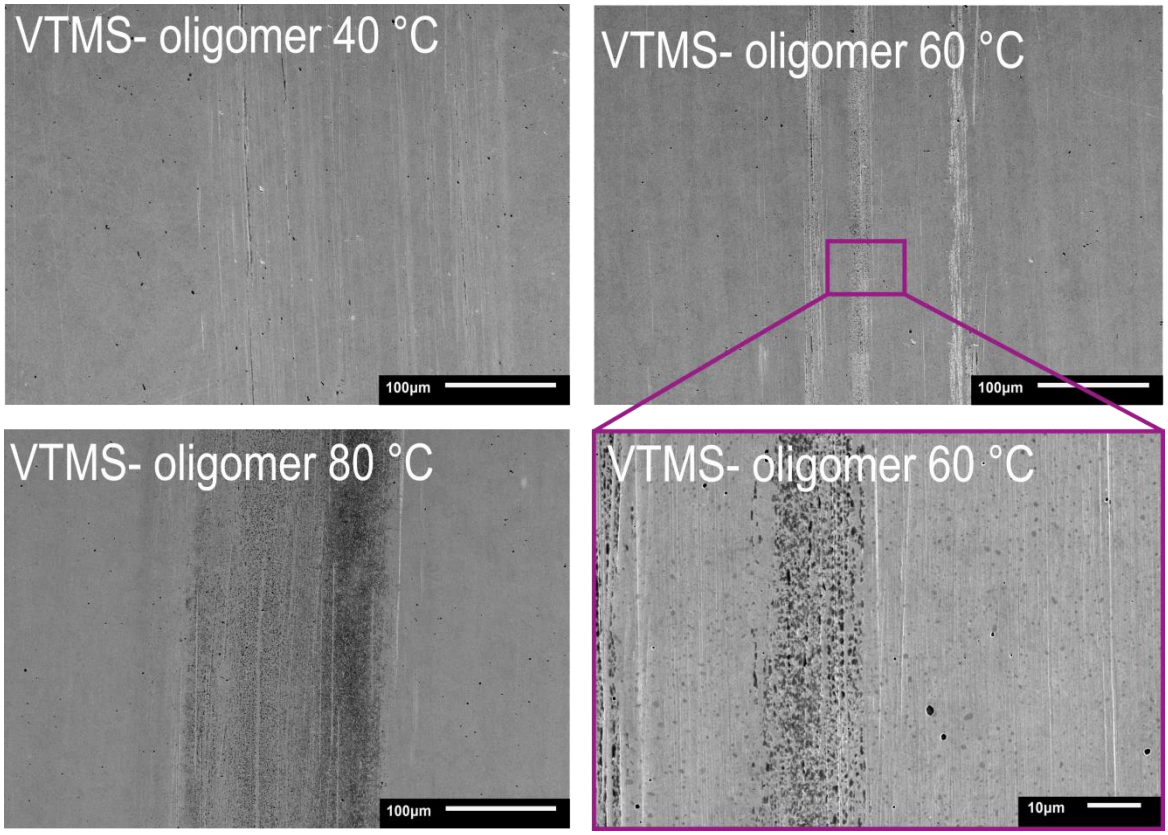

Figure 33: SEM images of wear tracks derived from VTMS-oligomer samples at different testing temperatures.

Raman spectra from these scratched areas, in Figure 34, prove that iron oxide is present also for the tests starting even at 40 °C, although the signals are weak. Again the signal intensities of the iron oxide bands corresponding to the VTMS-oligomer derived wear tracks are lower than for the corresponding base oil spectra. Interestingly, the signal intensity corresponding to the 80 °C derived wear track is even lower than that formed at 60 °C, which might be due to a thicker tribofilm and thus attenuation of intensity. The mechanical activation and oxide film growth in tribological contacts are already well investigated for steels [103]. It is stated, that thin oxide films form quickly by rubbing. Fe_3O_4 is known as the high temperature oxide, which generally forms at around 250 °C in rubbing contacts in normal atmosphere. In lubricated contacts, the oxygen diffusion is more limited and therefore magnetite is the expected oxide. It cannot be cleared from these experiments whether a thin oxide layer is necessary for the deposition of the tribofilm, but all results prove a clear correlation and is in accordance with literature. In addition, the growth of the siloxanic tribofilm on top of a magnetite modified surface is quite logical from the perspective of stronger polar attractions. Depending on the conditions, the presence of OH^- from the oxidation reactions may not only lead to attraction between the precursor and surface, but may also serve as a source for reactions with the siloxane precursor.

The iron oxide surface is also much more polar and exhibits higher surface tension than steel, which favor the attraction of siloxanic tribopolymer to the surface [45]. It must be noted, that stronger attraction between the polymeric species and the surface is the key property and crucial for the tribofilm formation. When the attraction onto the surface is strong enough, then the polymer cannot be sheared off, by the high shear rates during rubbing. The consequence is the transformation to a silica rich structure due to the severe conditions at the contacting asperity. Therefore, from this context the prior formation of magnetite is an important aspect for bonding and growth of the tribofilm. Thus, it would be of interest to investigate whether the pad-like structure of the tribofilm is determined by the growth of iron oxide on the surface.

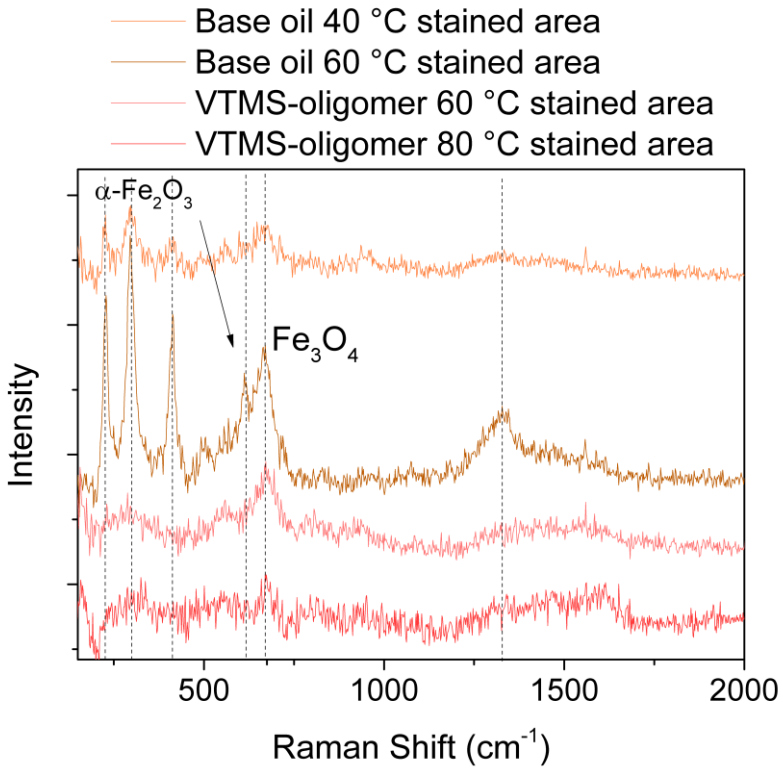

Figure 34: Micro-Raman spectra of MTM disc wear tracks tested with base oil as well as 2 wt.% VTMS-oligomer blend. The spectra are obtained at different testing temperatures only on stained areas on the wear track.

In total, all discussed dependences and influences on the tribopolymer and tribofilm formation are summarized in the following. It has been shown that the tribopolymer formation is highly dependent on the testing temperature. The investigations show that the tribopolymer is formed prior to the tribofilm and both stay in equilibrium so that the polymer formation balances the decomposition of the polymer into the tribofilm. Further it is shown that the tribofilm formation is dependent on the presence of the polymeric species. In addition, the observations from different loading as well as temperature testing conditions give a much better understanding of the role of iron oxidation on the tribofilm formation. The surface oxidation is shown to be crucial for the deposition of the adhesive tribofilm. Also it is suggested that the SiOC tribofilm is deposited onto layers of magnetite.

4.2. Lubrication mechanism and anti-wear effects of siloxane tribopolymer and tribofilm

This chapter builds on chapter 4.1, where a detailed description of the chemical and structural design of the reaction layers is given. Also some influences of the model precursor on friction have been introduced already, even for different testing conditions. However, no detailed derivation, which builds on and considers theory of lubrication, has been presented yet. Therefore, this chapter presents tribological test results and discussions, explaining the influences of the model precursor on tribological parameters, such as the impact on the lubricating film thickness and the shear strength of the formed polymer layers. With these results, a lubrication model for cross-linkable organosilane/-siloxane oil additives is presented. In addition, the anti-wear behavior of organosilane/-siloxane precursor is briefly discussed on the basis of their lubrication model.

4.2.1. Lubrication mechanism of organosiloxane tribopolymer and tribofilm

The following discussion is based on the findings from the previous chapter about the film formation and the knowledge about the structure and chemistry of the multi-layered film. It is already described that with the presence of the polymeric layers a reduction of friction is obtained in the boundary and mixed lubrication regimes. Also an increase in friction at higher speeds was observed as soon as a solid tribofilm emerged. The typical Stribeck curve profiles from the precursor tests, with lower cof at slow speeds but increased cof at higher speeds, suggest a shift of the EHD regime to higher entrainment speeds. Thus, which parameter and material properties cause these friction changes and shift the lubrication regimes is discussed in the following.

A short overview of properties and mechanism of friction modifier additives or anti-wear additives is already given in the theory chapter. The investigated tribopolymer does not fit into the category of typical friction modifier, as neither the polymer has a structure similar to stearic acid with long non-polar tails nor is a two dimensional crystal with low shear strength planes, such as graphene or MoS_2. As their mechanisms are structure dependent, another mechanism is expected for the polymeric cross-linkable siloxane. The lubricating behavior of polymeric oil additives and boundary lubricating layers has been extensively investigated by H.A. Spikes in the 1990's and 2000's, where he also defined the term boundary film as "Films which must have been formed by the physical or chemical interaction of the solids and the liquid during use and will have structure and thence properties distinguishable both from the bulk liquid and from the rubbing solids" [104, 105]. Significant advances have been made by

the development of optical interferometry, which enables *in-situ* measurements of the lubricating film thickness. The technique is generally abbreviated with "EHD measurement" and is applied in order to investigate the lubricating mechanism of the reaction films. Figure 35 shows the results from the EHD test, which is done with settings matching the standard MTM testing conditions. The slope of the base oil curve exhibits a value of 0.66 from around 30 mm/s to 3000 mm/s and matches with the theory and equation 19, where the film thickness dependence on speed is stated with a power of 0.67.

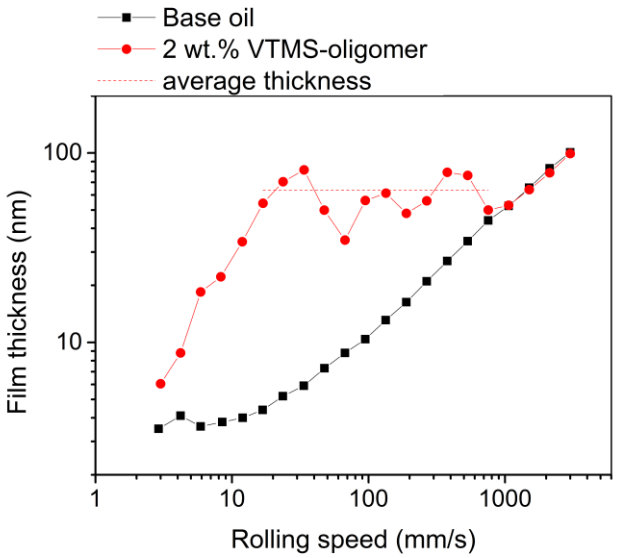

Figure 35: EHD measurement results, lubricating film thickness over rolling speed for base oil and 2 wt.% VTMS-oligomer mixture (30 N, 100 °C).

The red line presents the test results from the precursor mixture, the dotted line is the average lubricating film thickness over the given entrainment speed interval. The lubricating film thickness increases strongly already at low speeds from 3 to around 20 mm/s and reaches a plateau with an average value of 63.5 nm. This plateau displays a zig-zag profile with deviations in the lubricating film thickness of up to 30 nm and lasts until 800 mm/s. No differences between the base oil and precursor mixture test results can be observed at higher speeds. Based on these results it becomes clear, that the formation of a polymeric organosiloxane layer is supporting the lubrication at slow to medium speeds, by increasing the lubricating film thickness. Also these organosiloxane layers show a dependence on the entrainment speed and thus are of viscous rather than solid nature.

This behavior has been reported and investigated already with other dissolved polymeric oil additives [106, 107]. The investigated polymers form thick layers of adsorbed polymers at slow speeds, which possess much higher viscosities than the bulk fluid. At higher speeds these

polymer rich films break apart and the bulk fluid acts again as the main lubricant. This behavior is schematically sketched in Figure 36. Interestingly, these polymer rich boundary layers act similar to highly viscous oil or wax, so that their behavior can even be predicted by EHD theory [108]. Nevertheless, the literature EHD measurement results do not fully coincide with the investigated organosiloxane polymers. The reported boundary films generally start at film thicknesses of around 10 to 20 nm and then adapt at medium speeds to the lubricating film thicknesses of the bulk fluid [106, 107]. This means, the reported polymer films do not grow but diminish under shear stress [109].

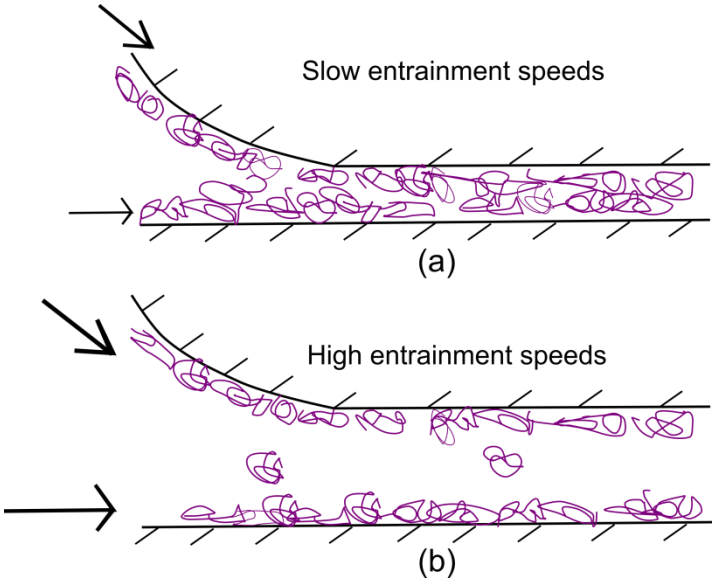

Figure 36: Schematic model of polymer rich boundary films. a) at slow speeds the adsorbed polymer fills the contact inlet and prevents asperity contact, b) at higher speeds, the inlet viscosity is based on that of the bulk fluid. Redrawn from [108].

This different behavior is connected to and can be explained by the molecular structure of the investigated polymers, which have also extensively been tailored. It was found out that (i) the polymers need polar functional groups able to adsorb on metal surfaces, (ii) the functional groups should be clustered, like in co-block-polymers rather than statistically distributed and (iii) high molecular weight polymer form more stable and thicker boundary films than that of low molecular weight polymers [19, 107].

Although, the findings from literature fit well with the behavior of the organosiloxane precursor, some differences in the properties and dependences are obvious. Similar to the hydrocarbon polymers, the model-precursor contributes to the lubricating film thickness at very slow speeds with additional 4 to 20 nm. However, the lubricating film thickness increases steadily until a plateau at high film thicknesses is reached. This build up features a slope of 1.2 compared to 0.67 from equation 19, which is contradictory with the given boundary film

model. Based on the polymer rich boundary film model and given testing conditions, three parameters must have changed with testing time or mean speed to cause such a change in slope. A reduction of the combined Young's modulus, an increase in pressure viscosity coefficient and most expected an increase in viscosity would lift the slope. The change of the combined Young's modulus can be neglected, because of the viscous nature of the polymeric films and their low thickness, since this contribution originates from the solid counterparts. Therefore, the viscosity and/or pressure viscosity coefficient must have increased with entrainment speed or time.

Luckily an easy estimation for the impact of the variation of viscosity pressure coefficient on the lubricating film thickness can be done with the help of T.J. Zolper et.al.'s work. They investigated different polysiloxane lubricants in terms of their lubricating behavior and material properties. Generally the coefficient becomes higher with higher fractions of bulky groups, such as phenyl groups [60]. From T.J. Zolpers work it can be read that a polysiloxane with a phenyl grafting on every second Si-O unit has one of the highest pressure viscosity coefficients in his work with 23.7 GPa^{-1}, the base oil in the present work has 14 GPa^{-1}. In order to check the impact of a change of pressure viscosity coefficient, the base oil viscosity is taken constant but the high pressure viscosity coefficient from the literature work is taken and the lubricant film thickness is calculated with equation 19. It has been shown that the base oil viscosity is nearly equal to the precursor oil mixture viscosity. This estimation would account to an increase of lubricant film thickness of around 24% by the change of the pressure viscosity coefficient. Thus the change or impact of the pressure viscosity coefficient is not comparable with the extreme differences, which are observed in EHD measurements with the model precursor. Nevertheless it is believed, that this contribution does also play a role, but not to a high extend, as it cannot describe the high film thicknesses. In total only the change of lubricant viscosity or in this case boundary film viscosity could have such a strong impact on lubricating film thickness and is discussed in the following.

Simple predictions of boundary film viscosities can be done by transposing equation 19 and taking the film thickness results from Figure 35. Accordingly equation 24 provides an average viscosity of oil and polymer films.

$$\eta_{avg} = \left(\frac{h/k}{U^{0.67}}\right)^{1/0.67} \tag{24}$$

The average viscosity is calculated with the pressure viscosity coefficient of the used base oil, k summarizes all other constants. Smeeth *et al.* used this approach to justify that polymer rich boundary films act similar to EHD films. The calculated viscosities are normalized to the base

oil viscosity at 100 °C and plotted in Figure 37. The figure describes how the boundary film viscosity of the VTMS-oligomer differs from the pure base oil viscosity, based on the EHD test results. The maximum viscosity is around 74 times higher than the base oil viscosity, which would attribute to a viscosity of 318 mPas. This value is achieved at a speed of 23.6 mm/s and also displays a point of inflection. A more detailed view for the change of the calculated relative viscosity is given by the right graph in Figure 37, which displays the first derivative of the relative viscosity by the variation of the rolling speed.

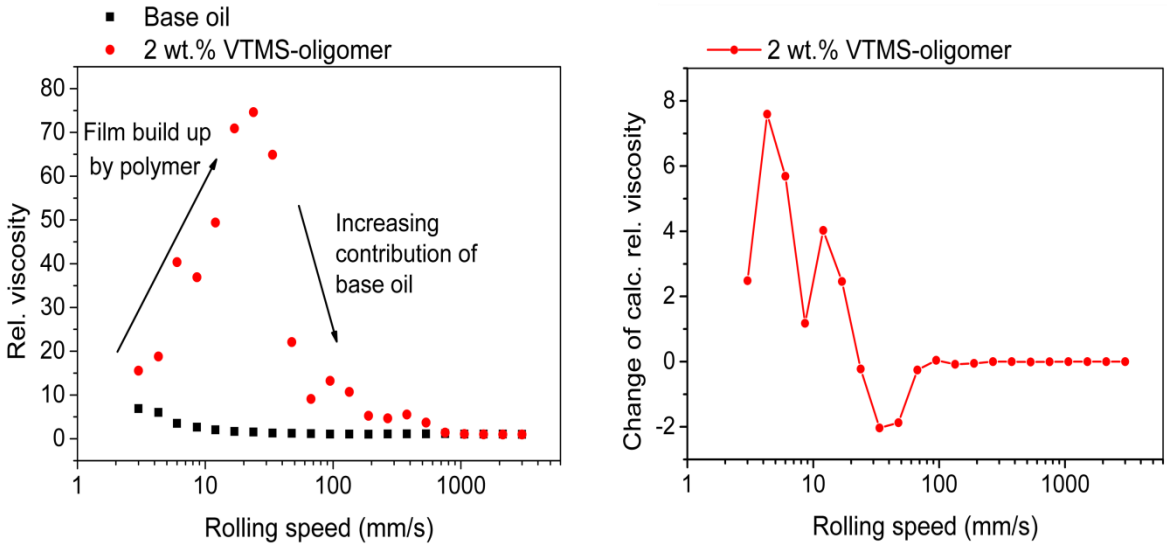

Figure 37: Calculated average viscosity (relative to base oil viscosity) over rolling speed for base oil and the VTMS-oligomer solution (left), (right) change of calculated relative viscosity of the VTMS-oligomer boundary film with rolling speed.

The profile of the graph illustrates that the biggest changes in viscosity and thus film thickness, relative to the base oils viscosity, appears during very low speeds and more or less steadily decreases. After the inflection point at 23 mm/s the change of the rel. viscosity becomes negative, as the base oil fraction of the boundary film increases. The variation of viscosity at higher speeds becomes small and levels to zero when the base oil viscosity is reached.

Although the values for the calculated rel. viscosities appear very high, they are in the same order of magnitude as other reported boundary films [19, 108]. Extraordinary is the high slope and increase of viscosity with the speed, compared to a steady decrease which is described in the given literature. This however, can be explained by the molecular structure of the polysiloxane tribopolymer. The reported hydrocarbon boundary film former have functional polar groups, which enable Van-der-Waal attraction towards the surface. The boundary film stability is therefore, only maintained by the fraction and design of the polar groups of the polymers. In case of the organosiloxane precursors a three dimensional network

by condensation reactions can be formed. First this network is generally polar, since it exhibits on every Si atom at least one polar alkoxy or Si-OH group. Second, the ability to form bonds between each other and with the surface increases the stability and thus offers the possibility to expand in concentration and volume in a much higher level. In contrast to the already reported boundary layers, the strong attraction and high stability of the organosiloxane polymer layers have the ability to grow even during motion.

Interestingly, even the zig-zag profiles, which are observed for the friction as well as for the film thickness measurements can be explained in this context. The EHD measurements show film thickness variations at a plateau from low to medium speeds, similar to an average cof at equal speeds. It is assumed, that during the growth of the polymeric boundary film, besides physical attraction and entanglement, also chemical bonding play an important role. Therefore, it is imaginable that these boundary layers become steadily more cross-linked with each other and with the surface, ending up in a gel-like film. While cross-linking continues, also elasticity increases with viscosity and thus film thickness of the gel-like film rises. Simultaneously the shear strength of siloxanic gels increase with their cross-linking degree and therefore, the gel-like tribopolymer layer resists stronger to motion, which is detected as increased friction. Since these layers are constantly exposed to a steadily increasing shear stress, bonds and entangled parts break apart, when a given film thickness and cross-linking is reached. The result is again a drop in friction due to lower shear strength of the network.

Up to now it was considered that the film thickness depends only on the change of entrainment speed, which is logical following hydrodynamic theory. But the applied lubrication theory by Hamrock does not account for liquids, whose viscosity may be time dependent.

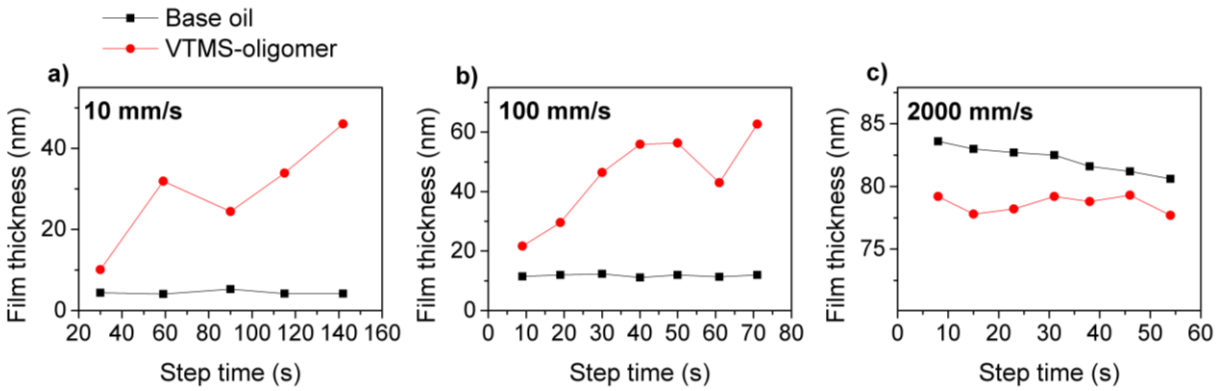

Figure 38: Measured film thickness versus time at constant entrainment speeds, a) 10 mm/s, b) 100 mm/s and c) 2000 mm/s, for base oil and 2 wt.% VTMS-oligomer mixture (EHD, 30N, 100 °C, pure rolling). A 2000 mm/s, 30 N, 10 s timed step was conducted between the 10 and 100 mm/s measuring steps to shear concentrated polymer out of the gap.

The observed decay of variation of rel. viscosity over rolling speed at low to medium speeds appears quite strong, therefore, the time dependence on lubricating film thickness build up is tested and results are shown in Figure 38. As predicted, the film thickness increases at slow and medium speeds over time. Whereas no significant changes on film thickness compared to base oil is observed at high rolling speeds. This behavior is consistent with the given explanation involving the interactions, primarily the attraction of the tribopolymer with one another. While the film thickness raise rather slow at low speeds with around 0.3 nm/s. For medium speeds a film built up of 1.1 nm/s is achieved during the first 30 seconds until a plateau at a film thickness of 56 nm is reached. With the rate of film built up over time, and the partial derivation of time of equation 24, the change of viscosity with time can easily be estimated. The result gives a change of the relative fluid viscosity of 5.6% per second in the case of 10 mm/s, while in the case of 100 mm/s the change of rel. viscosity is only 3.5% per second. Also the higher rate of viscosity change at lower speeds is similar to the previous derivation for the rel. viscosity changes with speed. The change of 3.5% per second at 100 mm/s is higher than predicted from Figure 37. The variation is ascribed to difference between constant and increasing speed conditions. In total it can be deduced that the cross-linking process and entangling is more disturbed at higher speeds and shear rates.

Unfortunately, longer testing times would be necessary to investigate the boundary film thickness limitations, but still the height of the plateau is quite similar compared to the test results with increasing entrainment speeds. Another interesting aspect is the boundary film stability, so which shear rates can the tribopolymer film withstand until it loses its lubricating function. In order to investigate this, MTM tests with different sliding to roll ratios at constant mean speeds are performed. The MTM owns the advantage of setting variable SRR accompanied with a high precision of acquiring friction torques. From the previous tests an average boundary film thickness is assumed and with equation 9 different shear rates can be achieved without the variation of the mean speeds. Also for this approach the assumption of Spikes, that polymeric boundary films act similar to EHD films is considered. A run-in procedure, with test conditions from chapter 4.1.1, of around 30 minutes is conducted so that equilibrium between tribopolymer and tribofilm formation is maintained. A sudden increase in friction can then be ascribed to the failure of the boundary film.

Figure 39 presents the results of the tests with mean speeds of 100 mm/s, 500 mm/s and 1000 mm/s. The friction values for 0 % SRR is only shown in a), the low values represent the friction in pure rolling conditions. Low coefficients of friction of around 0.06 are measured at 100 mm/s for SRRs between 25 and 75%, whereas a pronounced zig-zag profile is observed at a SRR of 25%.

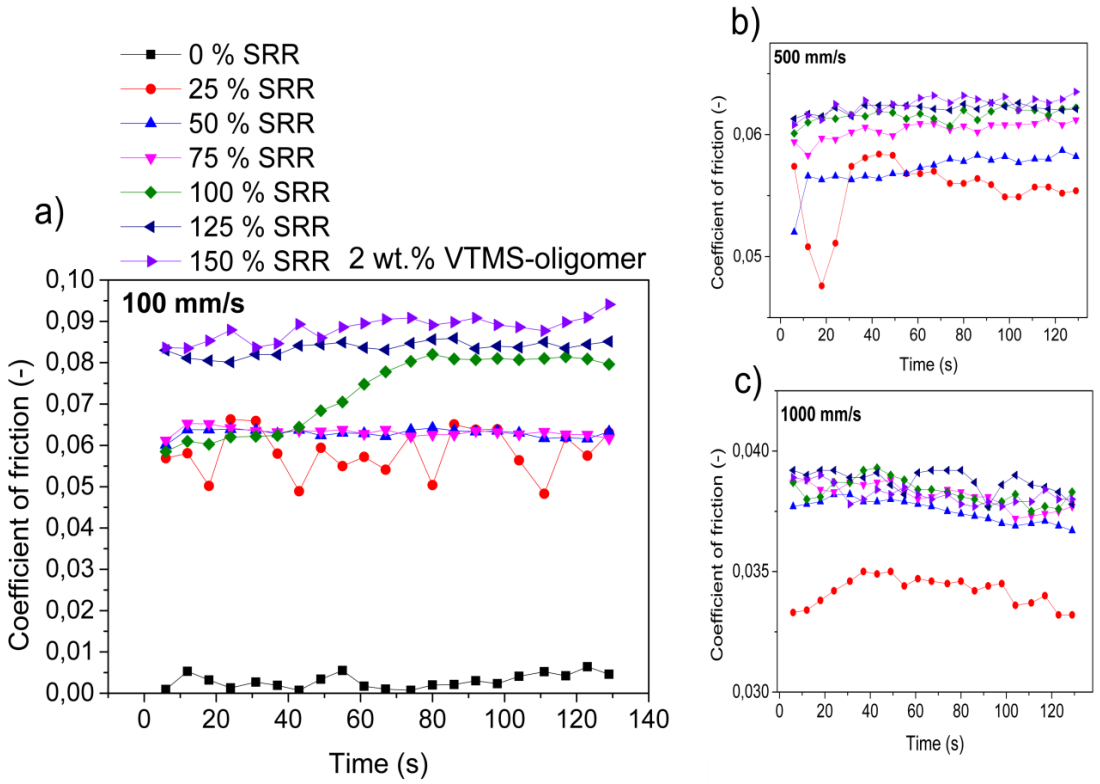

Figure 39: MTM test results with 2 wt.% VTMS-oligomer blends (30N, 100°C) for constant mean speeds a) 100 mm/s; b) 500 mm/s and c) 1000 mm/s over time and variation of the SRR. A 30 minutes run-in procedure with 100 mm/s rubbing steps was performed, prior to the variation of SRR steps.

At a sliding speed of 100 mm/s, a strong shift in the cof after around 40 s is detected, this levels then to a value of around 0.08. Higher sliding speeds start directly at cof values of 0.08 to 0.09 and stay constant during the timed steps.

A critical shear rate is seen at 100 mm/s sliding speed at which, no low friction and thus no boundary film formation is observed. In case of high sliding speeds no unexpected behavior or influences of the precursor on the lubrication is observed. The cof increases with increasing SRR, whereas the changes above SRR of 100% for the same mean speeds are rather low. Some interactions in the case of sliding speeds of 125 mm/s which account to a SRR of 25% at a mean speed of 500 mm/s are detected at the beginning of the sequence. However, the

course of the curves for SRR of 25% at higher speeds coincide very well with the base oil curves, so no influences can be attributed.

The test results coincide with the presented Stribeck curves from the previous chapters. The Stribeck curves show a transition from the boundary film lubricated regime into a mixed regime, observable by a change of slope, at around 150 to 200 mm/s. All previous test results are obtained with 50% SRR, which means that sliding speeds of around 100 mm/s are indeed critical for the boundary film stability. The sliding speeds can be transferred into shear rates by equation 9. Therefore, an average boundary film thickness of 60 nm is taken, which is obtained from the previous EHD test results. The critical shear rate would then account to $1.67*10^6$ 1/s. More interesting is the fact that the simplest approach for the prediction of viscosity by equation 7 gives results in the same order of magnitude, like estimated with the EHD boundary film approach of Spikes. The mean shear stress is calculated with equation 10 with the reduced friction values corresponding to a cof of 0.625 and a mean pressure over the Hertzian contact area, see equation 4 for the radius. The as calculated viscosity must be freed from the pressure contribution by the Barus equation 11. The obtained value accounts to 526 mPas compared to 318 mPas from the EHD results and the Hamrock approach for EHD films. Despite the big difference of the values, both values are only estimations for a cross-linking gel-like material, where fluctuations are expected. So the calculated values should not be taken at face value. Since they are in the same order of magnitude, they prove that the polymer rich boundary film approach of Spikes, which says that these films behave similar to EHD films, does also account for our used system, although their chemical nature and properties are quite different.

In line with the discussion from the previous chapter, the lubricating film thickness was measured at different testing temperatures and the results are given in the following. Figure 40 shows the difference in lubricating film thicknesses between base oil and VTMS-oligomer mixtures at different testing temperatures. The VTMS-oligomer has slightly higher film thicknesses at 40 °C, but no pronounced shifts can be observed. Nevertheless, it should also be noted that due to the higher viscosity at 40 °C the film thickness accounts to around 40 nm at 100 mm/s, which makes the detection of slight changes by the organosiloxane polymer difficult. But test results are consistent with the temperature program from the previous chapter, where first polymeric residues are observed at 60 °C in Table 7. Starting with 60 °C first increases of lubricating film thickness of around 20 nm between 10 and 300 mm/s can be observed. However, at 80 °C the film thicknesses are in the range of 50 to 60 nm at medium speeds and the curve profile exhibits the familiar zig-zag profile. Interestingly, the results indicate that the increase of film thickness appears at 100 °C already at lower entrainment speeds and also lasts for higher speeds.

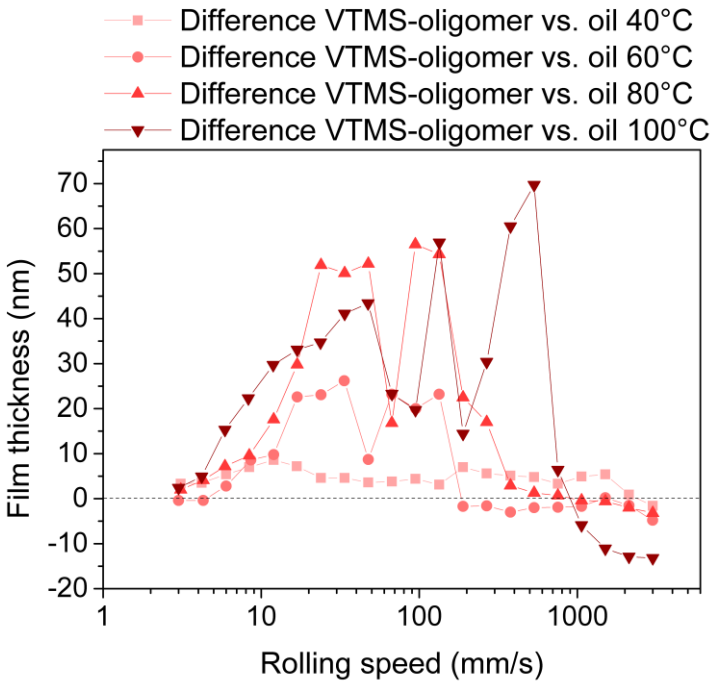

Figure 40: Difference of lubricating film thickness between base oil mixtures and 2 wt.% VTMS-oligomer mixtures, obtained by EHD measurements at different testing temperatures.

Also the comparison of the Stribeck curves of the 80 and 100 °C tests show, that at 100 °C the cof plateau lasts for slightly higher mean speeds, see Figure 31. Therefore, it is assumed, that due to the higher testing temperature also the tribopolymer formation is accelerated and favored. With increased reaction rates more polymer and also longer polymer are able to interact, which results in an earlier formation of a boundary film. The friction values and the

average lubricating film thickness appear however quite similar. This means, that the boundary film exhibits nearly the same properties as soon as a critical temperature of around 80 °C is reached. However, no information about influences by the different base oil viscosities on the boundary film formation is extractable.

Again, a decrease in film height compared to base oil, starting at around 2000 mm/s is seen for the 100 °C test, similar to Figure 38. It has been noted already, that the entrance of the EHD regime seems delayed, as the slope at 2000 to 2500 mm/s is still negative and no plateau is reached in the friction curves. Although the film thickness differences are not high at such high speeds, it may have an effect, if the surface is rough. Also the results from the 60 °C friction as well as lubricating film thickness measurements must be discussed by including the tribofilm influences into the theory.

Up to now the polymer rich boundary layer model was introduced and discussed. This model explains the behavior and function of the formed organosiloxane polymer. Unfortunately, the EHD test set-up is not appropriate to investigate the tribofilm lubrication and influence, as the thin glass layer is too fragile and thus no extended rubbing sequences can be performed. The advantage in examining the adhesive tribofilm influences on lubrication is that no dependence of speed is found concerning its micro structure and material properties. Therefore, the easiest approach to investigate its influence on friction and lubrication is to test a MTM disc and ball pair with deposited tribofilms.

Tribofilms have been deposited by a 120 min "standard" testing procedure, described in the experimental section with the precursor mixture. After the deposition, the specimens have not been demounted but extensively rinsed with benzene. The tribofilm Stribeck measurement has been performed with pure base oil. The results are given in the following as comparison between the different investigated surface conditions, polished steel, siloxanic boundary layer, tribofilm with boundary layer and only tribofilm.

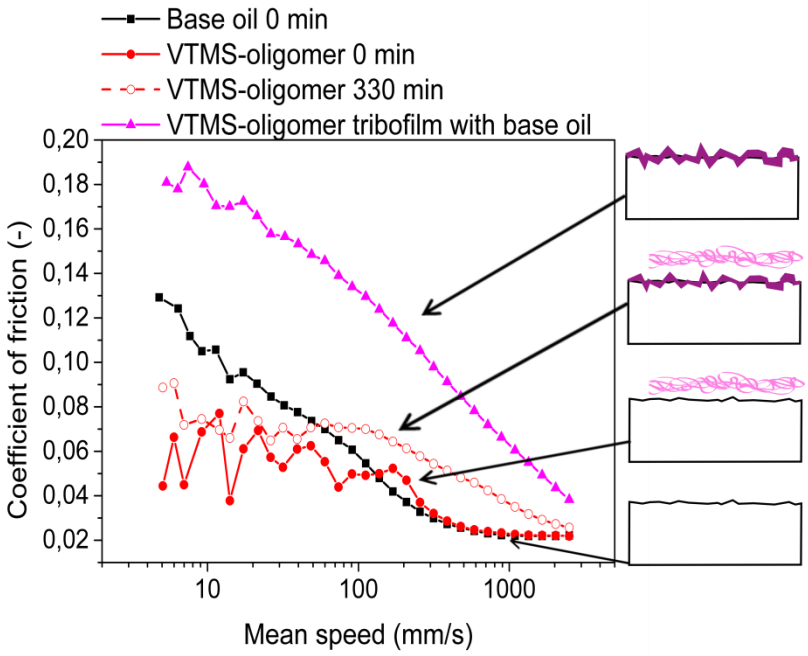

Figure 41: Effect of surface modification on friction (MTM, 100 mm/s, 30 N, 100 °C and SRR of 50 %). "VTMS-oligomer tribofilm with base oil" refers to a tribofilm obtained after 120 min testing under the same conditions and cleaned prior testing. The images on the right side are schematic sketches of the multi layered film.

Figure 41 demonstrates the influences by different obtained precursor modifications on friction, displayed in form of Stribeck curves. By comparison of all Stribeck curves, the one belonging to the tribofilm without tribopolymer layer exhibits much higher cof than the rest. The slope at high mean speeds suggests that the EHD regime is not reached under these conditions. Also the friction increases linearly from high to low speeds to cof values of around 0.18. So the cof in the boundary regime is thus much higher compared to 0.13 in case of the polished steel with base oil.

The surface roughness is a critical parameter for the determination of the lubrication regimes. Table 8 introduces the roughness values which are calculated from AFM measurements of the MTM reference disc and a VTMS-oligomer tribofilm, deposited under similar conditions. As expected, the roughness values of the polished steel and tribofilm surfaces differ quite strong from each other. The pad-like tribofilm structure exhibits around three times higher values for S_a and S_q compared to the polished steel surface.

Table 8: Roughness values expressed as average of two AFM measurements from two 25 x 25 µm sections for a MTM reference disc and a VTMS-oligomer tribofilm.

	S_a [nm]	S_q [nm]
MTM reference disc	6.15	8.03
VTMS-oligomer tribofilm	21.15	29

Tribofilms of other anti-wear additives, share similar disadvantageous behavior on boundary friction, which is referred to high roughness and constrictions in the oil film built-up [22, 35]. In total, the interplay of the extreme increase in roughness and the adhesive interactions are the reasons for the increase in friction.

A clearer image about the connection between roughness and lubricating film height is given by Stribeck curves with cof over the lubrication number λ. Figure 42 presents Stribeck curves with different surface modifications, similar to Figure 41. All cof and speed values for the calculation of λ are taken from the tests, displayed in Figure 41 and from Table 8. The calculated central lubricating film thickness h_c is taken for the base oil curves. In case of the tribofilm without polymeric boundary film, a strong shift of the Stribeck curve to lower λ values can be seen, which is due to the high roughness values. Also the curve ends at $\lambda = 2.07$ and therefore does not reach the EHD regime at a corresponding entrainment speed of 2500 mm/s. It is stated in the previous discussion, that not only tribofilm roughness can show such a strong influence on friction. This can clearly be observed by higher cof values for similar λ values, when comparing with base oil and polished steel results.

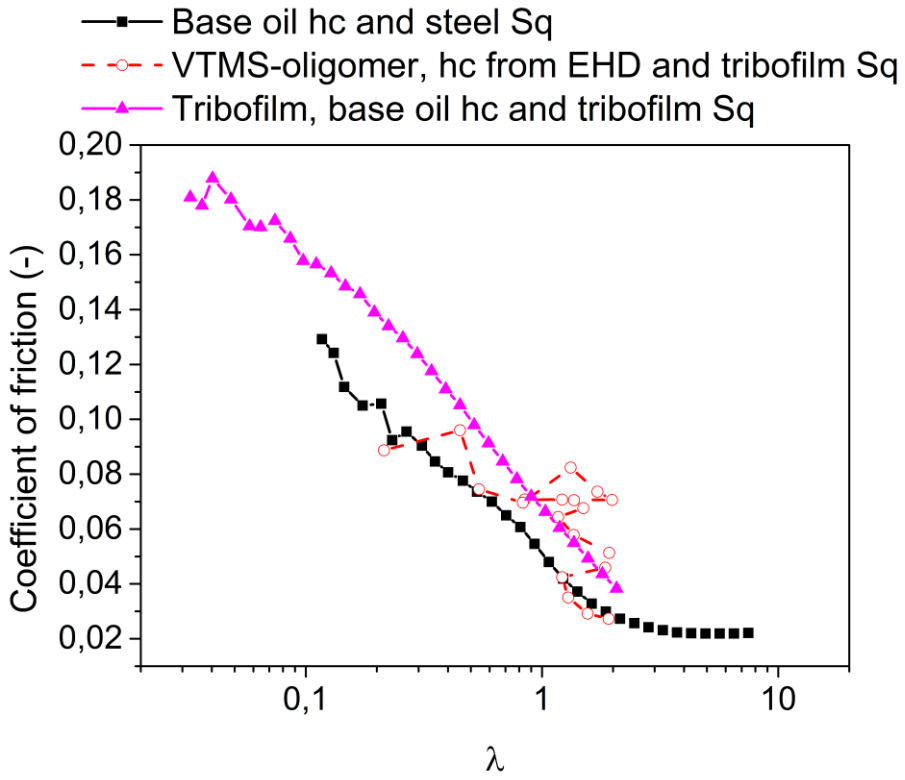

Figure 42: Stribeck curves with lubrication parameter λ and cof from standard test conditions (MTM, 100 mm/s, 30 N, 100 °C and SRR of 50 %).Film thicknesses for base oil tests are calculated and for the VTMS-oligomer curve are taken from EHD measurements. Roughness values S_q are taken for ball and disc roughness. EHD film height values do not fit exactly to Stribeck test conditions, due to glass disc and slightly different mean speed steps for friction / film thickness measurements. The sequence corresponds to the Stribeck measurement from 2500 to 5 mm/s.

The combination of the polymer rich boundary layer model and the tribofilm investigations can be summarized with the help of the red curve in Figure 42. The lambda values of the red curve are calculated from EHD results from Figure 35 and the roughness values are taken from the tribofilm. Despite the high roughness of the tribofilm, the Stribeck curve starts already at $\lambda = 0.21$ and ends at $\lambda = 1.92$, corresponding to 5 mm/s and 2500 mm/s, respectively. It is to notice that the fourth measuring point at 17.3 mm/s is with $\lambda = 1.3$ already in the mixed regime, thus the lubricating film is already thicker than S_q. The amount and sequence of values around λ = 1-2 displays that the system is for nearly the whole speed interval in the mixed regime. Although the cof values are much higher, compared to the reference, they match with the model, as the tribopolymer layer exhibits a much higher viscosity, compared to the base oil. The last four measurement points, which correspond to speeds from 721 to 2500 mm/s, show again the breakage of the polymer rich boundary layer, where the base oil becomes the primary lubricant. This is nicely seen by the perfect match of friction and λ values with the base oil and polished steel reference. However, due to the high roughness of the tribofilm, the EHD regime cannot be reached in the speed interval. One

remark should be commented regarding the region λ = 1-2 in which the polymeric boundary films act. It could as well be the case that during longer testing times even thicker boundary films form. Therefore, the lambda values could reach λ = 3-4 for longer testing times. This would mark a polymeric EHD regime, which would not contradict the friction results and lubrication model, as it is derived for EHD theory. In total and in combination with the shear tests it is clear, that a drop of λ will always be present when the critical shear rate occurs.

The lubrication model can now be summarized in short with the Stribeck curve example, which was recorded at 60 °C and is displayed in Figure 31. It was found out, that the formed siloxanic tribopolymer form viscous polymer rich boundary layer with highly increase viscosity compared to base oil. Due to their high viscosity, thick lubricating films can be formed at low entrainment speeds, which lead to a friction reduction. Though the formed tribofilms exhibit high roughness and therefore retard the lubrication and increase the friction. Nevertheless, if the polymer rich boundary layers are thicker than the tribofilm roughness, no disturbance of the tribofilm is present. The only remaining effect of the tribofilm on lubrication is then the retardation into the EHD regime. In case of the 60 °C tests an increase in lubricating film thickness of around 20 nm is detected, which however, cannot surpass the inhomogeneous tribofilm height of around 20 to 30 nm.

However, it cannot be resolved, why the tribofilm cof values exceed the multi-layer film cof values at higher mean speeds, such as λ > 1.5. From the given values only polymeric rest overs on the tribofilm surface may give a suitable explanation for the given behavior. Most probably, some stronger cross-linked polymeric layers could have resisted the cleaning procedure and give additional contributions, even at higher speeds. Another open point is the rather low friction decrease by the tribopolymer at loads of 10 N, which is shown in Figure 29. Possible explanations might be a stronger influence of the load on the tribopolymer formation than expected. Other possibilities might be a higher pressure viscosity influence or even shear thinning at higher loads.

4.2.2. Anti-wear investigation

Next to the investigations on the lubricating behavior of the organosiloxane model precursor, also anti-wear properties are tested and presented below. Due to the formation of polymer rich boundary layers and adhesive tribofilms advantageous influences are expected. Figure 43 presents the 4-ball wear results of the tests with base oil and the VTMS-oligomer addition. The tests have been performed with oil at room temperature, as well as under heated conditions at 100 °C. The expected anti-wear behavior can nicely be observed by comparison of the wear calotte diameters for the different oil blends. With increasing VTMS-oligomer addition smaller calottes, thus less wear occurs. Unfortunately, the opposite case, so wear increase with addition of the precursor is observed for the tests at 100 °C. It should be noted, that the wear test runs under severe conditions, where additional heating is generally not performed in DIN specifications. To get an impression, the estimated steel ball bulk temperature by frictional heating are calculated to 103 °C for the room temperature DIN conditions, following Ashby's derivation with a predicted cof of 0.1 and thermal conductivity of 45 W/mK [110]. However, since the base oil does not show a dependence of temperature on wear in this temperature interval, the strong differences in wear at 100 °C is attributed to the VTMS-oligomer addition. Nevertheless, a detailed description of the processes and mechanics which lead to wear reduction cannot be done with the obtained dataset and test results.

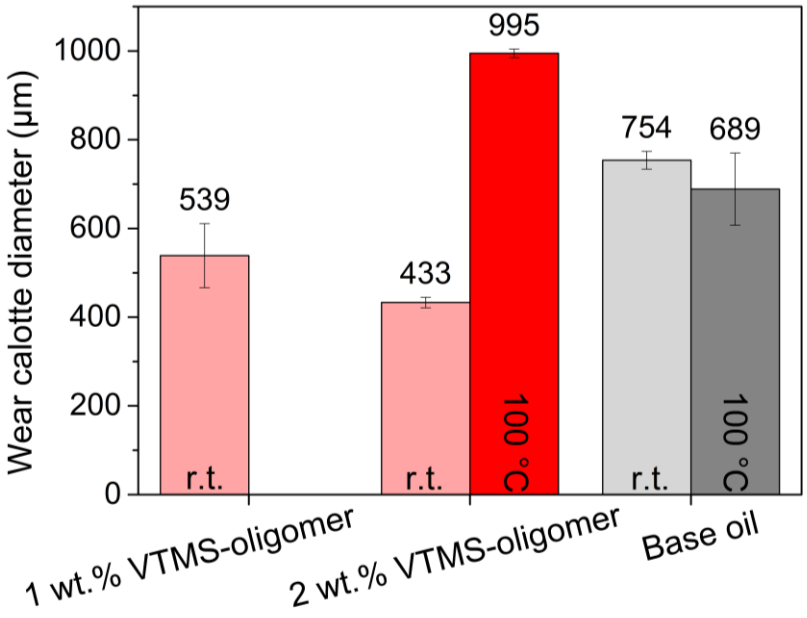

Figure 43: Calotte diameters obtained by 4 ball-wear tests following DIN 51350-3 for different oil samples. Test results are shown following the DIN at room temperature (r.t.) as well as with oil temperatures of 100 °C, otherwise also DIN conditions.

But by knowledge of the tribological behavior of the organosiloxane precursor it is clear that the viscous boundary films support the lubrication. Due to the existence of the polymeric layers the load carrying capacity of thin lubricating films increases.

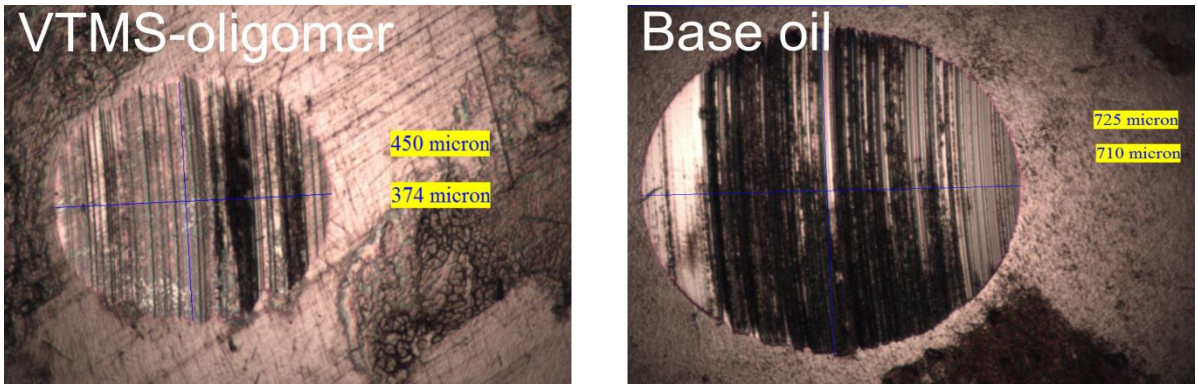

Figure 44: Exemplary wear calotte images from a 2 wt. % VTMS-oligomer test and from a base oil test.

Figure 44 gives an impression of the wear calottes from the tests with base oil and with VTMS-oligomer addition, for room temperature tests. Wear calottes from tests with VTMS-oligomer blends appear brighter without big dark stains around the wear calotte. Instead, colorful deposits on and next to the wear calotte can be seen, which are connected to the tribopolymer formation. Unfortunately no connection to tribofilms can be done and it is not clear, whether they play a role in the anti-wear behavior. When considering how much time the formation of tribofilms take, it is very likely that the abrasion of the steel surface hinders the deposition of tribofilms.

An explanation for the wear promotion at higher temperatures is discussed with additional information from Figure 45. Conspicuous is the extreme color change of the VTMS-oligomer mixture, compared to the slight color change of the base oil after the wear test. A color change from colorless to slightly yellowish or brownish is generally attributed to oxidized oil species. Furthermore a detailed look onto the ball surfaces, next to the wear calottes, can give additional information about the different anti wear behavior of the used lubricants. Ball surfaces from VTMS-oligomer tests show again traces of colorful deposits near and on the wear calotte. On the contrary, thick brownish to black deposits are present near the wear calottes of the base oil test. Due to the severe conditions and oil heating to 100 °C no cooling function by the oil can be expected. Thus, the generated frictional heat promotes oil decomposition and corrosion plus deposition of degraded oil species on the surface of the balls.

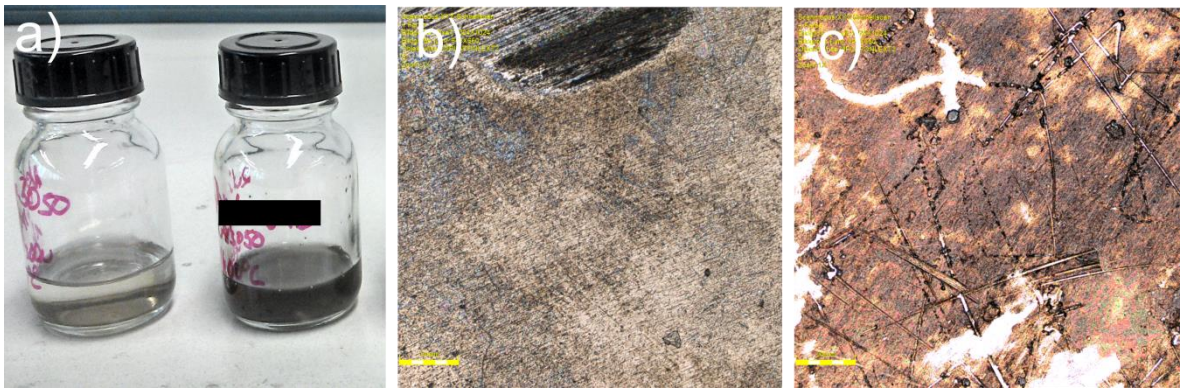

Figure 45: a) Differences of oil blend appearance of left base oil and right VTMS-oligomer blend after the 100 °C 4-ball test; b) ball surface from a VTMS-oligomer test and c) ball surface from a base oil test. The yellow scale bars from image b) and c) correspond to 100 µm.

Therefore, the strong color change of the VTMS-oligomer oil mixture can be attributed to dissolved degraded oil species and wear particles, which were not able to form thick deposits on the ball. This in turn must originate from interactions between the VTMS-oligomer and degradation products. Possible explanations could be that either the degradation products could not deposit on the surfaces, due to already coverage of the surface by the organosiloxane. Or the organosiloxane keeps these degradation products stabilized and dispersed in the oil. Apparently these dispersed wear products and particles intensify the wear process. Oxide films and wear deposits have extensively been investigated. Generally it can be summarized from literature work that oxide films, also with inclusion of degraded oil as binder, can show wear reducing properties [103, 111]. However, these films break apart when a critical film thickness is reached, as they also accelerate further decomposition. The resulting soot and wear particles lead to third body interactions, which highly promote wear [112, 113]. Therefore, it is considered that due to the dispersed wear particles by the VTMS-oligomer interactions, such a high wear is analyzed. In addition, it is imaginable that the VTMS-oligomer might act disadvantageous by actively agglomerating these particles or even itself forming hard silica species, both enhancing the wear.

4.3. Influences of precursor structure on lubrication and film formation

Chapters 4.1 and 4.2 introduced the tribological behavior of vinyltrimethoxysilane-oligomer as model precursor. Chemical and structural characterization is given, parallel to the influences on lubrication, friction and wear have been presented. As stated in 4.1 the described model should not only be valid for VTMS-oligomeric species, but for cross-linkable organosiloxane in general. Of particular interest is whether this model can be applied for monomeric silane species, so that this model fits and expands current knowledge [6, 7]. The findings are given in the following chapter 4.3.1. In chapter 4.3.2 the investigation of polymeric VTMS by sol-gel derived VTMS coatings and their behavior in tribological aspects is presented.

4.3.1. Differences between oligomeric and monomeric vinylmethoxysiloxane / -silane

The approach to show differences between oligomeric and monomeric VTMS is based on the discussion about the VTMS-oligomer. This chapter starts with differences in the viscosity of the oil mixtures and then goes on to test results of MTM tests at different temperatures. Afterwards similarities and differences of the chemical and structural properties, as well as the formation of the reaction films will be presented. Finally a discussion based on agreements and inconsistencies according to the proposed lubrication model is given.

As general remarks, the wording monomeric VTMS will be abbreviated by VTMS. In addition, in order to have comparable conditions all tests have been performed with 2.7 wt.% addition of VTMS. The amount is calculated to have an equal molar concentration of silicon similar to the VTMS-oligomer mixtures. Thus the wt.% increase is a result from higher alkoxy concentration.

Figure 46 displays the viscosity differences between the oligomeric and monomeric mixtures. The VTMS mixture has a lower kinematic viscosity at 40 and 100 °C than the oligomeric pendant. Also the manufacturer states the dynamic viscosities differently with 2-4 mPas for

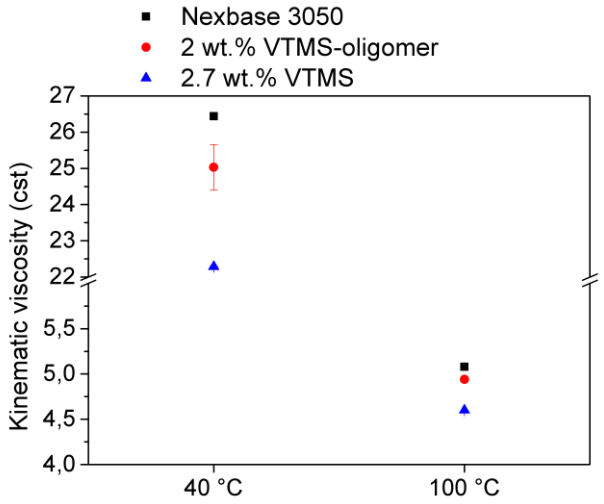

Figure 46: Kinematic viscosity over temperature of the base oil and the precursor + base oil mixtures, obtained following ASTM D445-18. Other error bars are too small to visualize.

the oligomeric and 1 mPas for the monomeric VTMS at 20 °C. The lower viscosities lead to slightly lower lubricating films and should be kept in mind in later discussions.

Influences on friction by VTMS are displayed with Stribeck curves in Figure 47, which have been measured over different testing and rubbing times. When comparing the test results with the curves of the oligomeric precursor in Figure 15 and Figure 26, it becomes obvious that the monomeric precursor does not show any friction reducing mechanism. In contrast to the oligomeric precursor, a friction increase in the boundary regime is detected during the first minutes of rubbing. Then the friction influence in the boundary regime becomes rather constant after already 5 minutes, but a clear contribution in the mixed regime with retardation of the EHD regime can be observed. This behavior has been discussed in the previous chapter and can be accounted to the formation and presence of a tribofilm.

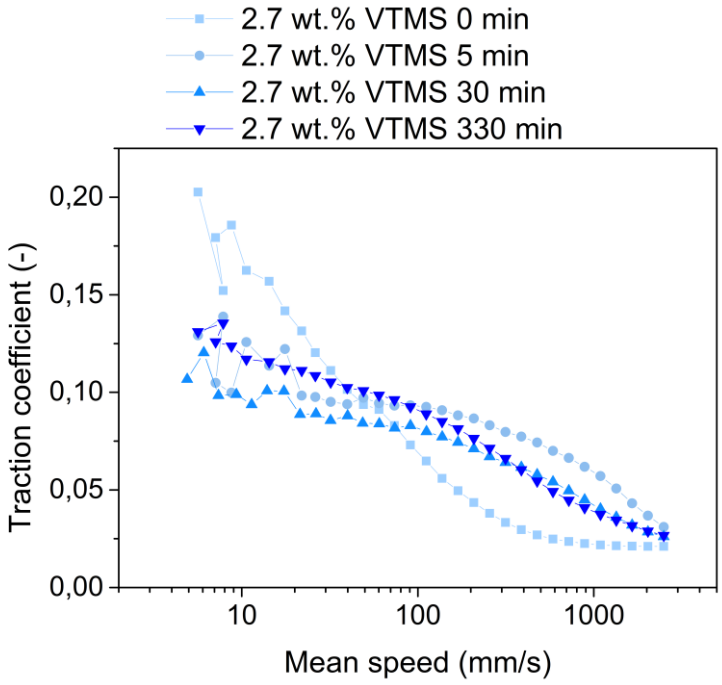

Figure 47: Stribeck curves measured after different testing / rubbing times (30 N, 100 °C, 50 % SRR).

Figure 48 displays the evolution of the tribofilm deposition over testing time. First it proves the expectations for the presence of tribofilms, but it also gives an interesting trend of film formation. Unlike the oligomeric precursor, VTMS deposits comparably thick adhesive tribofilms in shorter times, but the film height stays constant for longer testing times. Therefore, the average film thickness after 30 minutes stays constant with around 22.5 nm and is much thinner than the tribofilms produced by the oligomeric precursor. The friction curves provide no information concerning polymer evolution or influence.

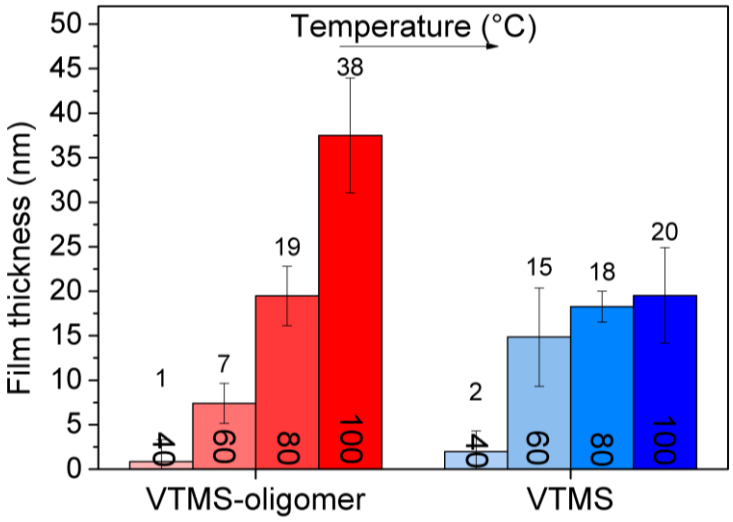

Figure 48: Measured average tribofilm step heights with profilometer for the different testing / rubbing times.

Also the tests, which have been run at different lubricant temperatures, see Figure 49, give no further information on polymer formation. The Stribeck curves have been obtained after 2 h testing time with the standard protocol, but at different temperatures. Again no friction reduction but similar cof values as presented are obtained for the tests from 60 °C to 100 °C. Only the test at 40 °C show no signs of friction increase by tribofilm formation. However, the formation and influences of tribofilms appear already at 60 °C, which was not the case for the oligomeric precursor.

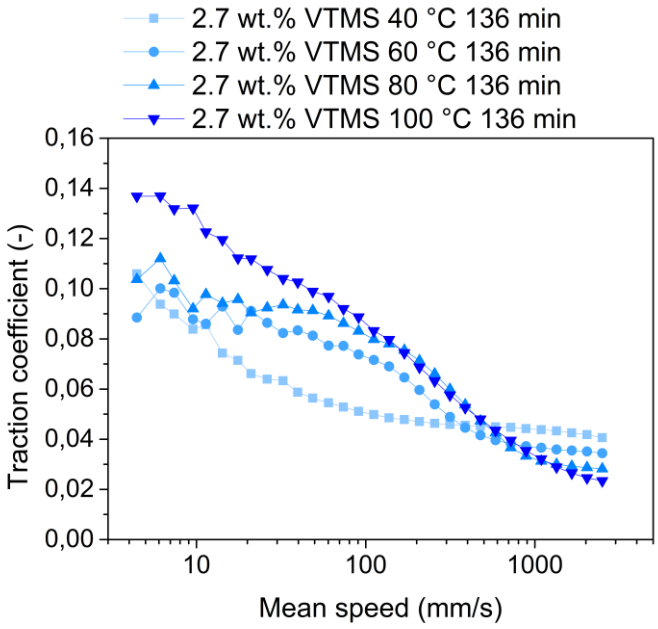

Figure 49: Stribeck curves measured after around 2 hours testing at different temperatures (30 N, 50 % SRR) with 2.7 wt.% VTMS samples.

More insights on the deposition and the formation of polymer residues are given by SLIM images in Table 9. As predicted, no pronounced signs of polymeric deposits are present on the wear tracks. For each test a color change to darker and more homogenous depositions over the testing time can be seen. These depositions can be traced back to the formation of adhesive films, whose film heights are given in Figure 50. Interestingly, also a color change for the test at 40 °C is present, although no influence on the cof and no tribofilm are detected.

Table 9: MTM SLIM (ball wear track) images recorded at different testing times, from tests at different temperature with VTMS-oligomer and VTMS addition. The stains on the VTMS 40 °C images are from fractures of the glass.

Time [min]	3	27	136	Time [min]	3	27	136
VTMS-oligomer 40 °C	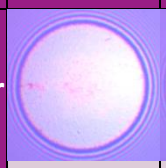	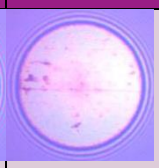	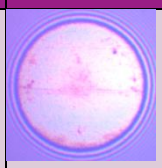	VTMS 40 °C		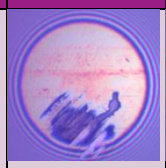	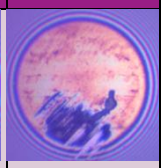
VTMS-oligomer 60 °C	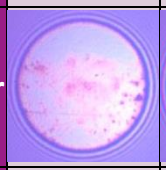	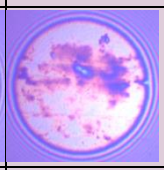	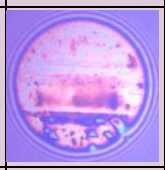	VTMS 60 °C	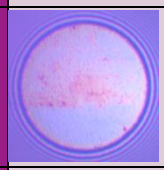	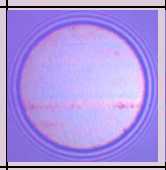	
VTMS-oligomer 80 °C		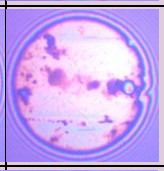	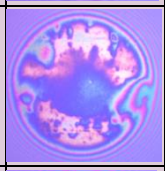	VTMS 80 °C	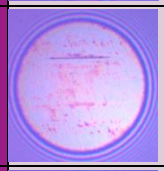	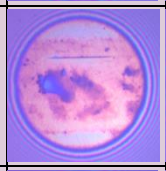	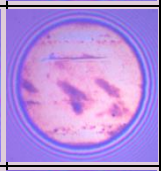
VTMS-oligomer 100 °C	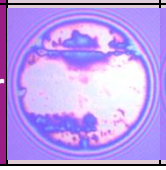	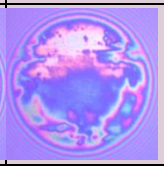	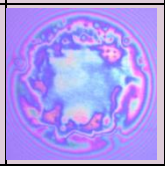	VTMS 100 °C	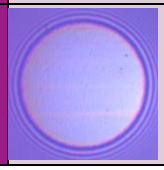	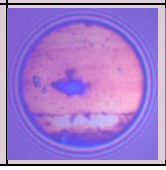	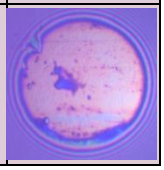

Figure 50 presents the tribofilm heights corresponding to the tests with the SLIM images. The tribofilm heights are consistent with the friction curves and explain the indicated influence on friction at already 60 °C. Also slightly lower film heights are seen for decreasing testing temperatures, similar for the case of the oligomeric precursor. This is attributed to lower reactivity and severity, which results in less cross-linking and decomposition of VTMS into polymeric or adhesive films.

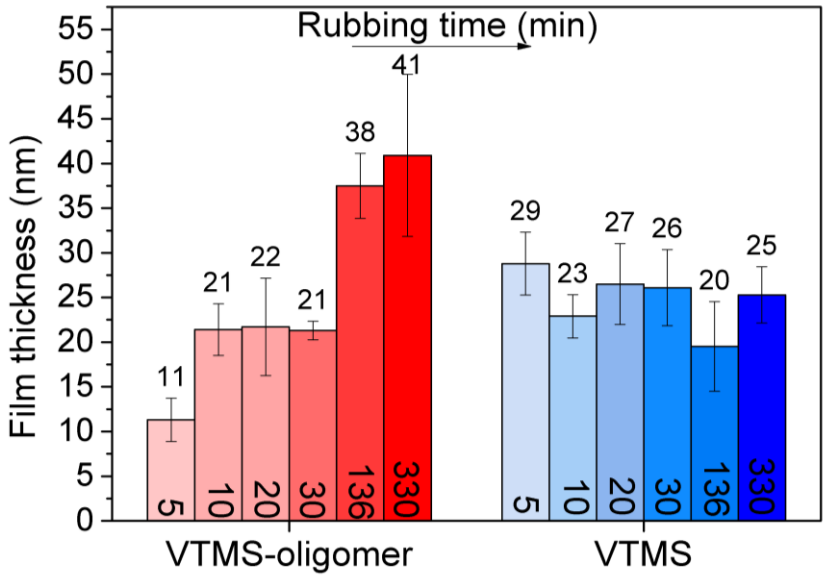

Figure 50: Measured average tribofilm step heights with profilometer for different testing temperatures and oil samples after around two hours testing.

In summary, pronounced tribofilm influences are observed, at even lower temperatures and after shorter rubbing times than with the oligomeric organosiloxane. The lack of friction reduction is, following the lubrication model, attributed to not sufficient formation of tribopolymer layers. In order to prove this assumption EHD measurements are performed and will be discussed after a short discussion about the chemical state of the formed reaction films.

All discussed differences about the formation and thicknesses of the reaction films indicate variation in their molecular structure. Figure 51 shows SEM micrographs of VTMS derived wear tracks. The wear tracks have been cleaned following the standard procedure and appear more homogenous and uniform or denser than the oligomeric derived wear tracks. Also the tracks appear rather bright and do not show strong color changes, like the oligomer derived tracks. EDX analysis proves the deposition of SiOC containing tribofilms, which have an average Si:O:C ratio of 1 : 1.51 : 1.55 and therefore indicate the formation of a strongly cross-linked network. The slight increase of silicon concentration over testing time suggest denser films, as their average thicknesses stay unchanged, also the SEM images appear more uniform with increasing testing time. More insights into their chemical structure are given by FTIR and Raman analysis in chapter 6.3, in the appendix. The chemical analysis shows that the monomeric and the oligomeric precursors derive similar chemical structures for polymeric residues and tribofilms. However, due to the lower amount of polymeric residues lower reaction rates and differences in film growth must be present, which should also explain the more uniform and dense films. These differences are discussed in detail after the following discussion about the polymer formation and their lubricating properties.

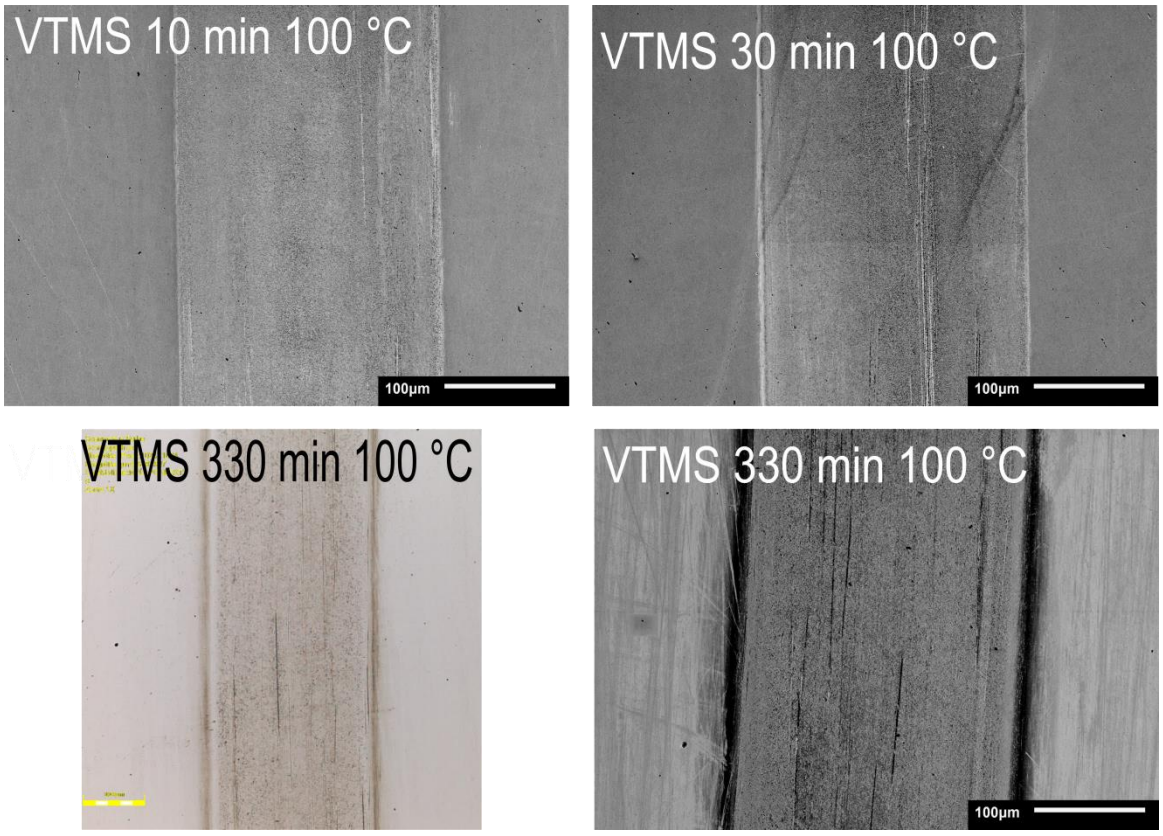

Figure 51: SEM and optical microscopy images of VTMS derived wear tracks after different testing times. The yellow scale bar corresponds to 100 µm in the optical microscopy image.

Table 10: EDX results of MTM disc wear tracks after different rubbing times. All area measurements are performed under similar conditions across the wear track, with 5 kV acceleration voltage.

Sample and rubbing time	Wear track composition [atom %]			
	Si	O	C	Fe
Reference Disc	0.4	0.2	4.7	94.7
VTMS 10 min	3.8	5.9	6.2	84.1
VTMS 30 min	4.1	6.5	6.3	83.1
VTMS 330 min	5.0	7.1	7.4	80.6

More insights on the polymer formation by VTMS are given with the help of EHD tests. Figure 52 presents a comparison of lubricating film thickness test results between the oligomeric and monomeric mixtures. The test results show that also VTMS increases the lubricating film thickness as it exhibits an average film thickness of around 30 nm in the range of 30 to 200 mm/s. Compared to the oligomeric precursor with 60 nm the effect is much lower and therefore does not differ from the base oil film thicknesses in a comparable extend. Similar to the oligomeric precursor, but at lower speeds of around 300 mm/s the base oil contribution takes control as the main lubricant. However, at higher speeds, contributions from the slightly lower fluid viscosity are present, which result in lower film thicknesses in the EHD regime. Nevertheless, the results prove also a contribution regarding the lubricating film thickness, which however do not show significant influence on frictional effects.

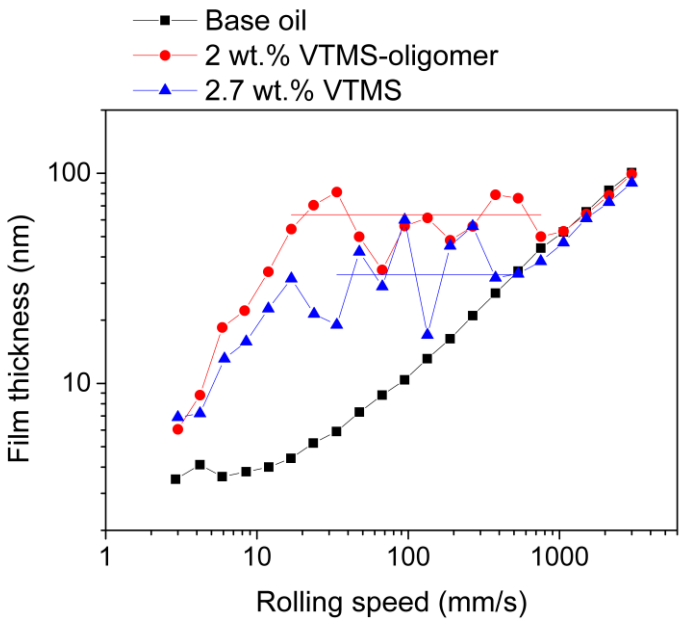

Figure 52: EHD measurement results, lubricating film thickness over rolling speed for base oil, 2 wt.% VTMS-oligomer and 2.7 wt.% VTMS mixtures (30 N, 100 °C). Straight red and blue lines represent the average film heights over the given interval.

Parallel to the MTM tests, also EHD measurements have been performed at different testing temperatures. Figure 53 shows the deviation between the film thicknesses obtained by the base oil and VTMS mixture tests. As expected, the contribution of VTMS on the lubricating film thickness decreases with lower temperatures, due to lower reactivity of the organosilane. So the increase of film height is about 5 nm at 80 °C. Below 80 °C no increases but decrease of lubricating film height is observable, however pronounced only at higher speeds. The effect of lower viscosity of the VTMS mixture can be predicted. Therefore, with the given viscosities and densities of ρ = 0.83 and 0.85 g/cm^3 for base oil and VTMS-mixture, respectively, the

lubricating film height h_c is calculated. The pressure viscosity coefficient at 40 °C is taken as 19.5 GPa^{-1}, which then results to calculated film thicknesses of 359 and 326 nm for base oil and for the VTMS mixture. Therefore, this strong decrease at higher speeds is mainly attributed to the differences in fluid viscosities.

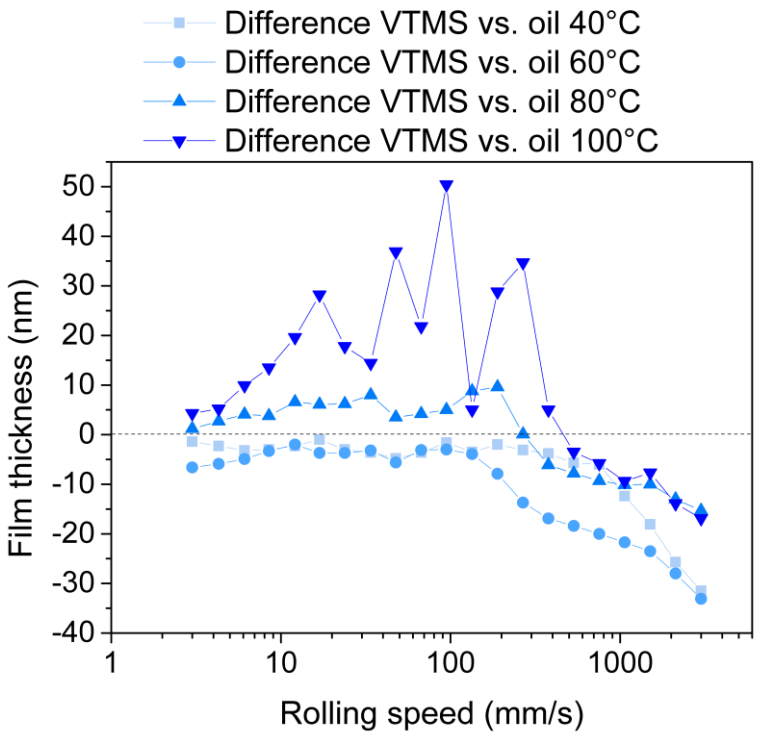

Figure 53: Difference of lubricating film thickness between base oil and 2.7 wt.% VTMS mixtures, obtained by EHD measurements at different testing temperatures.

To finally summarize the tribological behavior of VTMS, the lubricating film thickness results and the tribofilm roughness is taken into account and hence the cof is plotted vs. λ in Figure 54. The roughness values are given in Table 11 and describe the comparably smooth tribofilm surface, which is also indicated by the SEM images.

Table 11: Roughness values expressed as average of two AFM measurements of two 25 x 25 µm sections for a MTM reference disc, a VTMS-oligomer tribofilm and VTMS tribofilm.

	S_a [nm]	S_q [nm]
MTM reference disc	6.2	8
VTMS-oligomer tribofilm	21.2	29
VTMS- tribofilm	11.2	15.2

Figure 54 visualizes how the film thickness and cof between the oligomeric and monomeric derived boundary films mismatch. Although the obtained lubricating film thicknesses are lower for the case of VTMS, high λ values are obtained at low and medium speeds, because of the smooth tribofilms. The Stribeck curve of VTMS is shifted to higher λ values, but still exhibit high friction. Also the points corresponding to high speeds in the VTMS Stribeck curve do not match with the base oil curve, which is thought to be independent of the boundary film, due to the shearing off. In comparison most measuring points from oligomer results are in the same cof range, where boundary film lubrication is expected. The results for the monomeric case differ strongly from this and a clear decrease in friction can be seen for increasing entrainment speed, which corresponds to the sequence of points from top to bottom. A decrease of friction with entrainment speed can be attributed to stronger influences of base oil in the boundary layer, than observed in case of the oligomeric derived boundary layers. Therefore it cannot be said, that both precursor show similar behavior in terms of lubrication influences. At this point it is believed, together with the findings on film formation that the polymeric boundary films, derived by monomeric precursors differ in structure and in viscosity and thus shear behavior, from the oligomeric derived boundary films. The higher friction must be connected to immobile surface layers, which are less viscous than oligomer derived polymer films. Also the mismatch at high speeds indicates surface modifications, which influence the EHD lubrication of the bulk lubricant, similar to the tribofilm measurement from Figure 42.

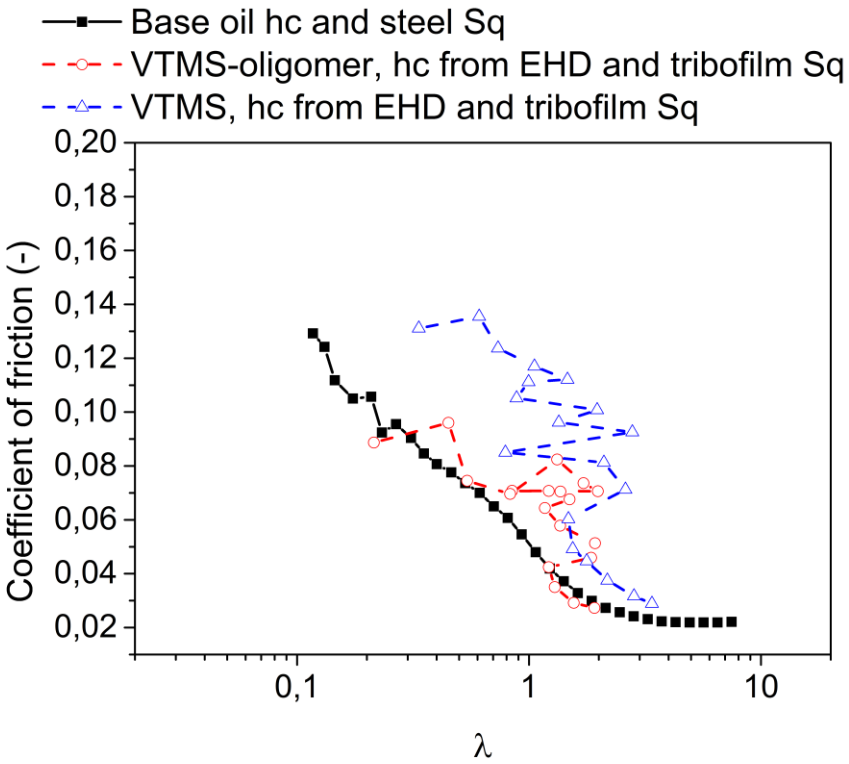

Figure 54: Stribeck curves with lubrication parameter λ and cof from standard test conditions (MTM, 100 mm/s, 30 N, 100 °C and SRR of 50 %).Film thicknesses for base oil tests are calculated and for the VTMS-oligomer curve are taken from EHD measurements. Roughness values S_q are taken for ball and disc roughness. EHD film height values do not fit exactly to Stribeck test conditions, due to glass disc and slightly different mean speed steps for friction / film thickness measurements. The sequence corresponds to the Stribeck measurement from 2500 to 5 mm/s.

From the given results it can be seen, that both precursor form polymeric and adhesive tribofilms, but act differently in terms of lubrication. These differences are now discussed in detail, while summarizing the findings in this chapter. The introduced model foresees first a formation of polymeric residues, which then decompose into partly glassy coatings. The results and findings of the monomeric precursor show some discrepancies. Valuable information for this answer was obtained by the EHD measurements. The results clearly show a viscous contribution from polymers on lubrication and thus also relation to the film formation. Why the boundary films from monomeric precursor do not decrease friction is related to the lower amount and probably smaller or more branched polymers. This can be estimated with the help of the Flory radius R_F which is comparable to half the polymer coil dimension in solutions. Cohen, Stuart and Spikes *et al.* have found out that polymer films in hydrodynamic contacts generally exhibit critical layer thicknesses, which are connected to polymer sizes [109, 114].

Their works show good agreements for different polymer sizes and boundary layer thicknesses. The Flory radius stands in following relation:

$$R_F = aN^{0.6} \tag{25}$$

where *a* stands for the monomer size and N for the number of monomers per chain. As stated, this model is in this case used as rough estimation, since organosiloxane and their ability to form three dimensional networks might have dependences different than the power of 0.6. Nevertheless, for the following comparison a boundary film thickness of 30 nm is considered, which is observed to be necessary to fulfill friction reduction by polymer layers. In the case of VTMS-oligomer at least 35 molecules have to react with each other to form polymer with a Flory radius of 30 nm. The oligomer consists of around five [Si-O] units, which means that at least 175 monomers have to react to reach a similar Flory radius. Additionally, the monomeric precursor needs to react in a chain-like configuration, which is highly doubtful owning to their molecular structure. Also it was already mentioned, that the molar ratio of hydrolysable Si-O-CH_3 groups to H_2O in the mixture is about 51 : 1, for the oligomeric case and even higher for the monomeric. Under the given conditions and the tribological stress it appears that monomeric precursor do not form polymer with comparable sizes or structure.

However, it can be noticed that a faster and more uniform tribofilm formation occurs for monomeric than for oligomeric precursor. This can be related to the lower yield of long chain-like polymer. Also due to three active cross-linkable groups on the silicon atom it is more likely, that the network grows in all directions, rather than in a chain. So polymers are less concentrated in solution and therefore also less sheared off the surface and grow into a more uniform fashion. This is consistent with the higher friction values during the first minutes of a test, which is considered to origin from attracting forces between the adsorbed or even chemisorbed monomer on the surfaces. From the given results, these surface networks form faster and more uniform than in case of the oligomeric precursor. In addition, these near-surface layers are exposed to tribological stress at already shorter testing times. The result is a faster and uniform tribofilm growth in case for the monomeric precursor.

4.3.2. Sol-gel derived coatings with Vinylmethoxysiloxane-polymer

In order to complete the investigations regarding the vinylmethoxysiloxane precursor, also friction tests with sol-gel derived coatings of vinylsiloxane have been conducted. The approach differs from the investigations with the oligomeric and monomeric precursor, due to solubility issues for aged vinylmethoxysiloxane sols and thus polysiloxane in the used base oil. The detailed coating and polymerization procedure is given in the experimental section. A major difference in the testing procedure is that sols have been prepared and aged for different times before deposition via a spin-coating procedure onto the MTM-discs prior the testing. The aged sols have been tested in MTM in two fashions, first as deposited, so without any curing step and also cured at elevated temperatures. All coated discs have then been tested with base oil as lubricant.

In the following, two coating parameters will be regarded. Whereas the first parameter is the aging time of the sols, which have been prepared as coating material, the second parameter is the curing process, especially how the coating properties and influences on friction vary with curing of the different gels. Therefore, sols have been deposited after 20 min (also referred as "fresh"), 1 day and 5 day ageing and cross-linking. The polymerization procedure is tracked via liquid NMR and information is given in the appendix. It should be kept in mind that the spin coating procedure did not differ for different aging durations therefore thicker coatings have been obtained by higher viscous, thus older sols. In summary, each aged sol has been tested in the MTM without a curing process and with a curing process for 4 days at 100 °C.

Friction curves for uncured coatings are presented in Figure 55. For each aged sol a Stribeck curve is measured at the beginning of the test and after around 36 min of rubbing. While the Stribeck curves from the fresh sol specimen show only marginal influences on friction, aged sol derived coatings show stronger influences.

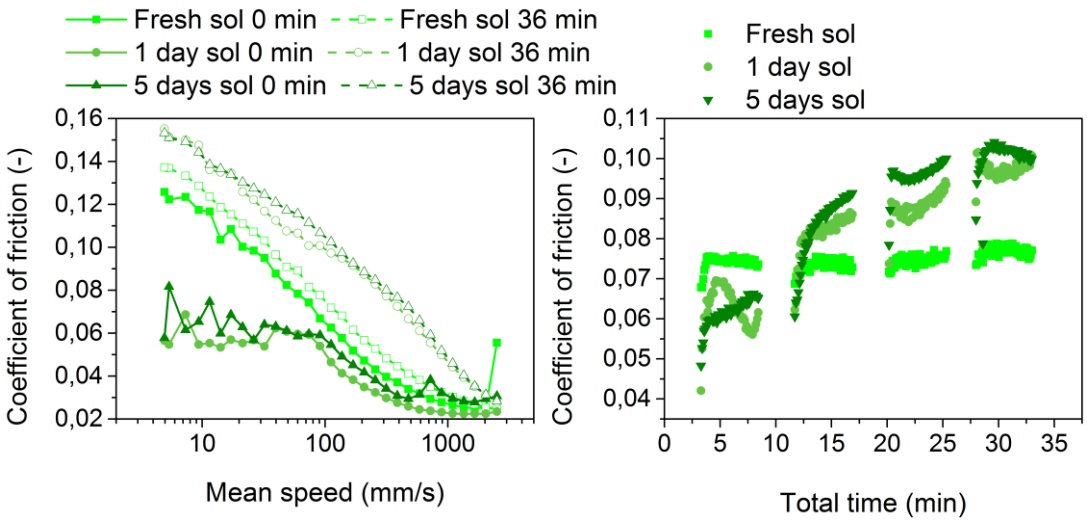

Figure 55: Left: Stribeck curves measured before and after around 30 min rubbing on coated MTM discs (30 N, 100°C, 50 % SRR). Right: Rubbing curves at 100 mm/s for the different coated MTM discs. MTM discs have been coated with VTMS-oligomer + ethanol+ water sols, aged for different times. The coatings have been tested with base oil directly after deposition, so no curing and drying was performed.

Before the rubbing sequences, the 1 and 5 days aged sol coatings show a similar Stribeck curve profile like from conventional oligomeric VTMS mixtures. Slightly lower cof values are obtained with the 1 day aged sol, especially in the mixed and EHD regime. However, after around 30 min of rubbing, the tested aged sols show a strong increase in cof displayed in the Stribeck curves, which seems to be independent of the aging time of the sols. Also the friction curves from the rubbing sequences are consistent with the observed friction increase for the 1 and 5 days aged sol tests. From the given test results, it can be concluded, that the polysiloxane aged for 1 and 5 days, are able to reduce the friction, as proposed by the lubrication model. Also the friction increase due to the degradation of the polymer and formation of tribofilms suits the model. Exemplary images of the obtained wear tracks are given in Figure 56, which also show clear signs of tribochemical reactions. The lack of friction reduction by the fresh sol may be attributed to either too small polymers or to the low active polymer volume, which was deposited on the MTM disc. Also it must be noted, that the active coating material is limited to the wear tracks, since the deposited polysiloxane form smooth coatings besides the wear tracks and thus do not contribute as solved polymer, see Figure 56. Polymers which were rubbed off during the beginning of rubbing might, besides further degradation and cross-linking also adsorb or chemisorb next to the wear track, where an unworn polysiloxane coating is present.

An unexpected observation can be deduced from the rubbing curve corresponding to the 5 day aged sol. All rubbing sequences show a steep increase from lower to higher cof values at

the beginning of each rubbing sequence. This curve profile suggests that viscous polymeric residues are able to form polymer rich boundary films in between the rubbing sequences, but can only withstand the shear rates during rubbing for short time.

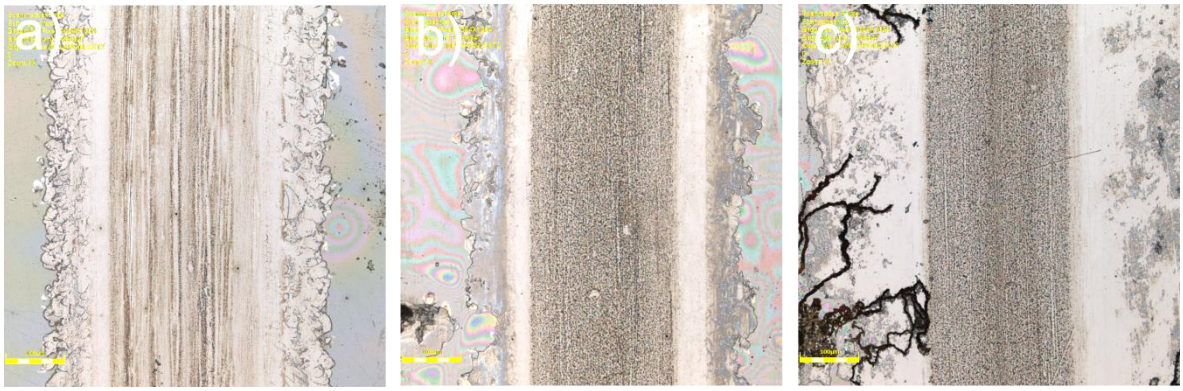

Figure 56: Wear track images after MTM tests with uncured sol-gel coatings; a) fresh sol; b) 1 day aged sol; 5 days aged sol.

Next the tribological behavior of cured coatings is discussed. Some coating properties are given in Table 12, which will be referred to for the discussion on friction curves. At first some general points will be cleared. The decreasing Martens hardness with increasing aging time can be explained by the increasing film thickness of the coatings in combination with less penetration into the substrate material. Therefore, it can be concluded, that especially in the case of the coating derived from a fresh sol, strong contributions from the substrate must be present and the Martens hardness cannot be taken as face value for the coating materials. The coating thicknesses can, additionally be taken as minimum coating thickness for the uncured samples. Contact angle measurements with base oil indicate worse wetting behavior of oil on the polysiloxane than on steel, as the reference steel disc shows contact angles of around 8 °. This can be related to the more polar structure of the polymers, the presented values for polysiloxane coatings are similar from literature [115].

Table 12: Overview of different coating properties from the cured coatings. All values are average values and obtained by at least three tests. Coating thickness is estimated with step height measurements between the wear track and coating. Strong variations might be present due to wave like profiles of the coatings, also next to the wear track.

Sample	Martens hardness [HM 0.05 / 20; N/mm^2]	Penetration depth [µm]	Coating thickness - profilometry [µm]	Contact angle with base oil [°]
Fresh sol cured	908	1.4	1.5+	20
1 day sol cured	297	1.5-2.7	1.8+	32
5 days sol cured	158	3.5	4+	35

The tribological behavior of the cured films is again investigated by MTM tests and the results are shown in Figure 57. Starting with the friction curves from the rubbing sequences, high starting cof values of around 0.1 to 0.11 are observed. The cof values decrease over the testing time for all cured samples. Interestingly, the cured fresh sol coating exhibits the highest cof values, while the cured coatings for 1 and 5 days show rather similar values. Except that the cof values of the cured 5 days aged sol-gel coating scatter strongly. The opposite behavior of friction influence, compared to the uncured samples, can be explained by a stronger networking and cross-linking due to the curing procedure. With increasing networking of the polymeric gel, the shear strength increases and therefore stronger resistance against motion is present, which in turn is reflected in higher friction. Nevertheless, the coatings exhibit only weak mechanical properties, so that the elastic coatings are continuously rubbed off during the tests and no stable contribution on lubrication is observed. The strong scatter can be attributed to polymer flakes which contribute arbitrarily as lubricant additive. The fact that these scatters are only present for the 5 days aged sol-gel coating can be referred to the thicker coating and thus more coating material and flakes.

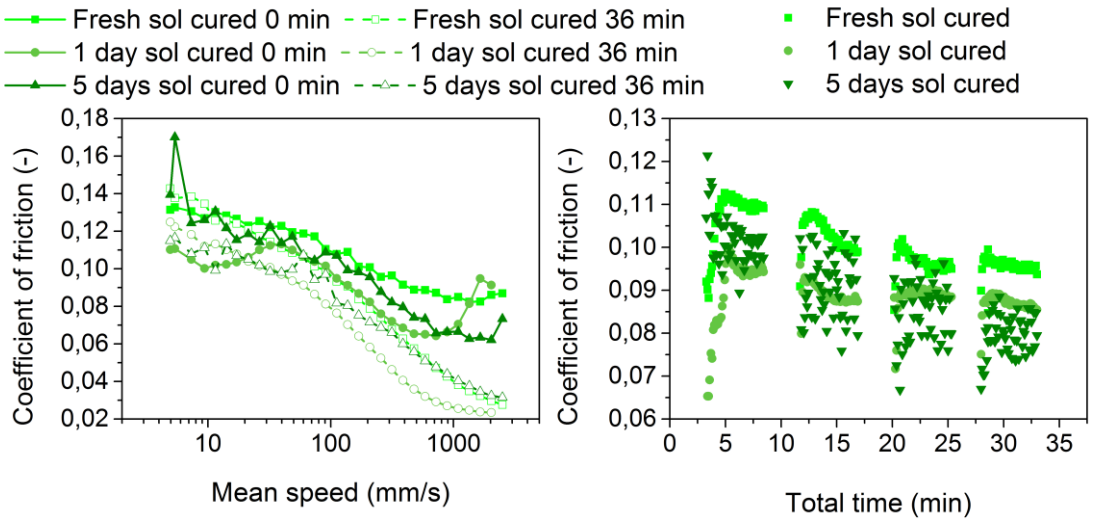

Figure 57: Left: Stribeck curves measured before and after around 30 min rubbing on coated MTM discs (30 N, 100°C, 50 % SRR). Right: Rubbing curves at 100 mm/s for the different coated MTM discs. MTM discs have been coated with VTMS-oligomer + ethanol+ water sols, aged for different times and afterwards cured for 4 days at 100 °C. The coatings have been tested with base oil.

Also Stribeck curves, which were recorded before and after the rubbing sequences, propose the degradation of the coatings. For each coating, the cof is in the range of 0.11 to 0.14 at low speeds at the beginning of the test. Interestingly no clear transitions from boundary to EHD regimes are observable and the cof values are still at 0.06 to 0.09 at high speeds. This behavior changes with testing time and transitions of the lubrication regimes are clearly

observable after 36 minutes of rubbing. Also no clear features for influences by polymeric boundary layers on friction can be observed after 36 minutes testing time. In total the Stribeck curves are in consistent with the rubbing curves as they show that the influences of the coating material diminish with testing time.

In addition, such high friction values for the not worn coatings at mean speeds above 1000 mm/s indicate no clear contribution of the base oil on the lubrication. The friction values are in the range of the mixed or even boundary regime for the base oil and steel couples and cannot be correlated to hydrodynamic friction of the base oil. Therefore, it can be deduced that not sufficient fluid entrainment into the tribo-contact is present. This behavior is due to the shearing of the coating material, what restrains lubricant inlet. SLIM images in Table 13 show transfer layers from the discs onto the balls and how they change with testing time. Especially in case of the 1 and 5 days aged sol-gel coatings clear evidences of polymeric deposits are present on the ball wear tracks.

Table 13: MTM SLIM (ball wear track) images recorded at different testing times, from tests with cured sol-gel coatings.

Time [min]	Fresh sol-cured	1 day sol-cured	5 days sol-cured
3	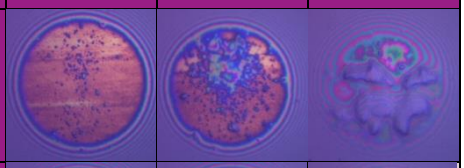		
36	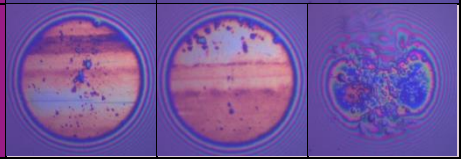		

The friction values after 36 minutes of rubbing are still higher than for pure base oil and standard steel couples. Reasons for this are polymeric residues, which are also shown in the SLIM images but also possible tribofilm generation. A similar influence on friction, at higher speeds, was also observed for the monomeric derived tribofilms. This behavior supports the hypothesis that stronger networked polymers can show disturbing influences on the fluid entrainment and lubrication.

Figure 58 displays the wear tracks from the cured coatings after cleaning. Despite the cleaning procedure still residues can be seen on the wear tracks. Also the coatings appear stained with a brownish or greyish color change.

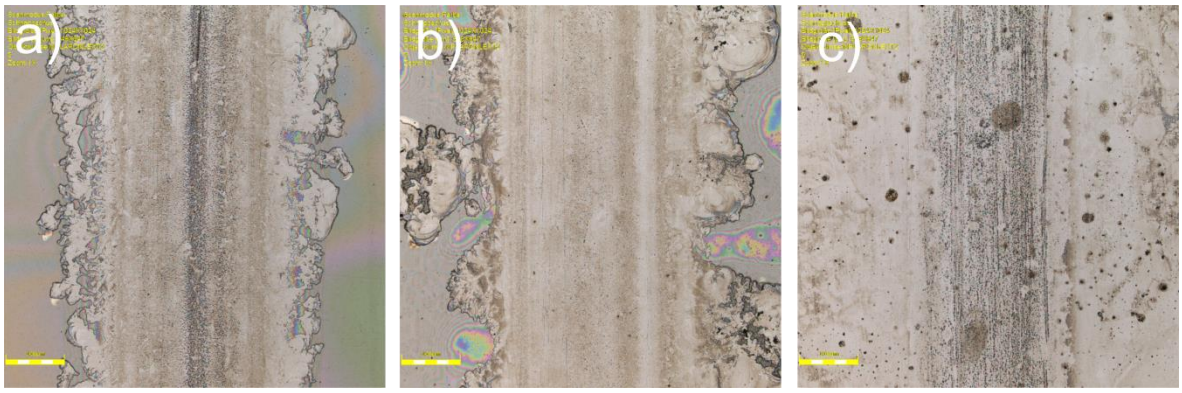

Figure 58: Wear track images after MTM tests with cured sol-gel coatings at 100 °C for 4 days; coatings are obtained from a) fresh sol; b) 1 day aged sol; 5 days aged sol.

All wear tracks have been analyzed by micro-Raman and EDX spectroscopy to obtain information about the degradation process and chemical reactions, the Raman spectra are shown in Figure 59 for the uncured coatings and Figure 60 for the cured coatings. The elemental composition of the wear tracks is given in Table 14. Unfortunately, the used FTIR set-up does not provide an adequate lateral resolution to only measure the wear track areas without contributions of the nearby coatings, thus it is difficult to state information about Si-O-Si bonds. The EDX measurements have been performed with a set-up different from the one with which the other results have been obtained, therefore, the reference disc results show much higher silicon, oxygen and carbon concentrations in Table 14. It cannot be argued whether, the reference disc has undergone oxidation on the surface, but it is clear, due to the higher silicon values that the results should not be taken by face value.

Nevertheless, the EDX analysis shows increased silicon values for all wear tracks, after the MTM tests. The increase of silicon, carbon and oxygen values is not significant, first due to low expected tribofilm thicknesses and second due to a high acceleration voltage of 10 kV, which means larger probe volumes and thus more substrate signals. All in all an adhesive tribofilm containing SiOC is expected, similar to the tribofilms obtained by the *in-situ* procedure.

Table 14: EDX results of coated MTM disc wear tracks after testing in MTM with base oil. All area measurements are performed under similar conditions in the center of wear track, with 10 kV acceleration voltage.

Sample and rubbing time	Wear track composition [atom %]			
	Si	O	C	Fe
Reference Disc	1.03	10.05	14.33	72.92
Fresh sol not cured	1.77	11.63	14.45	70.44
Fresh sol cured	1.81	12.12	14.78	68.79
24h sol not cured	1.68	10.99	17.37	68.28
24h sol cured	1.85	11.41	14.43	70.76
5 days sol not cured	1.57	11.34	15.08	70.51
5 days sol cured, rim of wear track	1.73	10.9	17.96	67.66
5 days sol cured, center of track	3.35	14.02	16.48	64.93

All micro-Raman spectra from wear tracks exhibit two bands at around 1350 and 1600 cm^{-1} which can be referred to D and G bands, respectively. Both bands originate from disordered graphitic like carbon structures which are the most striking features to investigate nanostructured carbon in SiOC glass ceramics [116-118]. It is rather surprising, since these features have not been obtained by all other wear tracks obtained by the *in-situ* procedure. However, it must be mentioned, that besides the showed friction curves also test sequences with 40 – 60 N load, so up to 240 MPa higher Hertzian pressures have been conducted after the here presented results. Therefore, it is difficult to argue, whether the appearance of disordered graphitic like carbon is a result of more severe testing conditions or of differences in the chemical and lubricating conditions by the ex-situ derived polymer coatings. In case of the uncured coatings no drying procedure was applied, which means that residual water and ethanol was present. The presence of water and alcohols is known to accelerate and promote base oil degradation [23, 119], which means, it is not clear whether the D and G bands arise from a polymer into ceramic transformation or from degradation of the base oil. Another difference is also the presence of corrosion in filament shape besides the wear track in the case of the uncured coating from the 5 days aged sol. The Raman spectrum obtained on these spots show strong signals for hematite, which has not occurred for all other tested conditions with in-situ formed polymer. Base oil reference spectrum, so without any coating material but otherwise under similar conditions show no clear signs of amorphous carbon. In the context of the given findings, the presence of D and G bands is ascribed to degradation products of the base oil, generally called “soot”.

Base oil degradation promotes generation of oil insoluble varnish deposits on the metal surfaces and often also triggers corrosive or abrasive wear. It is also observable that the Raman intensities of the D and G bands, as well as the dark wear track appearance reduce when the sols are cured to 100 °C, compared to the uncured coatings. This matches with the lower alcohol and water contamination of the lubricant by the coating material. However, on basis of the D and G bands of the dried coatings further influences of the coatings than water and alcohol contamination is expected. For example, the thick viscoelastic polymer layers might restrain the flow and cooling ability of the lubricating oil and thus accelerate or promote the degradation of oil.

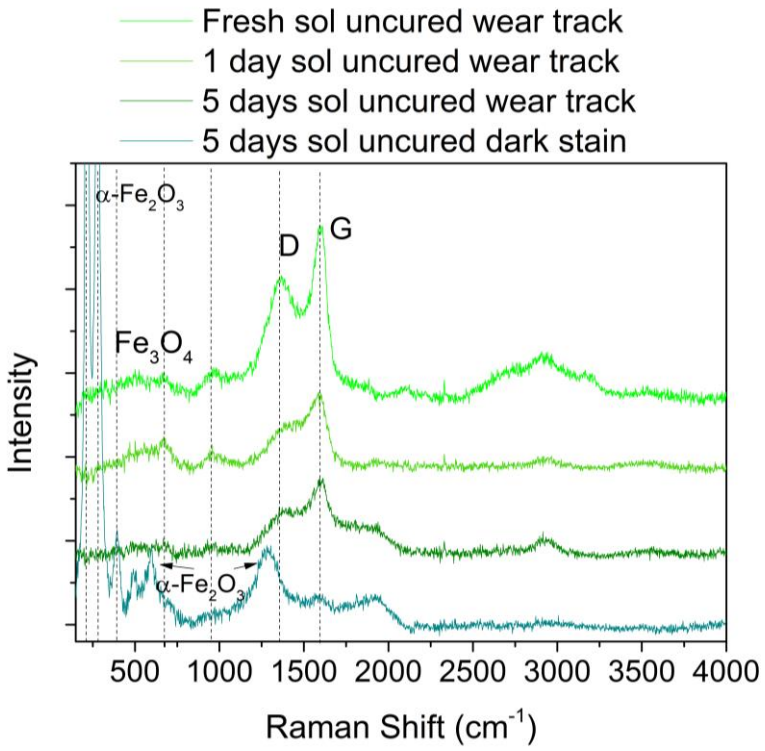

Figure 59: Micro-Raman spectra of MTM disc wear tracks tested with uncured VTMS sol-gel coatings. All spectra are from central regions of wear tracks, except the spectrum stated with "dark stain" which was obtained from a dark filament like looking area, see Figure 56.

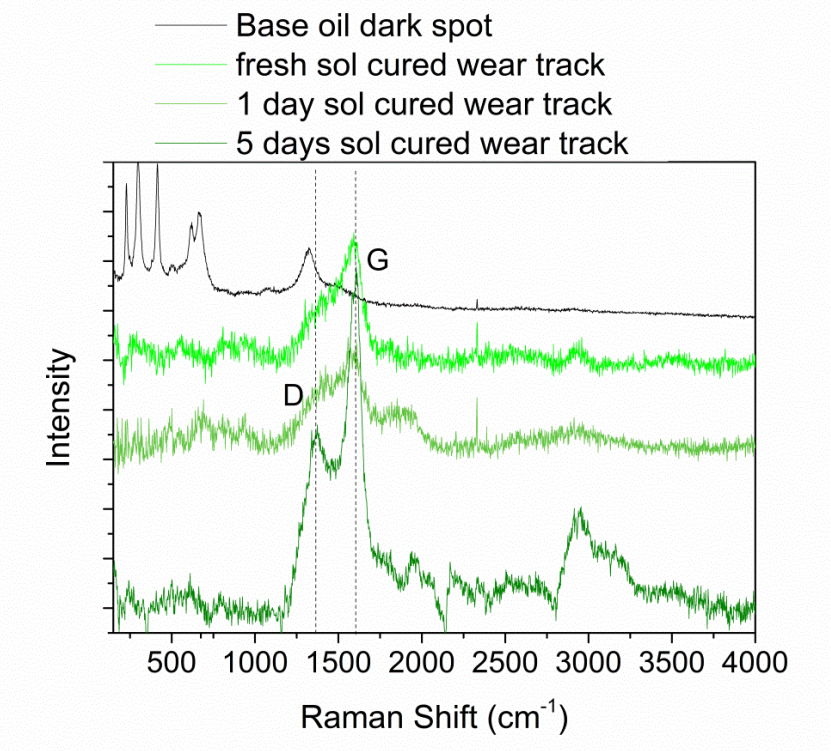

Figure 60: Micro-Raman spectra of MTM disc wear tracks tested with base oil and cured sol-gel coatings. All spectra showed strong background with fluorescence which was subtracted, except the spectrum of the base oil reference.

All in all the sol-gel experiments have given new insights for the lubrication behavior of cross-linked polymeric siloxanic coatings, but also the presented lubrication model could be verified by testing uncured polysiloxane, which act as ex-situ generated polymer rich boundary layers. It was shown, that uncured organosiloxane polymer behave similar to *in-situ* formed boundary layers. Differences in the lubricating behavior, especially for long-term testing could be explained by different boundary conditions. Cured polymeric coatings could not withstand the severe testing conditions, but the test results serve information about polymeric coatings and their lubricating behavior especially when breaking down. The chemical analysis shows that the thick polymeric coatings promote the degradation of base oil, which is argued mainly by the introduction of water and alcoholic residues.

5. Conclusion and Outlook

Different molecular weight vinyltrimethoxysilane and –siloxane have been tested as mineral oil additives and their tribological and tribochemical behavior have been investigated. It was found that the silicon species experience cross-linking reactions when they undergo tribological stress, which leads to the formation of multi layered reaction films. The reaction films exhibit a polymeric layer, which is rather weakly bonded and easy to shear off. Underneath the polymeric layer is an adhesive SiOC containing tribofilm, grown on the substrate material. Both layers differ in their molecular- and microstructure and, therefore, show different influences on the tribological performance and lubrication. A schematic evolution of film formation and molecular changes of organosiloxane in tribological contacts is given in Figure 61.

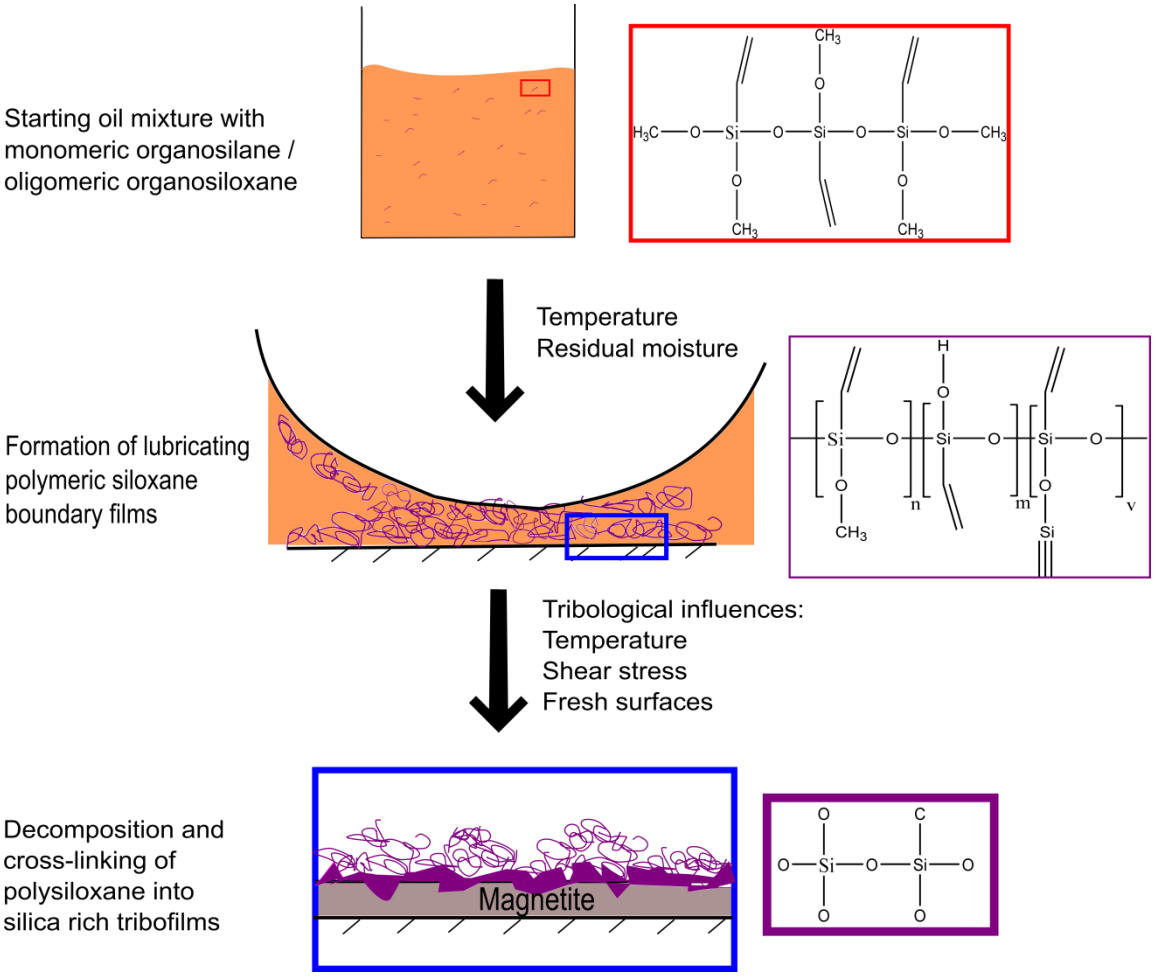

Figure 61: Schematic description of film formation and molecular changes of organosiloxane in tribological contacts.

Insights into dependences on the film formation could be obtained by the variation of testing conditions. The polymeric layers form mainly by polymerization of the precursors via condensation reactions. These reactions are temperature dependent, as no signs of polymers

were found from tests below 60 °C. Higher temperatures promote these reactions and thicker polymer films are formed. Test results suggest also differences in the microstructure of the formed gel films, depending whether oligomeric or monomeric silicon alkoxide precursors are used. It appears that the monomeric precursor forms a higher cross-linked network and elastic polymeric layers, while the oligomeric precursor forms rather viscous polymeric layers. These polymeric layers can be referred to as the source for the formation of adhesive tribofilms. It was found that the degradation and continuous cross-linking of the polymers results in silica rich adhesive tribofilms. The transformation is dependent on temperature. In addition, the influences of the load and the steel surface on film formation were discussed. First a critical contact pressure or shear stress is necessary to start the degradation and cross-linking reactions from organosiloxane into silica. Second, the role of iron oxide is not fully resolved yet but was found to be necessary for the tribofilm deposition. The results from surface characterization highlight, that the rough and pad-like SiOC tribofilm is grown on top of magnetite layers, which might catalyze the degradation reactions.

Furthermore, a lubrication model on the basis of the results from experiments with the oligomeric precursor has been presented. The model is derived from the polymer rich boundary film model by Spikes, which are described to act similar to elastohydrodynamic lubricant films. The major difference is the variation of viscosity with time and mean speed of the formed boundary films. This behavior is ascribed to the molecular structure and attractive forces of the polymers between each other and with the steel / tribofilm surface. In addition, a critical shear rate is found at which these boundary films lose their ability to maintain stable lubrication. The results from monomeric derived polymer layers do not fully support the model, which is referred to their different film formation behavior. Nevertheless, it could be shown that the polymeric layers are able to reduce the friction in boundary and mixed lubrication conditions by the formation of boundary films. In contrast, the adhesive tribofilms exhibit unfavorable influences on the friction and lubricating performance.

Sol-gel derived coatings are deposited under different conditions and their tribological behavior was investigated. The results from friction tests support the lubrication model and the theory of tribofilm formation of the in-situ generated reaction films. However, the coatings are not sufficiently mechanically strong enough to be used for conventional applications. All coatings got sheared off during the tests and no favorable influences on friction could be maintained over the whole testing time.

In summary, organosiloxane / -silane alkoxides as film forming oil additives show some advantageous and disadvantageous properties and mechanism in tribological contacts, which are summarized in Table 15.

Table 15: Advantages and disadvantages which were found by using vinylalkoxidesiloxane oil additives in terms of their tribological performance. The asterisks refer to the fact that a wear increase is obtained from wear tests with elevated temperatures.

+	-
Low friction by polymer layers	High friction from tribofilm
Good anti wear performance*	Bad anti wear performance after threshold*
Corrosion resistance	

The overall goal was to investigate organosiloxane containing alkoxide groups as suitable friction modifier and anti-wear additives for low viscous lubricants. This work shows that the in-situ condensation and formation of polysiloxane highly enhance the lubricating properties of the organosilane / -siloxane oil mixtures. Especially the main issue, the low viscosity and therefore low load capacity can effectively be improved in boundary conditions, while maintaining a low bulk viscosity, due to the surface near effects. The found corrosion resistance is mainly attributed to the adhesive tribofilm. However, the drawbacks by the adhesive tribofilm referring to influences on the lubrication are too big.

In consequence, further work should be directed into two directions.

First, the structure of the polysiloxane must be tailored in a way to reduce the possibility of the formation of silica rich tribofilms. At the same time, the condensation and polymerization must be controlled to ensure a stable boundary film formation without precipitation. This feature may be fixed by hydrocarbon / polysiloxane composites with a limited amount of siloxane and alkoxide fractions. This might establish an additive, which would not degrade and form adhesive tribofilms.

Second, the anti-wear performance of adhesive tribofilms may be enhanced in terms of their mechanical stability by higher deposition rates and higher silica fractions. Yu *et al.* found good anti-wear behavior by the use of calcium containing detergents and thus introduction of calcium into the tribofilm [6].

Besides these two general directions, further investigations are necessary for a better knowledge of the tribological behavior of organosiloxane oil additives. The following topics may provide a more detailed understanding:

- The resulting polymer structure of the boundary films is not resolved yet and should be studied. This may be simulated by the use of pre-condensed polysiloxane with different molecular weights.
- TEM investigations on the tribofilms should provide information about the microstructure and the role of magnetite.
- The dependence of the shear stress on the tribofilm formation should be in detail investigated to verify the possible boundary conditions for the use of this additive class. These investigations can be performed on the basis of Zhang`s work [33].
- The dependence of temperature can be reviewed with lubricant mixtures having the same viscosity for each temperature, to exclude viscosity effects of the bulk lubricant.

6. Appendix

6.1. TGA analysis and sol-gel annealing investigations

In moist atmosphere hydrolysis and condensation reactions are the main cross-linking reactions for alkoxysilane. Due to the negligible water content in mineral oil, TGA analysis in argon atmosphere has been performed to have a better understanding about the thermal stability of the used precursors. Of primarily interest is the decomposition behavior of methoxy groups. This way it can be discussed whether hydrolysis by water is necessary for cross-linking reactions or the cross-linking is triggered by radicals from scission reactions.

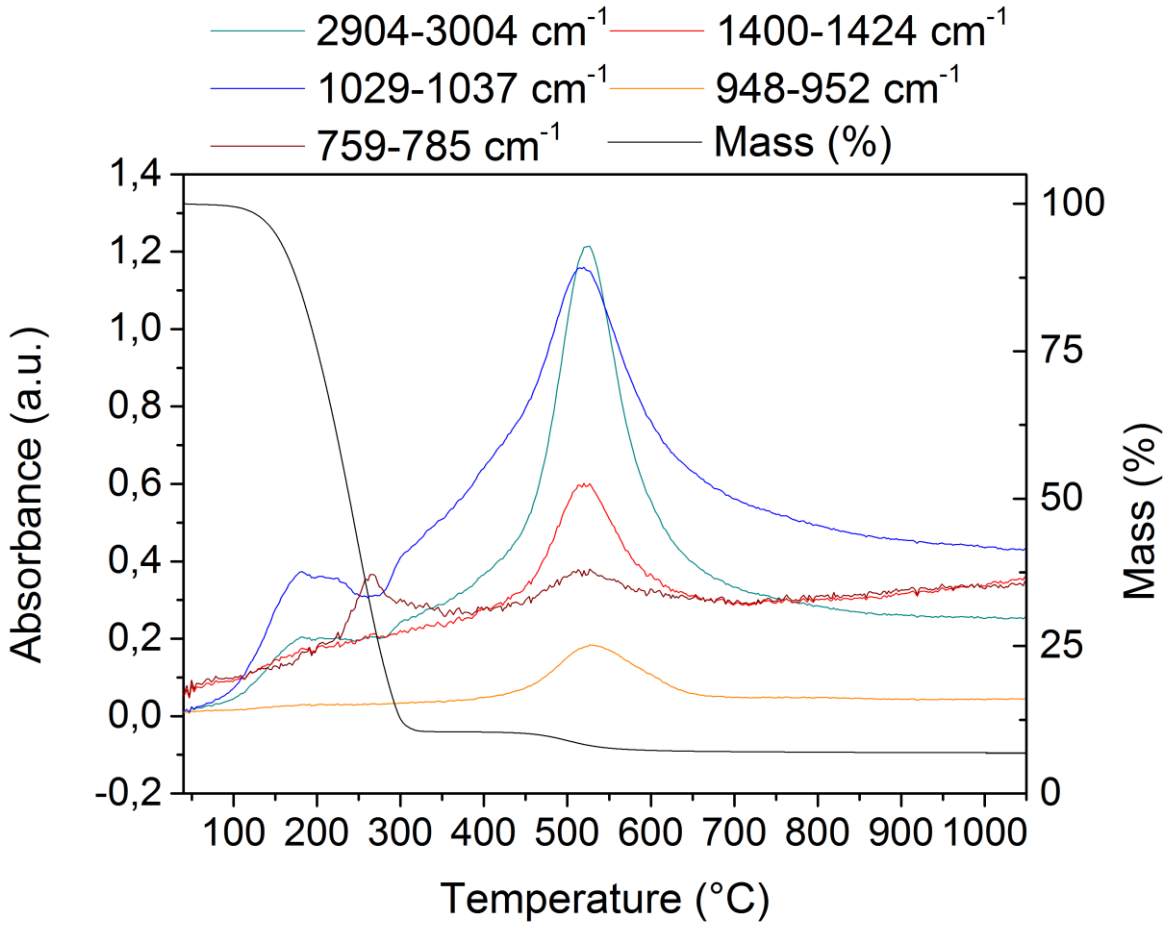

Figure 62: Absorbance from specific wavenumber regions over temperature from a VTMS-oligomer TGA analysis in argon atmosphere. The temperature ramp was set to 5 K/min.

Figure 62 presents results from the TGA analysis with FTIR absorption over temperature of the most interesting wavenumber regions and the mass change of pure VTMS-oligomer. First of all, the evaporation of the precursor can be observed from the mass change curve. The evaporation starts at 120 °C and the mass decreases linearly until around 10 mass percent is left at 300 °C, so after around 36 minutes of heating. Problematic is the differentiation of the evaporated species, because of similar organic groups and thus vibrations of

vinyltrimethoxysilane, methanol or CH_3 radicals. In addition, some condensed species have been found during the measurements, covering the tube in front of the FTIR detector. This makes a precise temperature range impossible as it cannot be said which species did condense to which extend. Therefore, the results can only be taken as estimation.

CH_3 corresponds to the range of 2904-3004 cm^{-1}, methanol or methanol radicals to 2904-3004 and 1029-1037 cm^{-1} and vinyltrimethoxysilane covers all ranges.

First FTIR signals can be seen at around 180 °C which correspond to C-H and C-O vibrations, followed by Si-C vibrations at around 260 °C. However, first vinyl signals are detected at 520 °C. All considered vibrations show the strongest intensity at this temperature, which might be a side effect of the condensation inside the tube of the TGA device. The earlier detection of C-H and C-O bonds would suite the hypothesis, what describes the separation of methanol fragments from the alkoxysilane, triggering cross-linking reactions of alkoxysilane. Although, binding energies would suggest the decomposition of C-O bonds rather than Si-O bonds at lower temperatures, the TGA analysis results are not very accurate in this regard.

Figure 63 shows a comparison of FTIR spectra obtained from VTMS-oligomer derived gels, which have been dried at 80 and 250 °C, respectively. The spectra from the annealed sample at 250 °C clearly show the vanishing of the bands, which are associated to the vinyl groups and the appearance of C=O vibrations. This information helps to estimate the conditions and possible reactions of the precursors during tribological stress, since C=O vibrations have also been observed for the tribopolymer deposits

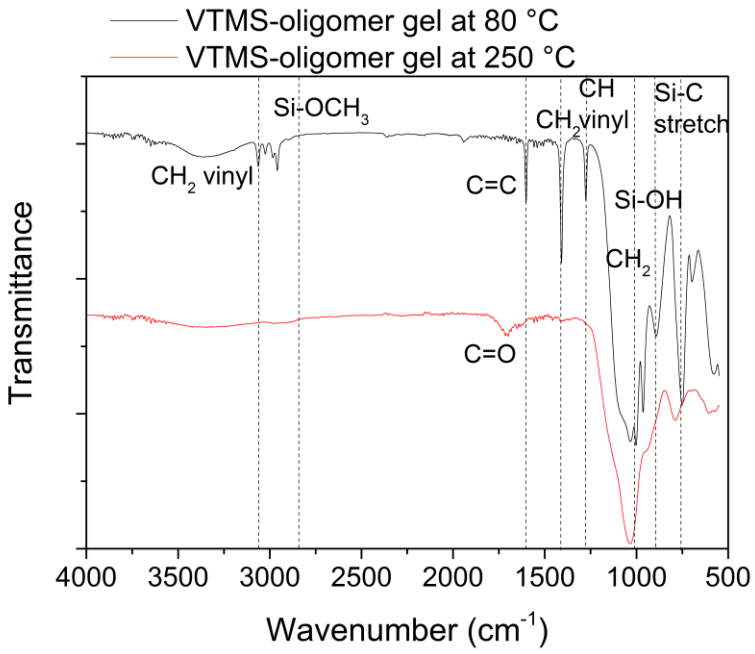

Figure 63: FTIR spectrum of dried gels, derived from VTMS-oligomers with ethanol and water.

6.2. NMR analysis of used base oil

In order to investigate changes of the tested mixtures NMR investigations have been performed and exemplary spectra are shown in Figure 64 and Figure 65. Figure 64 presents a comparison of the pristine base oil and of a VTMS-oligomer mixture after a MTM test in form of ^{1}H NMR spectra. In case of the VTMS-oligomer mixture peaks at around 3.5 ppm can be referred to methoxy groups from the precursor. A clear indication of methanol is difficult, since only very weak signals at 3.26 ppm might correspond to the hydrolyzed alcohol. Another new peak which does not fit with peaks from the pristine precursor nor from the oil appeared at 2.28 ppm. This range fits with signals from carbonyl groups unfortunately no other signals match to this assumption. Another assumption is a peak shift from an alcohol group due to hydrogen bonding, which is frequently observed and in the range of + / - 1 ppm shifts.

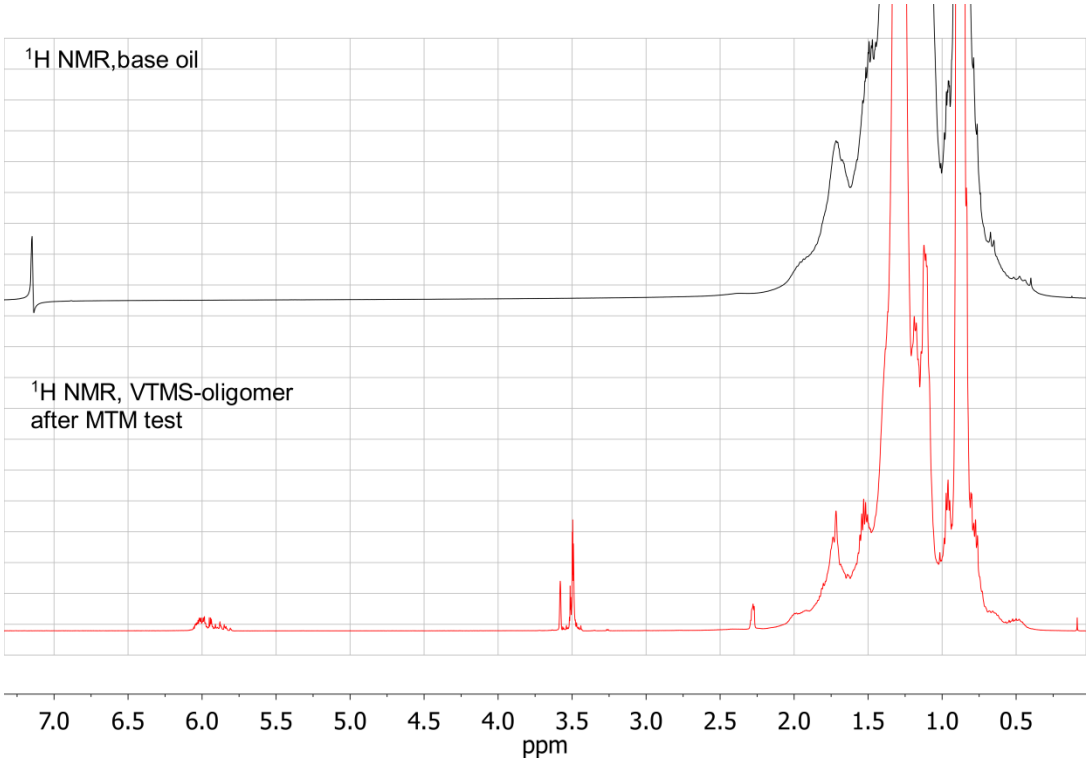

Figure 64: ^{1}H NMR spectra of base oil and a used VTMS-oligomer mixture after MTM test. The used solvents are benzene d-6 and tetrafuran d-8, respectively.

Coupled ^{1}H and ^{29}Si measurements are performed to increase the signal intensity for the silicon signals and the comparison of the pristine VTMS-oligomer precursor and the tested oil mixture is given in Figure 65. The pristine precursor shows signals for T1 and T2 structures at around -62 and -71 ppm. The silicon signals from the precursor after the MTM test are shifted to higher values of around -66 and -75 ppm. Sol-gel investigations, presented in chapter 6.4 show that condensed T3 structures appear at around -78 ppm. It is difficult to argue whether

condensed T3 units exist in the mixture, due to the very low concentration and therefore low signal to noise ratio. In addition, it cannot be said whether the shift towards higher ppm is attributed to formation and interaction of Si-OH or due to solvent effects.

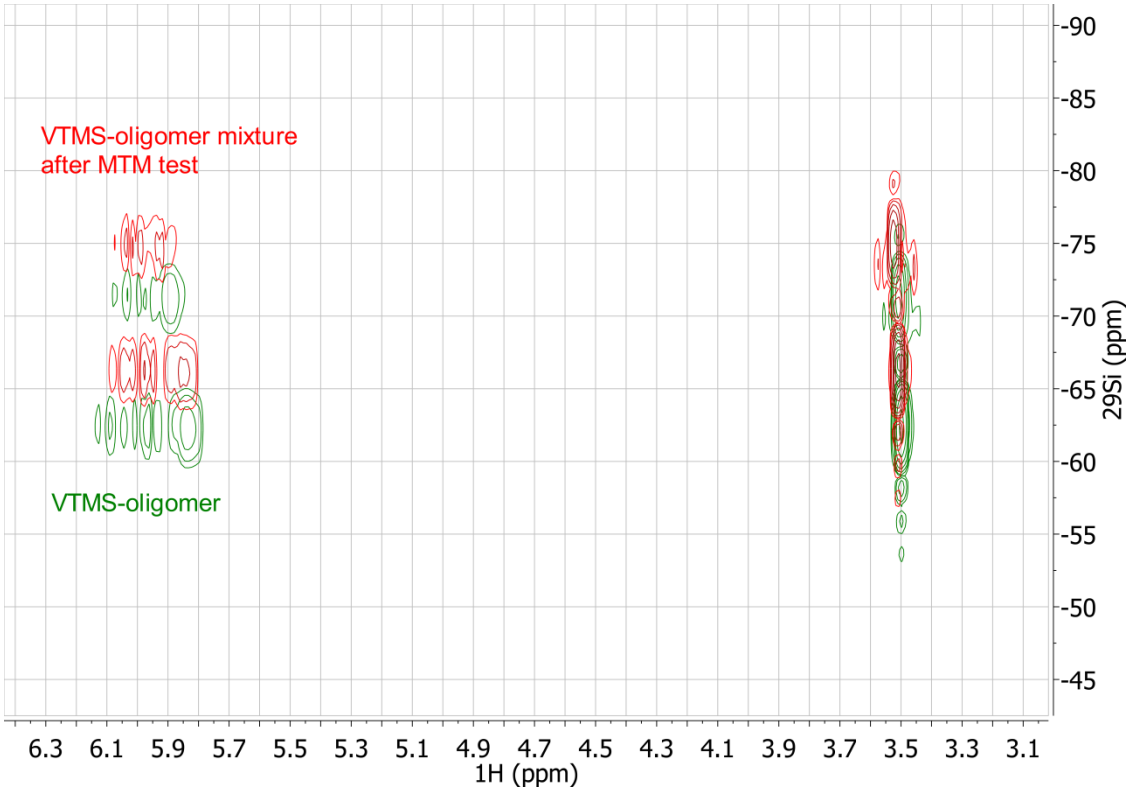

Figure 65: ^{1}H-^{29}Si-HMBC NMR spectra of pure VTMS-oligomer a used VTMS-oligomer mixture after MTM test.

6.3. FTIR and Raman analysis of VTMS wear tracks

FTIR and Raman spectroscopy has been used to investigate whether VTMS derived reaction films follow similar reactions like the oligomeric precursor. Therefore, disc wear tracks from MTM tests with VTMS addition have been investigated prior and after cleaning. Prior cleaning means, that the wear track surface is still covered with polymeric and oil residues. This is noted as "multi-layer film" in Figure 66, where tribofilm corresponds to the cleaned wear track, with an appearance like in Figure 51. The multi-layer film spectrum differs from the tribopolymer spectrum generated by the oligomeric precursor in Figure 18 by some points. First the broad O-H band at around 3400 cm^{-1} is much weaker, as well as the missing Si-O-H band. Also the only organic signs refer to C-H vibrations at 2925 and 2850 cm^{-1}. A indistinct band at 1600 cm^{-1} is also obtained with steel disc references and therefore no clear indication for the presence of C=C bonds. However, a clear Si-O-Si band is seen for the multi-layer film and for the tribofilm, which is in consistence with the EDX measurements of the wear tracks.

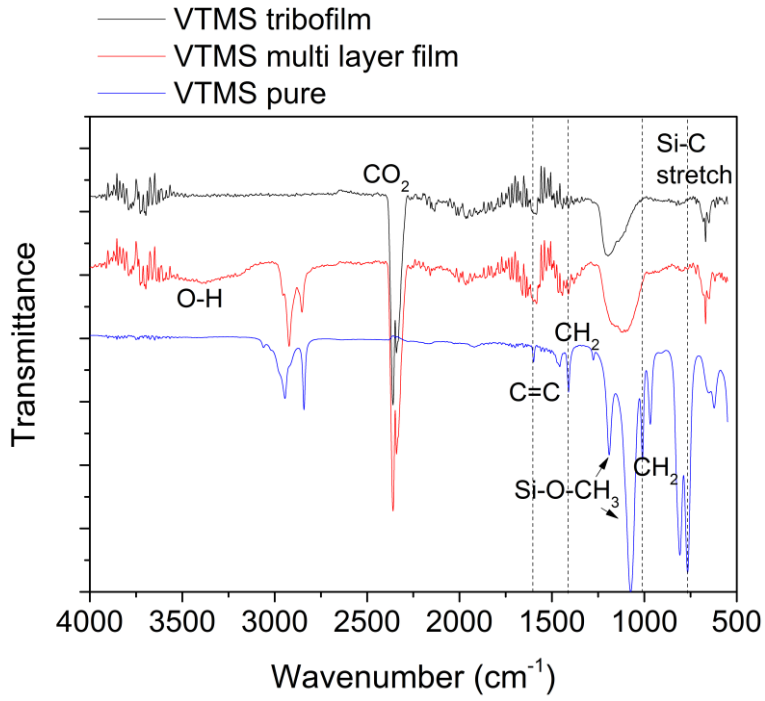

Figure 66: ATR-FTIR spectra of a MTM disc wear track tested with a 2.7 wt.% VTMS blend following the standard MTM procedure at 100°C. "multi-layer film" refers to the tribopolymer. "tribofilm" refers to the adhesive coating like reaction film.

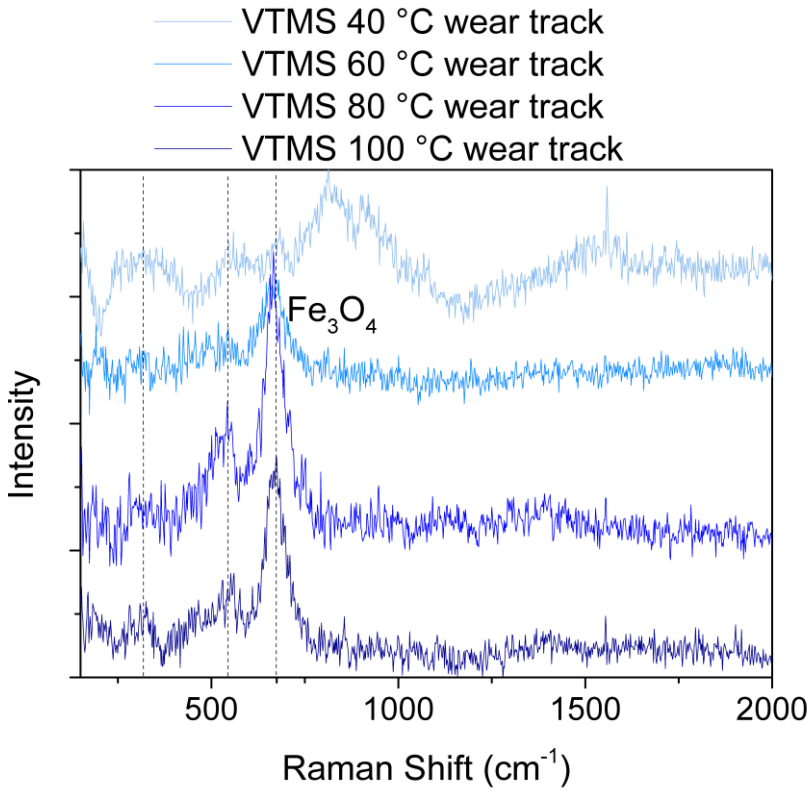

Figure 67: Micro-Raman spectra of MTM disc wear tracks tested with 2.7 wt.% VTMS blend. The spectra are from cleaned wear tracks, which were obtained at different testing temperatures.

Again similar to the VTMS-oligomer derived reaction films a strong shift of the Si-O-Si band is seen between the multi-layer spectrum and the tribofilm spectrum. Again this shift is ascribed to the stronger cross-linked and more silica like micro structure as is the case with the oligomeric derived tribofilms. The very weak signals of the multi-layer spectrum can be explained, by the low amounts or thin deposits of polymeric residues, which is also in consistence with the observations from the friction curves and the SLIM images.

Figure 67 presents Raman spectra from MTM disc wear tracks, which have been obtained at different testing temperatures. The spectra are similar to the VTMS-oligomer Raman spectra and show the presence of Fe_3O_4, in all cases, for 20 to 30 nm thick tribofilms. Nevertheless, it should be noted that the tribofilm from the 60 °C tests is much more uniform and expands over the whole wear track, opposite to the VTMS-oligomer tribofilm obtained at 60 °C, where only some regions were coated. The spectrum from the 40 °C sample does neither show a clear tribofilm formation nor signals corresponding to Fe_3O_4. A broad band at around 810 cm^{-1} is detected, which unfortunately does not fit with any iron oxide modification [91, 92].

Without the findings and the model of the oligomeric derived precursor it would be difficult to predict, which reactions the VTMS undergoes and whether the formation of the reaction films follows hydrolysis and condensation reactions. The presence of Fe_3O_4 again shows the connection and importance of iron oxidation on the tribofilm formation. The O-H band as well as the shift of the Si-O-Si band indicates that VTMS follows the same reaction pattern, like the oligomeric precursor. However, due to the low amounts of polymeric residues distinct differences in the reaction rates and thus film formation are likely and are explained in chapter 4.3.1.

6.4. NMR investigation of sol-gel polymer

The cross-linking and polymerization of the sols for the ex-situ test design have been tracked by FTIR and NMR spectroscopy. Due to an easier assignment for the polymerization degree, only NMR spectra are shown, see Figure 68 and Figure 69 for ^{29}Si-DEPT and ^{1}H-^{29}Si-HMBC spectra. Both spectra compare the ^{29}Si ppm shifts between pure VTMS-oligomer, a fresh sol and a 1 day aged sol, to follow hydrolysis and condensation reactions. The reference VTMS-oligomer spectrum exhibits T_1 and T_2 structures corresponding to the region around -62 ppm and -71 ppm, respectively. Only in case of the 1 day aged sol sample a new but rather undefined peak appears around -77.5 ppm in the ^{29}Si spectra. This peak is correlated to T_3 structures having a vinyl group and three bridging oxygen at a silicon atom. Thanks to the more sensitive ^{1}H-^{29}Si-HMBC method more information on the cross-linking can be obtained. While the VTMS-oligomer spectrum shows no clear signs for T_3 structures, small peaks can be

observed for the fresh and 1 day aged sol. Also the 1 day aged sol shows higher intensities for T_3 structures than for T_1. Also both sols show the highest intensities for T_2 structures, which clearly indicate a polymerization process, compared to the reference VTMS-oligomer spectra. Unfortunately, it is difficult to get more precise information via integration using ^{1}H spectra, due to hardly distinguishable signals from methanol and mono- or dimethoxy groups. Also transesterification reactions with ethanol should be also considered. Nevertheless, the ^{29}Si spectra show a clear trend of stronger cross-linking with aging time. As side note, a detailed specification of polymer structure on the resulting MTM disc can only be estimated due to the additional drying process on the steel surface during the spinning process.

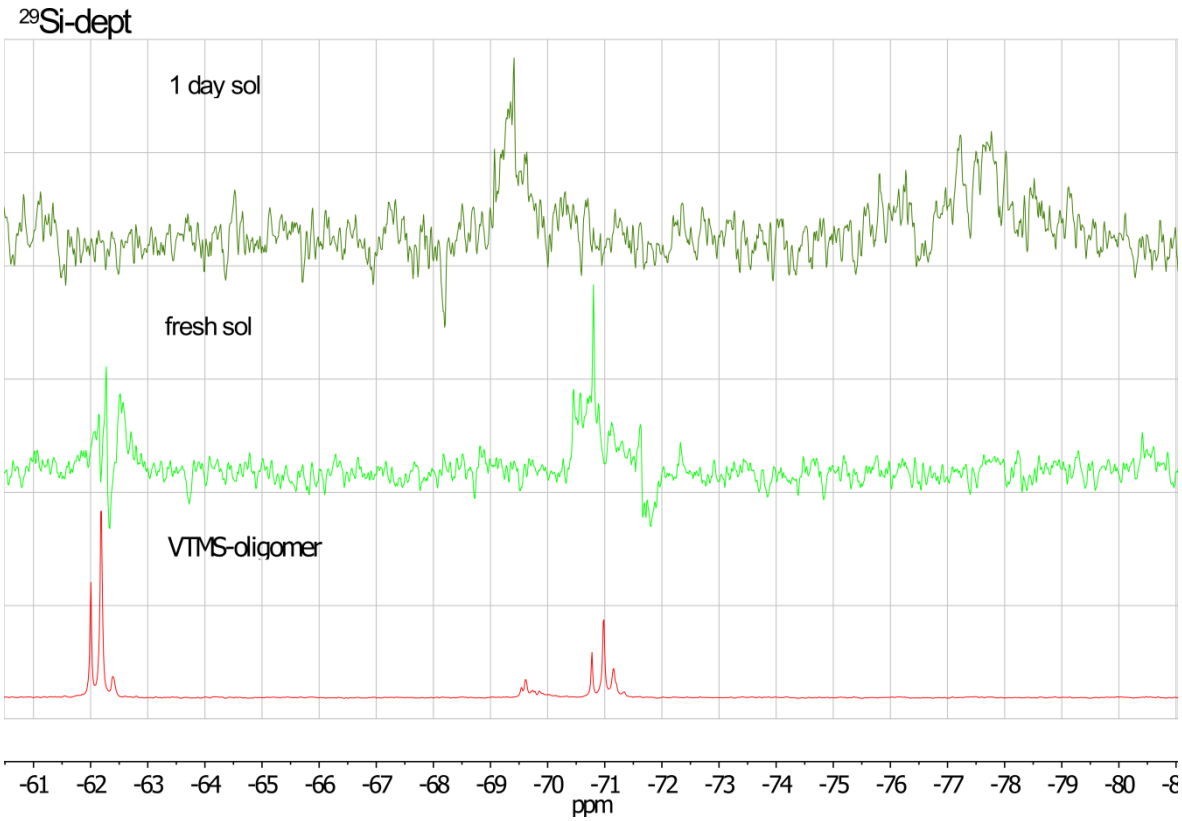

Figure 68: ^{29}Si-DEPT NMR spectra of pure VTMS-oligomer, the fresh sol and from the 1 day aged sol.

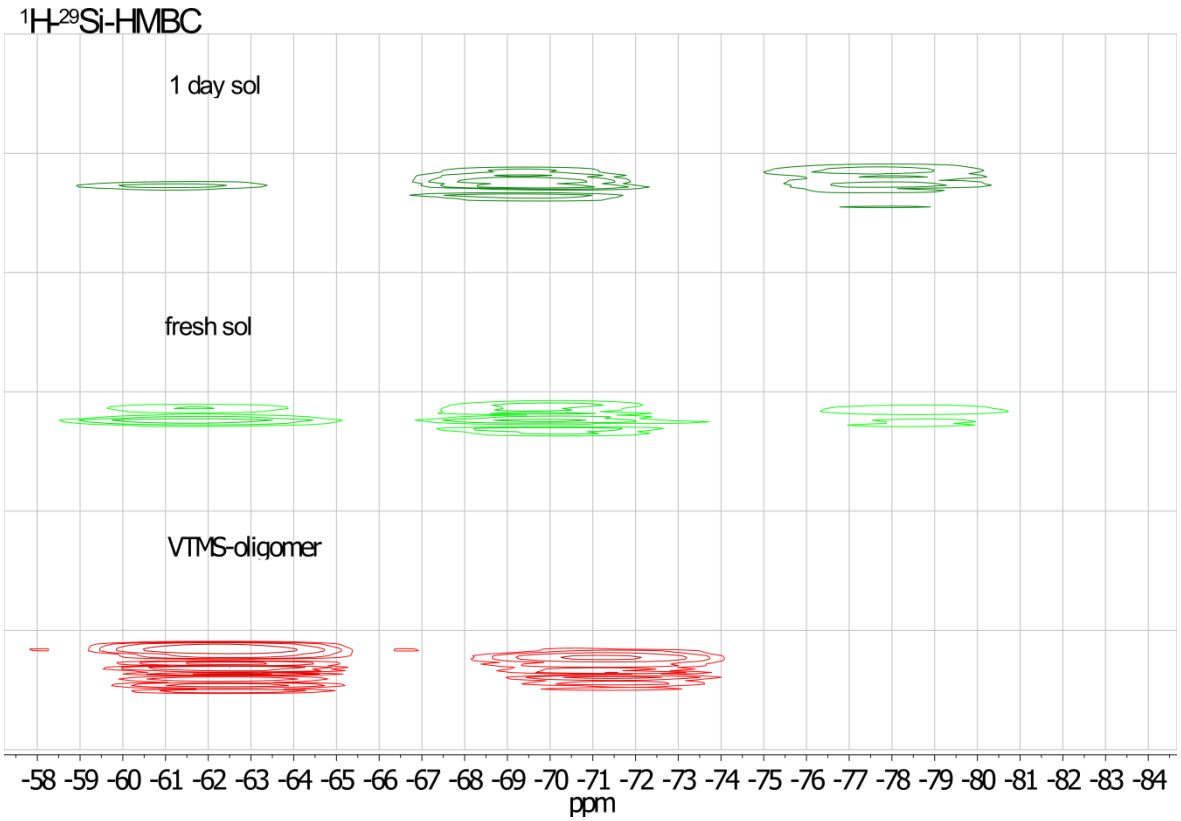

Figure 69: ^{1}H-^{29}Si-HMBC NMR spectra of pure VTMS-oligomer, the fresh sol and from the 1 day aged sol, the peaks correspond to the 5.9 – 6.2 ppm range from ^{1}H spectra, corresponding to couplings with vinyl groups, which showed most intense signals.

7. References

1. *Verordnung (EG) Nr.443/2009 Des Europäischen Parlaments und des Rates vom 23. April 2009 zur Festsetzung von Emissionsnormen für neue Personenkraftwagen im Rahmen des Gesamtkonzepts der Gemeinschaft zur Verringerung der CO2-Emissionen von Personenkraftwagen und leichten Nutzfahrzeugen*, 2009, Amtsblatt der Europäischen Union.
2. Holmberg, K., P. Andersson, and A. Erdemir, *Global energy consumption due to friction in passenger cars.* Tribology International, 2012. 47: p. 221-234.
3. K. Michaelis, B. Höhn, and M. Hinterstoißer, *Influence factors on gearbox power loss.* Industrial Lubrication and Tribology, 2011. 63(1): p. 46-55.
4. Minami, I., *Ionic liquids in tribology.* Molecules, 2009. 14(6): p. 2286-305.
5. Spikes, H., *Friction Modifier Additives.* Tribology Letters, 2015. 60(5): p. 1-26.
6. Yu, L.G., et al., *Study of silane-based antiwear additives: Wear and chemistry.* Tribology International, 2011. 44(6): p. 692-701.
7. D. Tabor, R.F.W., *The Formation Of Silicone Polymer Films On Metal Surfaces At High Temperatures and Their Boundary Lubricating Properies.* Wear, 1969. 13: p. 413-442.
8. Horst Czichos and K.-H. Habig, eds. *Tribologie Handbuch*. 2010.
9. Dowson, D., *History of Tribology*, ed. n. Edition1998.
10. Hutchings, I.M., *Leonardo da Vinci's studies of friction.* Wear, 2016. 360-361: p. 51-66.
11. Hertz, H., *Über die Berührung fester elastischer Körper.* J. für die reine und Angew. Math., 1881. 92: p. 156-171.
12. Hamrock, B.J., *Fundamentals of Fluid Film Lubrication.* NASA Reference Publication 1991. 1255.
13. M. Esfahanian and B.J. Hamrock, *Fluid-film lubrication regimes revisited.* Tribology Transactions, 1991. 34: p. 628-632.
14. Minami, I., *Molecular Science of Lubricant Additives.* Applied Sciences, 2017. 7(5): p. 445.
15. H.B. Hardy and L. Doubleday, *Boundary Lubrication-the paraffin series.* Proc. R. Soc. Lond., 1922. A100: p. 550-557.
16. C.F. Prutton, et al., *Corrosion of metals by organic acids in hydrocarbon solvents.* Ind. Eng. Chem., 1945. 37: p. 90-100.
17. Tang, Z. and S. Li, *A review of recent developments of friction modifiers for liquid lubricants (2007–present).* Current Opinion in Solid State and Materials Science, 2014. 18(3): p. 119-139.
18. Graham, J., H. Spikes, and R. Jensen, *The Friction Reducing Properties of Molybdenum Dialkyldithiocarbamate Additives: Part II - Durability of Friction Reducing Capability.* Tribology Transactions, 2001. 44(4): p. 637-647.
19. Fan, J., et al., *Reduction of Friction by Functionalised Viscosity Index Improvers.* Tribology Letters, 2007. 28(3): p. 287-298.
20. Dai, W., et al., *Roles of nanoparticles in oil lubrication.* Tribology International, 2016. 102: p. 88-98.
21. Li, B., et al., *Tribochemistry and antiwear mechanism of organic–inorganic nanoparticles as lubricant additives.* Tribology Letters, 2006. 22(1): p. 79-84.
22. Taylor, L.J. and H.A. Spikes, *Friction-Enhancing Properties of ZDDP Antiwear Additive: Part I—Friction and Morphology of ZDDP Reaction Films.* Tribology Transactions, 2003. 46(3): p. 303-309.
23. Theo Mang and W. Dresel, eds. *Lubricants and Lubrication*. 2007, Wiley-VCH.
24. Forbes, E.S. and A.J.D. Reid, *Liquid Phase Adsorption/Reaction Studies of Organo-Sulfur Compounds and Their Load-Carrying Mechanism.* A S L E Transactions, 1973. 16(1): p. 50-60.
25. Forbes, E.S., *THe Load Carrying Action of Organo-Sulfur Compounds-A Review.* Wear, 1970. 15: p. 87-96.

26. Fujita, H. and H.A. Spikes, *The formation of zinc dithiophosphate antiwear films.* Proc. Instn Mech. Engrs., 2004. 218(J): p. 265-277.
27. Johnson, D. and J. Hils, *Phosphate Esters, Thiophosphate Esters and Metal Thiophosphates as Lubricant Additives.* Lubricants, 2013. 1(4): p. 132-148.
28. Hiratsuka, K. and C. Kajdas, *Mechanochemistry as a key to understand the mechanisms of boundary lubrication, mechanolysis and gas evolution during friction.* Proceedings of the Institution of Mechanical Engineers, Part J: Journal of Engineering Tribology, 2013. 227(11): p. 1191-1203.
29. Shakhvorostov, D., et al., *Mechanical properties of zinc and calcium phosphates.* The European Physical Journal B, 2010. 76(3): p. 347-352.
30. D. Shakhvorostov, et al., *Smart Materials Behaviour in Phosphates: Role of Hydroxyl Groups and Relevance to Antiwear Films.* The Journal of Chemical Physics, 2009. 131.
31. Martin, J.M., *Antiwear mechanisms of zinc dithiophosphate a chemical hardness approach.* Tribology Letters, 1999. 6: p. 1-8.
32. Z. Yin, et al., *Application of soft x-ray absorption spectroscopy in chemical characterization of antiwear films generated by ZDDP Part I: the effects of physical parameters.* Wear, 1997. 202: p. 172-191.
33. Zhang, J. and H. Spikes, *On the Mechanism of ZDDP Antiwear Film Formation.* Tribology Letters, 2016. 63(2).
34. M. L. Suominen Fuller, et al., *Solution decomposition of zinc dialkyl dithiophosphate and its effect on antiwear films and thermal film formation studied by X-ray absorption spectroscopy.* Tribology International, 1998. 31: p. 627-644.
35. Taylor, L.J. and H.A. Spikes, *Friction-Enhancing Properties of ZDDP Antiwear Additive: Part II—Influence of ZDDP Reaction Films on EHD Lubrication.* Tribology Transactions, 2003. 46(3): p. 310-314.
36. Hüsing, N., *Sol-Gel Processing of Ceramics*. Ceramic Science and Technology, ed. Ralf Riedel and I.-W. Chen2011: Wiley-VCH.
37. Ebelmen, J.J., Ann., 1846. 57: p. 331.
38. Berger, W.G.a.E., *Verfahren zur Änderung des Reflexionsvermögens optischer Gläser*, in *German Patent*1939.
39. H. Schroeder, *Physics of Thin Films: Advances in Research and Development.* Phys. Thin Films, 1962. 5: p. 87-141.
40. Banerjee, D.A., et al., *Tribology of silica nanoparticle-reinforced, hydrophobic sol–gel composite coatings.* Surface and Coatings Technology, 2014. 260: p. 214-219.
41. Wang, D. and G.P. Bierwagen, *Sol–gel coatings on metals for corrosion protection.* Progress in Organic Coatings, 2009. 64(4): p. 327-338.
42. Muromachi, T., et al., *Application of functional coatings by sol-gel method.* Journal of Sol-Gel Science and Technology, 2006. 40(2-3): p. 267-272.
43. Penard, A.L., T. Gacoin, and J.P. Boilot, *Functionalized sol-gel coatings for optical applications.* Accounts of Chemical Research, 2007. 40(9): p. 895-902.
44. Arcos, D. and M. Vallet-Regi, *Sol-gel silica-based biomaterials and bone tissue regeneration.* Acta biomaterialia, 2010. 6(8): p. 2874-88.
45. C.J. Brinker and G.W. Scherer, *Sol-Gel Science*1990: Elsevier Science Publishing Co Inc.
46. Claudionico, W. *Sol-Gel Process*. 21.03.2020 19:33]; Available from: https://en.wikipedia.org/wiki/Sol%E2%80%93gel_process#/media/File:SolGelTechnologyStages.svg.
47. E.R. Pohl, et al., *Sterically hindered silanes for waterborne systems: a model study of silane hydrolysis*. Silanes and Other Coupling Agents, ed. K.L. Mittal. Vol. 2. 2000, London: TaylorFrancis.
48. Innocenzi, P., ed. *The Sol to Gel Transition*. ed. P. Innocenzi2016, Springer.
49. Brochier Salon, M.-C. and M.N. Belgacem, *Competition between hydrolysis and condensation reactions of trialkoxysilanes, as a function of the amount of water and the*

nature of the organic group. Colloids and Surfaces A: Physicochemical and Engineering Aspects, 2010. 366(1-3): p. 147-154.
50. *The Chemistry of Silica: Solubility, Polymerization, Colloid and Surface Properties and Biochemistry of Silica*, ed. R.K. Iler1979, New York: Wiley.
51. P. G. Chantrell and P. Popper, *Inorganic Polymers for Ceramics*. Special Ceramics, ed. P. Popper1965, New York: Academic Press.
52. S. Yajima, et al., *Development of a silicon carbide fibre with high tensile strength.* Nature, 1976. 261: p. 683-685.
53. Colombo, P., et al., *Polymer-Derived Ceramics: 40 Years of Research and Innovation in Advanced Ceramics.* Journal of the American Ceramic Society, 2010: p. 1805-1837.
54. Gabriela Mera and E. Ionescu, *Silicon-Containing Preceramic Polymers*. Encyclopedia of Polymer Science and Technology. Vol. 1. 2013, New York.
55. Ionescu, E., H.J. Kleebe, and R. Riedel, *Silicon-containing polymer-derived ceramic nanocomposites (PDC-NCs): preparative approaches and properties.* Chemical Society reviews, 2012. 41(15): p. 5032-52.
56. Sorarù, G.D., et al., *On the shrinkage during pyrolysis of thin films and bulk components: The case of a hybrid silica gel precursor for SiOC glasses.* Journal of the European Ceramic Society, 2012. 32(3): p. 627-632.
57. Lewis, G., *The atom and the molecule.* Journal of American Chemical Society, 1916. 38(4): p. 762-785.
58. *Inorganic polymers*, ed. R. De Jaeger and M. Gleria2007, New York: Nova Science Publishers Inc.
59. Zolper, T.J., et al., *Energy Efficient Siloxane Lubricants Utilizing Temporary Shear-Thinning.* Tribology Letters, 2013. 49(3): p. 525-538.
60. Zolper, T.J., *Friction and Wear Protection Performance of Synthetic Siloxane Lubricants.* Tribol Lett, 2013. 51.
61. G.V. Vinogradov, N.S. Nametkin, and M.I. Nossov, *Antiwear and Antifriction Properties of Polyorganosiloxanes and Their Mixtures With Hydrocarbons.* Journal of Basic Engineering, 1965: p. 747-752.
62. Tabor, D. and R.F. Willis, *The formation of silicone polymer films on metal surfaces at high temperatures and their boundary lubricating properties.* Wear, 1969. 13(6): p. 413-442.
63. Willis, R.F., *The formation of polysiloxane films on metal surfaces and their lubricating properties.* Tribology, 1969. 2(3): p. 175-178.
64. Jemmett, A.E., *Review of recent silicone work.* Wear, 1970. 15: p. 143-148.
65. Kuribayashi, T. and Y. Yamamoto, *Effect of Friction and Wear on Formation of Polysiloxane Films at Iron Oxide Surface in Viscous Couplings.* Tribology Transactions, 2000. 43(4): p. 579-586.
66. Elaine S. Yamaguchi and K.-S. Ng, *Method for Forming Tetraoxy-Silane dervided Antiwear Films and Lubricating Oil Compositions Therefrom*, 2008: United States.
67. E. Nyberg, C. Y. Respantiningish, and I. Minami, *Molecular design of advanced lubricant base fluids: hydrocarbon-mimicking ionic liquids.* Royal Society of Chemistry, 2017. 7: p. 6364-6373.
68. Hansen, J., et al., *Performance and mechanisms of silicate tribofilm in heavily loaded rolling/sliding non-conformal contacts.* Tribology International, 2018. 123: p. 130-141.
69. Marsal, A., et al., *Mechanical properties and tribological behavior of a silica or/and alumina coating prepared by sol-gel route on stainless steel.* Surface and Coatings Technology, 2013. 237: p. 234-240.
70. Hanetho, S.M., et al., *Synthesis and characterization of hybrid aminopropyl silane-based coatings on stainless steel substrates.* Surface and Coatings Technology, 2014. 238: p. 1-8.

71. Dante, R.C. and C.K. Kajdas, *A review and a fundamental theory of silicon nitride tribochemistry.* Wear, 2012. 288: p. 27-38.
72. Jin, L., *Ultra-low friction of sintered silicon carbide in aqueous tribological environment of mechanical seals*, in *Institut für Werkstoffwissenschaften*2018, Technische Universität Darmstadt: Darmstadt.
73. Y. Hibi and Y. Enomoto, *Chemical analyses of mechanochemical reaction products of alpha-Si3N4 in ethanol and other lower alcohols.* Journal of Materials Science Letters, 1997. 16: p. 316-319.
74. Neste, *Safety Data Sheet Nexbase® 3050*, Neste, Editor 2015.
75. Instruments, P., *MTM2 Mini-Traction Machine brochure*, 2017.
76. Instruments, P., *MTM2 3D SLIM Option*, 2014.
77. Instruments, P., *MTM Standard Specimen Specifications.* 2015.
78. Scientific Polymer Products, I. *Refractive Index of Polymers by Index*. 14.06.2019]; Available from: https://scientificpolymer.com/technical-library/refractive-index-of-polymers-by-index/.
79. Cristina Eliza Brunchi, et al., *Properties of Some Poly(siloxane)s for Optical Applications.* High Performance Polymers, 2009. 21: p. 31-47.
80. J.M. Perez, G.C. Caufmann, and L. Holland. *Using Biodegradable Lubricants in Farm Equipment*. 14.06.2019]; Available from: https://www.machinerylubrication.com/Read/28598/biodegradable-lubricants-farm-equipment.
81. Efficiency, E.R., *Product information Dynasylan 6490*, July 2017.
82. Topolovec-Miklozic, K., T.R. Forbus, and H.A. Spikes, *Film thickness and roughness of ZDDP antiwear films.* Tribology Letters, 2007. 26(2): p. 161-171.
83. Philip J. Launer and U.b.B. Arkles, *Infrared Analysis of Organosilicon Compounds: Spectra-Structure Correlations.* Reprinted from Silicon Compounds: Silanes & Silicones, 2013 Gelest, Inc Morrisville, PA: p. 175-178.
84. Ishida, H. and J.L. Koenig, *Vibrational Assignments of Organosilanetriols. I. Vinylsilanetriol and Vinylsilanetriol-D3 in Aqueous Solutions.* Applied Spectroscopy, 2016. 32(5): p. 462-469.
85. Li, Y.S., et al., *Vibrational spectroscopic studies of vinyltriethoxysilane sol-gel and its coating.* Spectrochimica acta. Part A, 2004. 60(12): p. 2759-66.
86. N. Primeau, C. Vautey, and M. Langlet, *The effect of thermal annealing on aerosol-gel deposited SiO2 films a FTIR deconvolution study.* Thin Solid Films 1997. 310: p. 47-56.
87. Singh, A., et al., *Lubricant degradation and related wear of a steel pin in lubricated sliding against a steel disc.* ACS applied materials & interfaces, 2011. 3(7): p. 2512-21.
88. Hyuncheol Kim and J. Jang, *Infrared Spectroscopic Study of SiOx Film Formation and Decomposition of Vinyl Silane Derivative by Heat Treamtent. I. Ony KBr and Gold Surface.* Journal of Applied Polymer Science, 1997. 68: p. 775-784.
89. Wang, T.B., Z.G. Liu, and C.Z. Tan, *Relationship between the frequency of the main LO mode of silica glass and angle of incidence.* The Journal of Chemical Physics, 2003. 119(1): p. 505-508.
90. Zanchetta, E., et al., *Stereolithography of SiOC Ceramic Microcomponents.* Advanced Materials, 2016. 28(2): p. 370-6.
91. Colomban, P., *Potential and Drawbacks of Raman (Micro)spectrometry for the Understanding of Iron and Steel Corrosion*, in *New Trends and Developments in Automotive System Engineering*, M. Chiaberge, Editor 2011, IntechOpen: London.
92. D. L. A. de Faria, S. Venâncio Silva, and M.T.d. Oliveira, *Raman Microspectroscopy of Some Iron Oxides and Oxyhydroxides.* Journal of Raman Spectroscopy, 1997. 28: p. 873-878.
93. Spivak, A., et al., *Raman study of MgCO3–FeCO3 carbonate solid solution at high pressures up to 55 GPa.* Physics and Chemistry of Minerals, 2014. 41(8): p. 633-638.

94. Linda Jayes, et al., *Vibrational Spectroscopic Analysis of Silicones A Fourier Transform-Raman and Inelastic Neutron Scattering Investigation.* Anal.Chem., 2003. 75: p. 742-746.
95. Post, P., et al., *Characterization and Applications of Nanoparticles Modified in-Flight with Silica or Silica-Organic Coatings.* Nanomaterials, 2018. 8(7).
96. Dahiya, R., G. Gottardi, and N. Laidani, *PDMS residues-free micro/macrostructures on flexible substrates.* Microelectronic Engineering, 2015. 136: p. 57-62.
97. Simonsen, M.E., et al., *XPS and FT-IR investigation of silicate polymers.* Journal of Materials Science, 2009. 44(8): p. 2079-2088.
98. Becker, S., et al., *Solvent cleaning and wettability of technical steel and titanium surfaces.* Adsorption Science & Technology, 2016. 34(4-5): p. 261-274.
99. Biesinger, M.C., et al., *Resolving surface chemical states in XPS analysis of first row transition metals, oxides and hydroxides: Cr, Mn, Fe, Co and Ni.* Applied Surface Science, 2011. 257(7): p. 2717-2730.
100. Tien-Chih Lin, Gayatri Seshadri, and J.A. Kelber, *A consistent method for quantitative XPS peak analysis of thin oxide films on clean polycrystalline iron surfaces.* Applied Surface Science, 1997. 119: p. 83-92.
101. Tse, J.S., Y. Song, and Z. Liu, *Effects of Temperature and Pressure on ZDDP.* Tribology Letters, 2007. 28(1): p. 45-49.
102. Jaeger, J.C., *Moving sources of heat and the temperature at sliding contacts.* Proc. R. Soc. NSW, 1942. 76: p. 203-224.
103. Batchelor, A.W., G.W. Stachowiak, and A. Cameron, *The Relationship Between Oxide Films and the Wear of Steels.* Wear, 1986. 113: p. 203-223.
104. Spikes, H.A., *Boundary Lubrication and Boundary Films.* 1993. 25: p. 331-346.
105. Spikes, H.A. and A.V. Olver, *Basics of Mixed Lubrication.* Lubrication Science, 2003. 16(1): p. 3-28.
106. V. Anghel, C. Bovington, and H.A. Spikes, *Thick-Boundary-Film Formation by Friction Modifier Additives.* Lubrication Science, 1999. 11(4): p. 313-335.
107. Müller, M., et al., *The Design of Boundary Film-Forming PMA Viscosity Modifiers.* Tribology Transactions, 2006. 49(2): p. 225-232.
108. Smeeth, M., H.A. Spikes, and S. Gunsel, *The Formation of Viscous Surface Films by Polymer Solutions: Boundary or Elastohydrodynamic Lubrication?* Tribology Transactions, 1996. 39(3): p. 720-725.
109. Cann, P.M. and H.A. Spikes, *The Behavior of Polymer Solutions in Concentrated Contacts: Immobile Surface Layer Formation.* Tribology Transactions, 2008. 37(3): p. 580-586.
110. Ashby, M.F., J. Abulawi, and H.S. Kong, *Temperature Maps for Frictional Heating in Dry Sliding.* Tribology Transactions, 1991. 34(4): p. 577-587.
111. Diaby, M., et al., *Understanding carbonaceous deposit formation resulting from engine oil degradation.* Carbon, 2009. 47(2): p. 355-366.
112. Green, D.A. and R. Lewis, *The effects of soot-contaminated engine oil on wear and friction: A review.* Proceedings of the Institution of Mechanical Engineers, Part D: Journal of Automobile Engineering, 2008. 222(9): p. 1669-1689.
113. Hu, E., et al., *The role of soot particles in the tribological behavior of engine lubricating oils.* Wear, 2013. 304(1-2): p. 152-161.
114. Stuart, M.A.C., et al., *Hydrodynamic thickness of adsorbed polymer layers.* Macromolecules, 1984. 17(9): p. 1825-1830.
115. Shingo Katayama, et al., *Preparation of Organosiloxane Based Inorganic Organic/Hybrids with High Affinity toward Engine Oil.* Journal of the Ceramic Society of Japan, 2002. 110(6): p. 549-553.

116. Stephan Trassl, G.M., Ernst Rössler, Günter Ziegler, *Characterisation of the free-carbon phase in precursor-derived SiCN ceramics.* Journal of Non-Crystalline Solids, 2001: p. 261-267.
117. Liu, G., et al., *Electrochemical performance of DVB-modified SiOC and SiCN polymer-derived negative electrodes for lithium-ion batteries.* Electrochimica Acta, 2013. 106: p. 101-108.
118. A. C. Ferrari and J. Robertson, *Interpretation of Raman spectra of disordered and amorphous carbon.* Physical Review B, 2000. 61: p. 14095-14107.
119. Wu, Y., et al., *Oxidative degradation of synthetic ester and its influence on tribological behavior.* Tribology International, 2013. 64: p. 16-23.

8. Acknowledgements

At first I would to give big thanks to my doctoral thesis supervisor Prof. Dr. Ralf Riedel who offers me the possibility to obtain a doctorate in materials science and who also supported me through his interest in a field of science which is partly aside his common research.

I would also like to thank Prof. Dr. Robert Stark for willingly accepting the position as second assessor and for surveying this thesis.

Special thanks go to Dr. Günter Schmitt who gave me the possibility to join his team and work in his lab at Evonik Darmstadt and for sharing so much interest. At this point I would also like to thank Dr. Stephan Fengler for accepting and funding this work as research project.

Luckily I had many nice colleagues at Evonik, who I also like to thank. Dr. Robert Kolb, Dr. Can Turhan, Dr. Michael Hagemann, Dr. Stephan Wieber and Dr. Roland Wilkens thank you for all your help, time and energy, they put into all the discussions. Thank you Robert for realizing this project and thanks to Dr. Anja Kaspar for your help with the patent.

I want to address a big thank you to the whole FriMo and Test Lab Team. Steffen Ulzheimer, Rebecca Göttig, M. Sc. Jennifer Schranz, Markus Stephan and Detlef Birth thanks for the funny time and introducing me to different testing techniques.

Apart from my colleagues at Evonik I would like to thank my colleagues in DF group. First I would like to thank Dr. habil. Emanuel Ionescu and Dr. Gabriel Mera for all the helpful discussions and also teaching me necessary chemical background.

Very big thanks go to the whole DF group! Thanks especially to Dr. Christina Stabler, Dr. Dragoljub Vrankovich, Dr. Felix Rosenburg, Dr. Fangton Xie, Dr. Xingmin Liu and Dipl. Ing. Dario de Carolis for the great time and vast amount of discussions we had about all kind of topics, including science ☺. Also thank you Dipl. Ing. Claudia Fasel for all your help in the lab.

Also thanks to M.sc. Björn Büker for the FIB-SEM investigations, to M. sc. Andreas Hubmann for your help with the XPS measurements and Dr. Christian Dietz for your help with the AFM measurements.

I am grateful to my parents, my brother and my sister, who supported me through my whole life. It is impossible for me to put my gratitude for you into words. I am happy to have you always near me.

Finally, I would like to thank my wife for all the support and all the strength you led me through this time. You always kept me motivated and helped me to focus on the important parts of life. Thank you for being the person you are.

9. Curriculum Vitae

Personal information

Benjamin Juretzka

Date of birth	29. March 1989
Nationality	german
Family status	married, 1 child

Education

3/2016 – today	**PhD program to Dr.-Ing in Materials Science** Technical university Darmstadt / Evonik Resource Efficiency GmbH Title of dissertation: „*Systematic investigation of organosiloxane derived surface modifications by tribochemical processes*“
5/2014 – 2/2016	**Master of Science in Materials Science** Technical university Darmstadt Title of master thesis: „*Formation and Characterization of Polymer Derived Tribofilms*“ in cooperation with Evonik Industries
10/2010 – 5/2014	**Bachelor of Science in Materials Science** Technical university Darmstadt Title of bachelor thesis: „*Stromlose Abscheidung von superhydrophoben, mikro- und nanostrukturierten Silberoberflächen durch Halogenidzusatz*“
8/1999 – 6/2009	**Abitur** Martin-Luther Schule, Rimbach

Internship

4/2015 – 2/2016	**Evonik Resource Efficiency GmbH, Oil Additives** Internship and master work on silicon containing polymers as film forming oil additives
9/2013 – 10/2013	**Staatliche Materialprüfanstalt Darmstadt, Kompetenzbereich Werkstoffanalytik** Characterization of silicon carbon nitride based thin films

Work Experience

11/2019 – today	**Development engineer** at **Dentsply Sirona / Degudent GmbH** Development of new products and process validations referring to dental ceramics
3/2016 – 3/2019	**PhD-student** at **Evonik Resource Efficiency GmbH, Oil Additives / Technical University Darmstadt, Dispersive solids Prof. Riedel** PhD program about the tribological behavior of organosilane and organosiloxane oil additives
4/2012 – 9/2014	**Student research assistant** at **Staatliche Materialprüfanstalt Darmstadt, Kompetenzbereich Werkstoffanalytik** Assistance in external work assignments and scientific projects regarding thin film characterization and deposition (10 hours/week)
5/2010 – 7/2010	**Worker in production** at **ESM Energie- und Schwingungstechnik, Mitlechtern** Assembly of vibration damper for wind engines and support at packaging
8/2009 – 4/2010	**Civilian service** at **Diakoniestation Fürth/Odw.** Care of elderly and office work

Abilities and achievements

Languages	German (mother tongue), English (business fluent), Italian (basics)
Trainings	Project management, time management, „Crucial Conversations“ (communication training), leadership training, Process validation for medical products (
Software	MS Office (advanced), OriginLab (advanced)

Publications & presentations

4/2020	**Patent**, Juretzka Benjamin; Wieber Stephan; Wilkens Roland; Hagemann Michael; Kolb Robert; Schmitt Günter; Turhan Can Metehan; Albert Philipp; Riedel Ralf „WO2020064619 (A1), USE OF TRIALKOXYSILANE-BASED COMPOUNDS FOR LUBRICANTS", registered 09.23.2019 published 04.02.2020
3/2020	**Publication**, Benjamin Juretzka, Stephan Wieber, Roland Wilkens, Michael Hagemann, Robert Kolb, Ralf Riedel "*Tribological Behavior of Film Forming Organosilane/-Siloxane Oil Additives: Film Characterization and Influences on Lubrication",* Tribology Letters, Issue 01/2020
9/2018	**Presentation**, 59. Jahrestagung der Gesellschaft für Tribologie, Göttingen, „*Tribological behavior of Organosilane Oil Additives*"
7/2015	**Publication**, F. Muench, B. Juretzka, S. Narayan, A. Radetinac, S. Flege, S. Schaefer, R.W. Stark and W. Ensinger "*Nano- and micro-structured silver films synthesised by halide-assisted electroless plating*", New Journal of Chemistry, Issue 9/2015